1964 Annual Report

CONFERENCE ON ELECTRICAL INSULATION

National Academy of Sciences—
National Research Council

Publication 1238

CONFERENCE ON ELECTRICAL INSULATION

Conference Organization for 1963-64

Chairman . . . . . Louis J. Frisco
General Electric Company, Schenectady, New York

Vice Chairman . . . . . A. J. Warner
De Bell and Richardson, Inc., Hazardville, Connecticut

Secretary . . . . . E. L. Brancato
Naval Research Laboratory, Washington, D. C.

Staff Executive . . . . . D. W. Thornhill

Secretarial Assistant . . . . . Marian Miller
National Academy of Sciences-National Research Council

CONFERENCE EXECUTIVE COMMITTEE

Chairman . . . . . Louis J. Frisco

E. L. Brancato
R. G. Breckenridge
J. C. Devins
A. M. Sletten
Joseph Sticher
A. J. Warner

COMMITTEE ON DIGEST OF LITERATURE

Chairman . . . . . J. C. Devins
General Electric Company, Schenectady, New York

Vice Chairman . . . . . A. M. Sletten
Westinghouse Electric Corporation, Pittsburgh, Pennsylvania

Daniel Berg

DIGEST CONTRIBUTORS

R. C. Anderson
W. R. Cook, Jr.
J. I. Cooperman
R. J. Coswell
J. Eustance
L. W. Frost
T. J. Gallagher
A. E. D. Heylen
C. M. Huggins
K. H. Illinger
L. A. Kitchman
O. H. LeBlanc, Jr.
J. Lupinsky
R. C. Merrill
F. Mopsik
H. M. Philofsky
B. Salvage
M. P. Strier
R. W. Tucker

ANNUAL REPORT
1964

CONFERENCE ON ELECTRICAL INSULATION
Division of Engineering and Industrial Research
National Academy of Sciences—National Research Council

Publication 1238
National Academy of Sciences—National Research Council
Washington, D. C.
1965

Available through the
Printing and Publishing Office
National Academy of Sciences—National Research Council
Washington, D. C. 20418
$5.00

Inquiries concerning this publication should be addressed to:
The Staff Executive, Conference on Electrical Insulation,
National Academy of Sciences—National Research Council,
2101 Constitution Avenue, N. W., Washington, D. C. 20418.

Library of Congress Catalog Card No. 51-28575

REPORT OF THE CHAIRMAN

The Conference on Electrical Insulation, sponsored by the Division of Engineering and Industrial Research of the National Academy of Sciences—National Research Council, held its thirty-third annual meeting at the Parma Research Center, Union Carbide Corporation, Cleveland, Ohio, October 11 - 14, 1964. One hundred and seventy members and guests registered for the meeting.

The Conference is indebted to the Union Carbide Corporation for its generous hospitality in providing the use of meeting facilities. In particular, Mr. David H. Bain devoted a great deal of time and effort to the local arrangements for the meeting. His efforts are appreciated.

Again this year there were so many papers submitted that time was not available for round table discussions. Eight papers were contributed by scientists from Canada, England, Germany, Israel, and Japan. The increased participation by foreign scientists in recent Conference meetings is indicative of the growing importance of the Conference as an international forum. The Office of Naval Research, Washington, D. C. provided transportation for some of the foreign academic participants. This support is deeply appreciated.

A special session of invited papers on the technology of thin films was organized by Professor N. M. Bashara, The University of Nebraska. The efforts of Professor Bashara and the contributors of the invited papers contributed greatly to the success of the meeting.

The Whitehead Memorial Lecture was delivered by Dr. Kenneth S. Cole, National Institutes of Health, Bethesda, Maryland. Dr. Cole, who has been primarily interested in understanding the structure and function of living cell membranes in general and of nerve membranes in particular, concentrated largely on the electrical approach to these problems. In his talk, "Dielectrics Alive," Dr. Cole reviewed the advances that have been made in this field.

The banquet speech was delivered by Dr. Augustus B. Kinzel, Vice President of Research, Union Carbide Corporation. "Innovations" was the title of Dr. Kinzel's stimulating talk.

For the over-all program arrangements and the preparation of the Annual Report, the Conference is indebted to Mr. A. J. Warner, Conference Vice Chairman.

At the business session of the Annual Meeting, the Chairman reviewed the status of the Conference within the National Academy of Sciences. It was reported that the first draft of a constitution had been prepared in response to a request from the Division Executive Committee. The final version will be submitted for the approval of the membership before it is adopted.

Dr. R. G. Breckenridge, Chairman of the Finance Committee, presented a detailed report of the financial status of the Conference. Financial support from the U. S. Army Research Office (Durham), under Contract DA-31-124-ARO(D)-22, which expired in September 1964, and from the National Aeronautics and Space Administration, Washington, D. C., under Task Order Contract NSR-09-012-902 has enabled the Conference to expand its activities while attaining financial solvency. A special effort is now being made to improve the income of the Conference by increasing the sale of publications, particularly the Digest. An increased income is necessary if the Conference is to function effectively without relying on the support of Government agencies.

In recent years it has become apparent to the Executive Committee that a one-year term of office for the Conference officers is not conducive to the most efficient operation and the establishment of closer relations with the Staff and the Division of Engineering and Industrial Research of the National Academy of Sciences—National Research Council. With this limitation in mind, the Nominating Committee recommended that the present officers serve for another one-year term. This recommendation was endorsed by the membership at the business session. Subsequently, the following appointments were made by the Chairman of the Division of Engineering and Industrial Research with the approval of the President of the National Academy of Sciences.

Louis J. Frisco	-	Chairman
A. J. Warner	-	Vice Chairman
E. L. Brancato	-	Secretary

The 1963 Digest of the Literature on Dielectrics, Volume 27 (NAS-NRC Publication 1230) was prepared this year under the editorship of Dr. John C. Devins, Chairman of the Digest Committee, and Dr. Andreas M. Sletten, Vice Chairman of the Committee. As is recognized, the publication of the Digest is one of the important functions of the Conference. The editors and the authors of the individual chapters richly deserve the gratitude of the Conference. Dr. Andreas M. Sletten was appointed Chairman and Dr. David W. Swan, Vice Chairman of the Committee for the 1964 Digest of Literature on Dielectrics.

The 1965 meeting will be held at the Inn, Buck Hill Falls, Pennsylvania, October 24 - 27. The 1966 meeting is scheduled for October 2 - 5 at the Pocono Manor Inn, Pocono Manor, Pennsylvania.

I wish to express my appreciation to the members of the Executive Committee, who devoted a great deal of time and effort to Conference affairs during the past year. The able assistance of Mr. D. W. Thornhill, Staff Executive, and Mrs. Marian Miller, Secretarial Assistant, National Academy of Sciences—National Research Council, is also appreciated.

Louis J. Frisco, Chairman
1964 Conference on Electrical Insulation

Schenectady, New York
November 1964

CONTENTS

ELECTRICAL CONDUCTIVITY AS A FUNCTION OF PRESSURE IN FIVE CONJUGATED AROMATIC MONOMERS

R. G. Fitzgerald

Sandia Corporation
Albuquerque, New Mexico

I. Introduction

In the last few years an increasing amount of emphasis has been directed toward obtaining the properties of materials at high pressure. The piezo-resistive effect is one of the properties receiving a considerable amount of attention as expressed in the recent papers by Drickamer[1] and others. A majority of the data obtained, however, is under static conditions. The investigation of materials under dynamic conditions is of prime importance at this laboratory since efforts are being made to find a correlation between impulse loading, conductivity, and pulse dielectric strength.

It is not anticipated that the basic pressure induced conduction mechanism will be elucidated as a result of this study; instead, the purpose of this study is to determine the effect of molecular variation of a basic organic system on electrical conductivity during impulse loading. A broader purpose of this study is to examine the general behavior of conductivity in organic compounds as a function of pressure.

II. Theory

The theoretical aspects of material selection for this study were done in association with D. M. Carlton. The criteria used in selecting the organic materials to be investigated were: (1) the material is to be a good electrical insulator, (2) the material should be readily available or easily synthesized, (3) the basic molecule selected should lend itself to structural variation, and (4) the material should have a crystalline structure in order that future studies can be conducted on single crystals of relatively high purity. Based on these criteria, the materials selected were: fluorene, diaminofluorene, biphenyl, benzidine, and tetramethyl benzidine. The structure of these materials is illustrated in Figure 1.

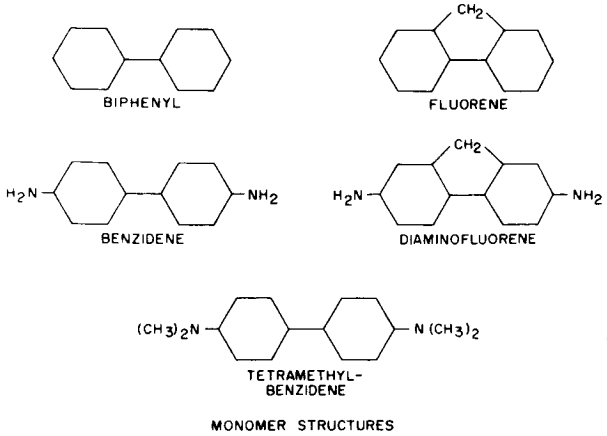

Fig. 1

Because of the steric interference between the ortho hydrogen atoms on the biphenyl molecule, there is incomplete conjugation between the phenyl rings[2,3]. The degree of conjugation is unknown. By adding a methyl bridge to the biphenyl molecule, the planar, and completely

conjugated, molecule of fluorene is formed. Conductivity measurements in the two materials should qualitatively establish the contribution of complete π orbital overlap to the conduction process in organic molecules.

Additional structure variation is realized by adding the amine groups to fluorene and biphenyl in order to form diaminofluorene and benzidine. Two new factors have been introduced: (1) there is a concentration of negative charge at the nitrogen atoms, and (2) higher intramolecular bonding energy results because of hydrogen bonding. It is believed that these additions will reduce the barrier for intramolecular charge transfer.

The third structure variation is a substitution of four relatively bulky methyl groups for the amine hydrogen atoms in benzidine. It is believed that the resulting tetramethylbenzidine will have reduced intramolecular bonding energy, an increased barrier for intramolecular charge transfer, and reduced conductivity.

III. Experimental Procedure

Standard explosive plane wave generators 1.6 inches in diameter were used to develop the high pressures required in this study. A shock wave developed by the explosive lens assembly is transmitted to the specimen under test by a metal buffer plate fabricated from copper, aluminum, or magnesium. Since the shock transfer characteristics of each buffer material to the specimen is different, a wide range of pressure levels may be established by varying the type or thickness of the buffer plate used.

The pressure developed in the specimen is determined graphically by a technique described by Walsh,[4] et al. Shock and free surface velocities are measured using a procedure given by Goranson,[5] et al. As shown in Figure 2, free surface velocity determination involves the measurement of the closure times of pins spaced at known distances from the buffer plate. Shock velocity is obtained by measurement of the closure times of pins placed at the buffer-specimen interface and at the specimen-back electrode interface. The error in pressure measurement is estimated at 5 to 7 per cent.

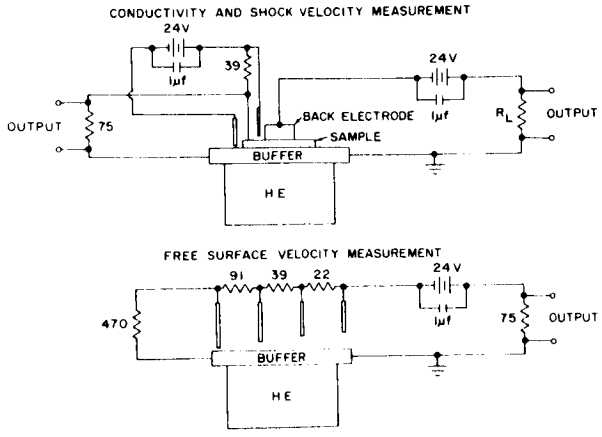

Fig. 2

Specimens were obtained by compressing polycrystalline monomers into pellets 1.00 inch in diameter and approximately .035 inch thick. A pressure of 13,000 psi was used to obtain the monomer compact. Four of the monomers have been obtained commercially at the highest purity level offered by the manufacturer. Tetramethylbenzidine was synthesized and manufactured by D. K. McCarthy. In order

to eliminate any effects of water absorption by the amine groups, specimens of benzidine, diaminofluorene, and tetramethylbenzidine were vacuum dried for a minimum of 48 hours at a pressure of 10^{-5} mm of mercury.

The resistance of the monomer specimen during shock loading is measured using the circuit shown in Figure 2. The specimen is clamped to the buffer plate by a 1/2-inch diameter aluminum back electrode. A change in resistance of the specimen normal to the shock front is noted as a change in voltage across the load resistance and is recorded by oscilloscopes. The error in resistance measurement is estimated to range from 5 to 10 per cent.

IV. Results

A plot of minimum resistance versus pressure for the five materials is shown in Figure 3. In the pressure range of 30 to 80 kilobars the resistance of all materials is many orders of magnitude lower than at ambient pressure and is decreasing rapidly with increasing pressure. This plot also shows relative resistance values to be in accord with those predicted by theory with the exception of tetramethylbenzidine. It is likely that impurities are responsible for the low resistances observed for this material. A metallic state is being approached for fluorene and diaminofluorene and would probably be attained for the remaining monomers at sufficiently high pressures.

The effect of complete conjugation is readily apparent when the data for fluorene and biphenyl are compared. A similar comparison for benzidine and diaminofluorene can also be made. The importance of hydrogen bonding and electron rich amine

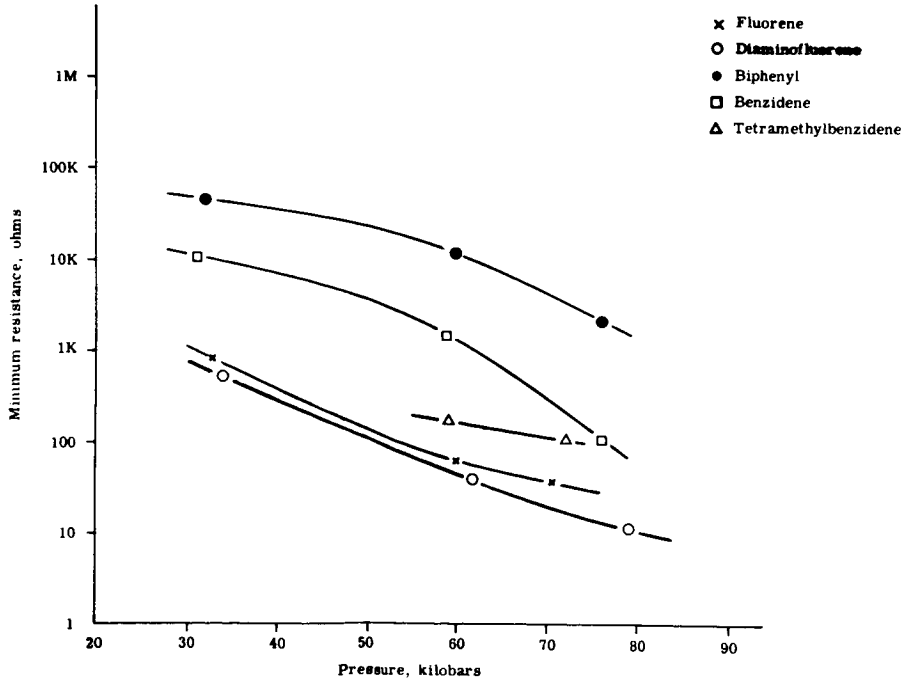

Resistance vs. Pressure for Five Conjugated Aromatic Monomers

Fig. 3

groups on conductivity is illustrated by a comparison of fluorene to diaminofluorene and biphenyl to benzidine. These comparisons are valid only if the temperature rise developed as a consequence of shock loading is the same for all materials, and that the intramolecular charge transfer mechanism is also similar. Due to the similar structures and mechanical properties of the five materials, the above assumptions seem to be reasonable.

V. Summary

In summary, it has been determined that: (1) the resistance of all materials tested at pressures of 30 to 80 kilobars is at least nine orders of magnitude lower than at ambient pressure, (2) a near metallic state is attained at 80 kilobars for fluorene and diaminofluorene, and (3) conductivity is enhanced by complete conjugation and hydrogen bonding.

References

1. Drickamer, H. G., Journal of Chemical Physics, 37, 474 (1962).
2. Hargreaves, A. and Rizvi, S. H., Acta Crystallographica, 15, 365 (1962).
3. Wheland, G. W., The Theory of Resonance, p. 92, John Wiley and Sons, New York 1947.
4. Walsh, J. M., Rice, M. H., McQueen, R. G., and Yarger, F. L., Physical Review, 108, 196 (1957).
5. Goranson, R. W., Bancroft, D., Burton, B. L., Blecher, T., Houston, E. E., Gittings, E. F., and Landeen, S. A., Journal of Applied Physics, 26, 1472 (1955).

CAVITATION IN TRANSFORMER OIL DUE TO ELECTRIC FIELDS

N. Klein, Y. Amariglio, and E. Burstein

Israel Institute of Technology
Haifa, Israel

It has been known for the last forty years that cavitation arises in oil under the influence of electric fields and that this cavitation is apparently not accompanied by electrical discharges. Local heating, field emission, electrolysis, growth of nuclei of cavities and other causes were suggested for the effect, but no conclusive evidence has been produced yet in support of any of these explanations[1,2]. To shed further light on these phenomena experiments were carried out with the following arrangement:

An 18 cm diameter condenser system was built consisting of a bottom brass disk, of a 0.012 cm thick oil impregnated cable paper layer placed on top of the brass electrode, of a 0.02 cm polyethylene disk on top of the paper and of a transparent, plane glass disk on top of the polyethylene. The under side of the glass disk adjacent to the polyethylene was coated with a transparent, conducting SnO_2 layer, forming the upper electrode of the system. The SnO_2 layer was produced by pyrolysis and its resistivity varied according to sample from 10 to 1000 Ω/square. Connections to this layer were made with Silverdag paste.

Top and bottom electrodes were parallel within ±1 per cent. The cable paper was impregnated in vacuum. The polyethylene disk contained 64 uniformly distributed 0.2 cm diameter holes, which were clearly visible through the top electrode. The system was placed in transformer oil in a desiccator vessel, the oil being nearly saturated with air at atmospheric pressure.

Experiments were carried out by changing pressure in the vessel, or voltage on the condenser system and by observing cavities arising in consequence in the holes of the polyethylene. For equal voltage and pressure the probability of cavitation varied from system to system. Cavitation was observed at fields as low as 5000 V/cm under conditions of supersaturation of air in the oil. The following observations were made at room temperature:

1. On repeated experiments the cavities tend to arise in the same holes.

2. On decreasing pressure at a constant voltage the probability of cavitation increases, as shown in Figure 1 for a 50 c/sec energy source. Without application of voltage cavitation begins below 50 mm Hg absolute pressure.

3. On changing the frequency of the source, cavitation occurs at lowest voltages around 7 c/sec, as indicated by Figure 2. To obtain this figure use was made of a large number of experiments on cavitation carried out at 80 mm Hg absolute pressure in the desiccator at varying frequencies.

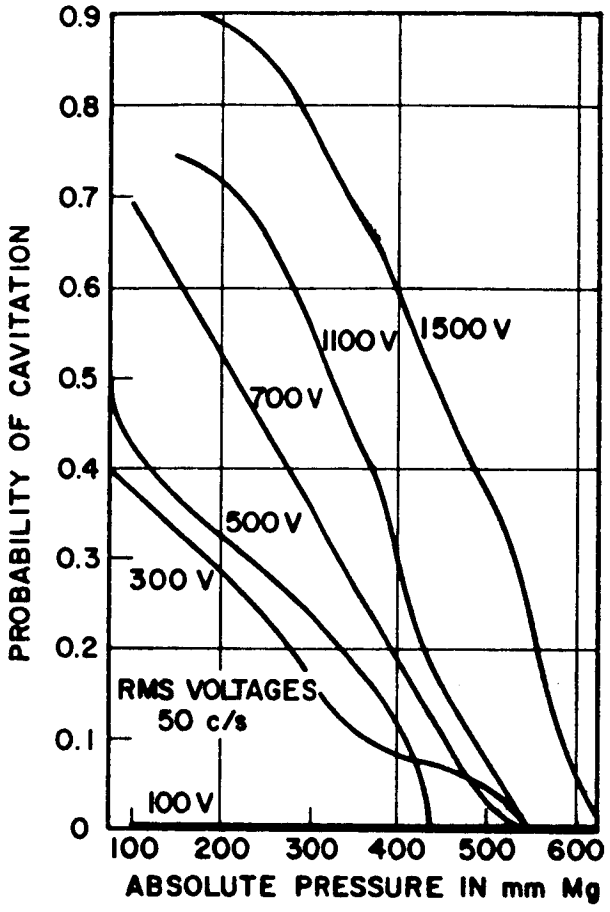

Fig. 1

4. There is less cavitation in the holes in the vicinity of the periphery.

5. Tests with the discharge detector showed that discharges do not occur during the beginning of the visible growth of the cavities.

Some conclusions regarding the causes of cavitation may be drawn from these results:

The frequency dependence of cavitation shown in Figure 2 does not support the assumption that resistive heating causes cavitation. Explanations by field emission are not acceptable in view of the very low fields causing cavitation.

Electrolysis might be understood as the cause of cavitation at low frequencies, but not at higher frequencies and this is in accordance with Figure 2. Assuming, however, electrolysis as the cause, it is not easy to explain higher cavitation inception voltages on dc than at 7 c/s. Bubbles arise occasionally not

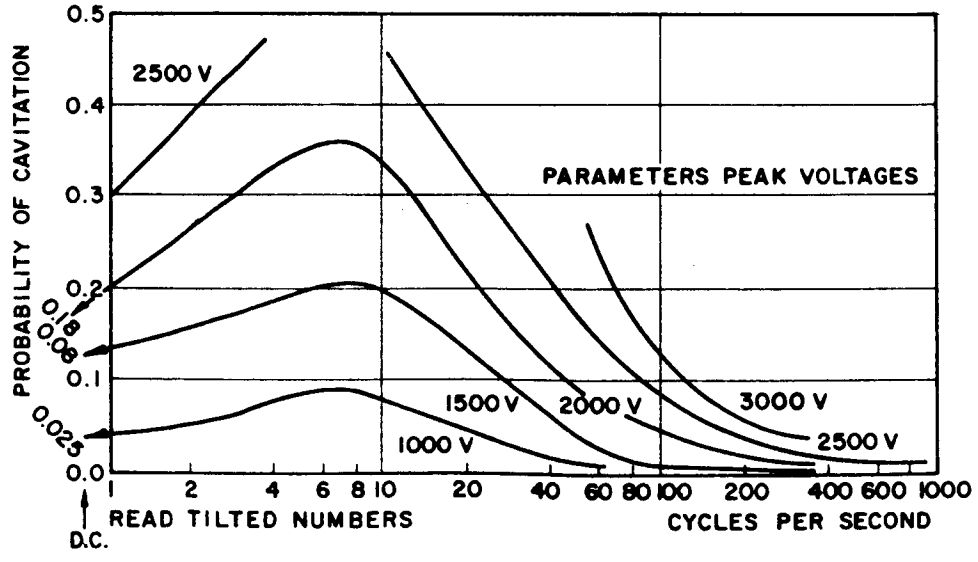

Fig. 2

at the electrodes, e.g. between the paper and polyethylene and such cavities are not due to electrolysis.

Experimental investigations on cavitation continue, to determine what the role of electrolysis is in these phenomena and whether other mechanisms can cause cavitation.

References

1. Sharbaugh, A. H. and Watson, P. K., Conduction and Breakdown in Liquid Dielectrics in J. B. Birks and J. Hart, Progress in Dielectrics, Vol. 4, Academic Press, 1962.

2. Kogan, P., Behavior of Moist Oil-impregnated Paper Under Electric Stress. Proc. IEE, London, Vol. 110, 1963, pp. 2257-66.

THE EFFECT OF HYDROGEN ACCEPTORS ON ELECTRICAL CONDUCTIVITY OF TRANSFORMER OIL AND LIQUID PARAFFIN UNDER VERY HIGH ELECTRICAL STRESS*

L. Angerer and H. Tropper

Battersea College of Technology
London, England

Queen Mary College
London, England

I. Introduction

Conductivity of insulating liquids is not yet adequately explained and more experimental work is needed to collect sufficient data for a better understanding of its mechanism. The study presented in this paper gives an account of the effects of organic hydrogen acceptors when present in transformer oil and liquid paraffin. These additives when used, up to a certain concentration, exhibited some beneficial effects giving a substantial reduction of conduction current. For all of them an optimum concentration was found which gave maximum reduction. Concentrations in excess of the optimum gave less reduction and ultimately increasing the concentration introduced harmful effects.

Measurements of conduction current for different gap settings revealed a "bulk effect" of the additives as their beneficial effects increased with the gap length. The results obtained with uniform field and small gap settings showed also that the compounds containing oxygen in their molecular structure exhibited, in addition to the bulk effect, a "surface effect", i.e., formation of a protective layer on the electrode surface.

Results obtained in tests with liquid paraffin, contaminated by aromatic constituents of transformer oil showed that the presence of the more volatile unsaturated compounds in the test liquid has a significant effect on its conduction properties. Some results are shown in Figure 1.

The effect of azocompounds was found to be less pronounced in liquid paraffin than in transformer oil. Addition of aromatic constituents to liquid paraffin containing azobenzene showed a cumulative effect of both additives.

II. Test Procedure

The apparatus consisted of a glass cell with two optical flat windows, degassing flask, liquid reservoir and No. 5 sintered glass filter, all elements arranged in a close-loop system. The oil system was connected to a vacuum line and each part of the oil system could be evacuated to a pressure of 10^{-3} mm Hg.

---

*The work was carried out in conjunction with a study of the effects of additives on breakdown of transformer oil and liquid paraffin at High Voltage Laboratory, Queen Mary College, London, England.

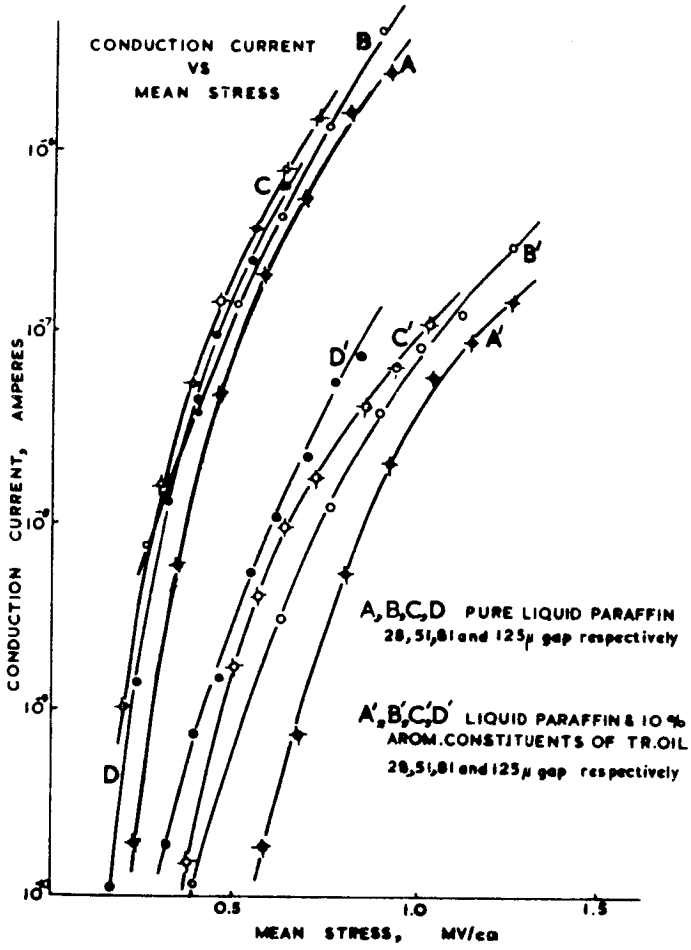

Fig. 1. Current Stress Characteristics of Liquid Paraffin and Liquid Paraffin Containing 10% of Aromatic Constituents of Transformer Oil. Nickel Electrodes. Uniform Field.

For uniform field tests two nickel spheres were used each of 5 mm in diameter. Non-uniform field tests were made with a 5 mm dia sphere opposite a nickel plated fine sewing needle with a point radius of about 16 microns. A Brandenburgh stabilized R. F. unit was used as the dc supply with an output from 0 - 20 kv at a maximum current of 200 microamperes.

Two basic liquids were used in tests, namely: B30 transformer oil supplied by Gulf Oil (Great Britain) Ltd., and liquid paraffin supplied by British Drug House. The choice of additives was suggested by their effects on gassing tendency of insulating oils[1,2] and it was decided to use the following additives: azobenzene, azoxybenzene, diphenyl, benzophenone, benzil, anthracene, 1.4 naphthaquinone and 1.4 anthraquinone. The basic solutions were obtained by filtering the basic liquid through a No. 5 filter and then admixing to it the additive. Typical concentrations were: 4.59×10^{-3} mole/100 g of solvent for azobenzene, azoxybenzene, diphenyl, benzophenone and benzil, - 1.15×10^{-3} mole/100 g of solvent for anthracene and 1.4 naphthaquinone and 1.15×10^{-4} mole/100 g of solvent for 1.4 anthraquinone. The lower concentrations were prepared by mixing a suitable portion of basic solution with filtered transformer oil or liquid paraffin.

The test samples were again filtered through a No. 5 filter and then carefully degassed in the degassing flask of the oil system. During the degassing process the liquid was vigorously stirred by a magnetically driven stirrer.

The test liquid was then "stress conditioned" in the test cell. For the uniform field tests a 125 micron gap was adjusted and the voltage increased to produce a mean stress in the liquid of about 600 kv/cm. For the non-uniform field tests, a 200 micron gap was used and the mean stress was about 400 kv/cm.

III. Test Results

The current was measured reducing the applied voltage from prestressing value and taking readings at each step. The measurements were repeated with increasing voltage by similar steps. The steady conditions for measurements were obtained for stresses as high as 1200 kv/cm for the 28 micron gap.

The test results showed that the effects of additives used depended on: (1) the type of additive and its concentration, (2) the volume of the solution under electrical stress, and (3) the electrical stress for a given gap setting.

Figure 2 shows the conduction current in solutions containing different amounts of additives for the 125 micron gap and an electrical stress of 765 kv/cm. All curves indicate an optimum concentration for a given additive. 1.4 anthraquinone

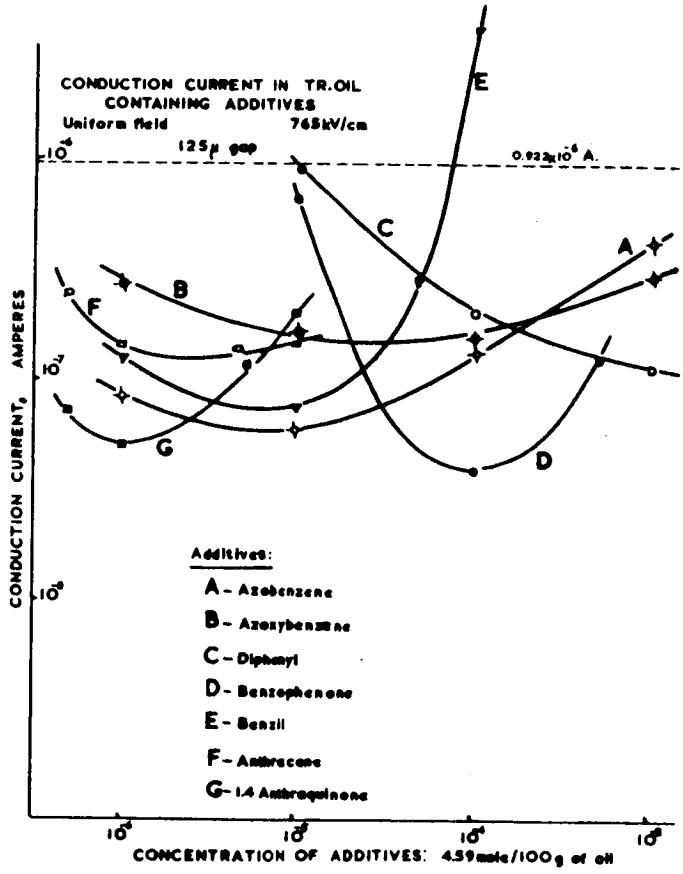

Fig. 2. Conduction Current of Transformer Oil as a Function of Concentration of Additives. Nickel Electrodes. Uniform Field.

was found to be the most effective. For diphenyl the optimum concentration is probably 2.3×10^{-2} mole/100 g of transformer oil. Oxidized compounds, namely, azoxybenzene, benzophenone, and benzil showed two optimum concentrations, one for small gap setting and the other, higher, for larger gaps. Quinones gave the same optimum for all gap settings. Similar results were obtained for azobenzene, diphenyl, and anthracene.

The beneficial effects of all additives used increased with the volume of the solution under electrical stress. This effect was observed with uniform field and non-uniform field configurations. In Figure 3 the characteristics of conduction current of solutions are compared with that of pure transformer oil, for different gap settings, to show the bulk effect of additives.

For the 28 micron gap, the effect of non-oxidized compounds greatly depended on stress, while that of oxidized compounds was less stress dependent. The results obtained for azobenzene and azoxybenzene are shown in Figure 4. On the other hand, their effects were similar for the 125 micron gap and far less stress dependent.

The effect of aromatic constituents on conduction current of liquid paraffin depended also on their concentration. The optimum concentration was found to be 10

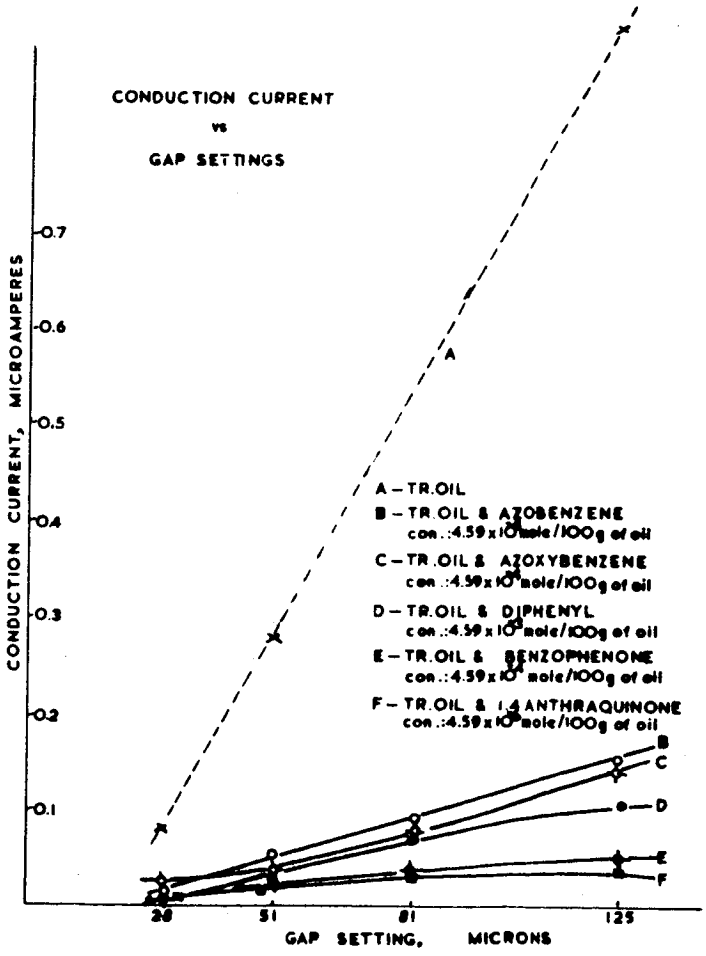

Fig. 3. Conduction Current of Transformer Oil and its Solutions Containing Additives as a Function of Gap Setting. Mean Stress 765 kv/cm. Nickel Electrodes. Uniform Field.

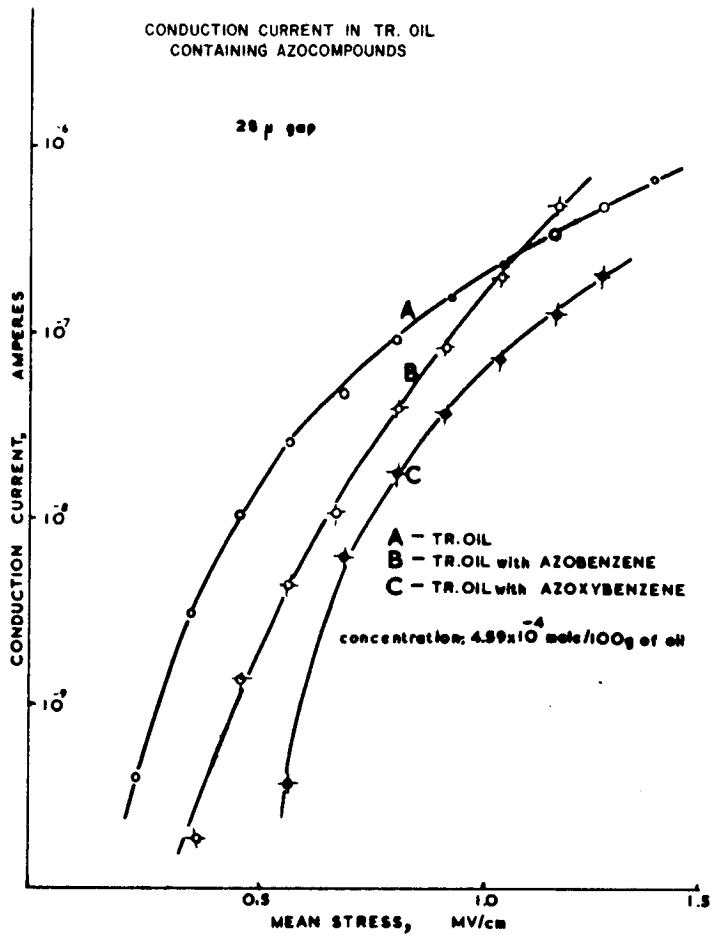

Fig. 4. Conduction Current of Transformer Oil Containing Azocompounds for the 28 Micron Gap Setting. Nickel Electrodes. Uniform Field.

per cent. No harmful effects were observed even with such a high concentration as 33 per cent. For the 28 micron gap the effects depended on stress but for the 125 micron gap the ratio of solution current to that of pure paraffin was practically constant for all the applied stresses.

Cumulative effect of additives was observed in solution of liquid paraffin containing azobenzene and aromatic constituents of transformer oil (5 per cent).

Even minute concentrations of oxidized compounds affected considerably the conduction current for small gap setting but further increase in concentration of the additive did not result in greater change of the current. It probably indicated formation of a protective layer on the electrode surface, which when formed, was not controlled by the amount of the additive in the solution. An interesting fact is that azoxybenzene when present in liquid paraffin considerably affected its current for the 28 micron gap while azobenzene at the same concentration produced no effects. Both additives gave similar reduction of conduction current when the 125 micron gap was tested. In general the effect of azocompounds in liquid paraffin was less pronounced than in transformer oil.

IV. Conclusions

An attempt was made to correlate the effects of additives with their molecular structure and resonance energy of molecule but the information available was not

sufficient for a quantitative statement of such a relationship. The results suggest that the additive having more rigid molecular structure and higher resonance energy is more effective as a stabilizer.

Different effects obtained for oxidized compounds for small gap settings revealed the effect of the condition of the electrode surface on conduction current[3]. For bigger gap settings, with diminishing surface effect the effects of oxidized compounds were similar to that of non-oxidized compounds.

The bulk effect of additives, found in uniform field tests and confirmed by the results obtained with non-uniform field and negative point electrode, probably indicates their electron quenching ability and other action which is somehow restricted and only apparent when larger volumes of liquid are tested.

The pronounced effect of more volatile aromatics in liquid paraffin together with rather small effects of non-volatile hydrogen acceptors in the same liquid strongly suggest the existence of the vapor phase in the stressed liquid. Assuming the presence of the gas or vapor bubbles in the stressed liquid the effectiveness of more volatile aromatics can easily be explained as they can operate inside the bubble, bringing about a number of different effects[4]. The less volatile hydrogen acceptors will mainly be active outside the gas bubble, able only to scavenge the atomic hydrogen escaping from this bubble. Their effect, therefore, should be more pronounced when aromatics are present in the liquid and when the larger volumes of the liquid are under the stress. This was shown by the results for both transformer oil and liquid paraffin.

References

1. Basseches, H. and McLean, D. A., "Gassing of Liquid Dielectrics under Electrical Stress," Ind. Eng. Chem., Vol. 47, 1955.

2. Basseches, H. and Barnes, W. M., "Gassing of Liquid Dielectrics under Electrical Stress," Ind. Eng. Chem., Vol. 5, 1958.

3. Zein Eldine, M. E., Zaky, A. A., Hawley, R., and Cullingford, M. C., "Influence of Electrode Coatings on Space Charge Distribution in Transformer Oil," Nature, Vol. 201, 1964.

4. Frank, J. and Rabinowitsch, E., "Some remarks about Free Radicals and the Photochemistry of Solutions," Trans. Faraday. Soc., Vol. 30, 1934.

ELECTRIC CONDUCTION IN SODIUM CHLORIDE AND SODA-LIME GLASS

J. H. Calderwood, K. C. Kao, and M. F. Pac Soo.

Royal College of Advanced Technology
Salford, England

I. Experimental Techniques

Sodium chloride specimens of about 3 cm diameter were produced by cleaving single crystals grown from analar grade material by the Kyropoulos method, and a flat bottomed recess of about 1 cm diameter was drilled in the center until the thickness was reduced to about 0.1 cm. Both surfaces were polished, and the thickness was measured with a dial gauge micrometer. The specimens were then annealed, the thickness being checked before metal electrodes were deposited by evaporation in vacuum.

The glass specimens were in the form of discs of about 5 cm diameter. After the thickness measurement with the micrometer, they were cleaned in boiling trichlorethylene and dried in an oven before electrodes were deposited as for NaCl.

The dc supply was an electrostatic generator, with output stable to 1 part in 10^5. Voltage was measured with a calibrated micrometer in series with a high stability resistor chain of 200 megohms. Conduction current was determined by the voltage drop across a known high stability resistance, measured with a Vibron electrometer, a guard ring technique being used for all specimens. All leads were shielded and measurements were carried out in a double screened room.

Figure 1 shows the electrode system inside its glass cell. To ensure good contact the lower hollow brass electrode was spring loaded, providing a force of about 150 grams weight on the specimens. The guarded and guard electrodes were separated by a concentric P.T.F.E. ring. A platinum wire in contact with the end of the upper hollow brass electrode was used to measure specimen temperature. For low temperatures, the test cell was immersed in a Dewar flask, the specimen temperature being controlled by adjustment of gas flow between the double glass walls of the cell: solid CO_2 and liquid nitrogen were used as coolant. For high temperatures, the test cell was placed in a thermostatically controlled bath with castor oil as heating medium. Before each test the cell was evacuated for half an hour, and was then flushed out several times, filled and sealed with dry nitrogen at atmospheric pressure.

II. Experimental Results

For sodium chloride crystals, although the general characteristics were reproducible, the absolute value of conduction current measured under the same experimental conditions varied from specimen to specimen, while for glass similar tests yielded identical results within the limits of experimental error. Although each test was repeated at least three times with different specimens, the results reported refer to a typical specimen.

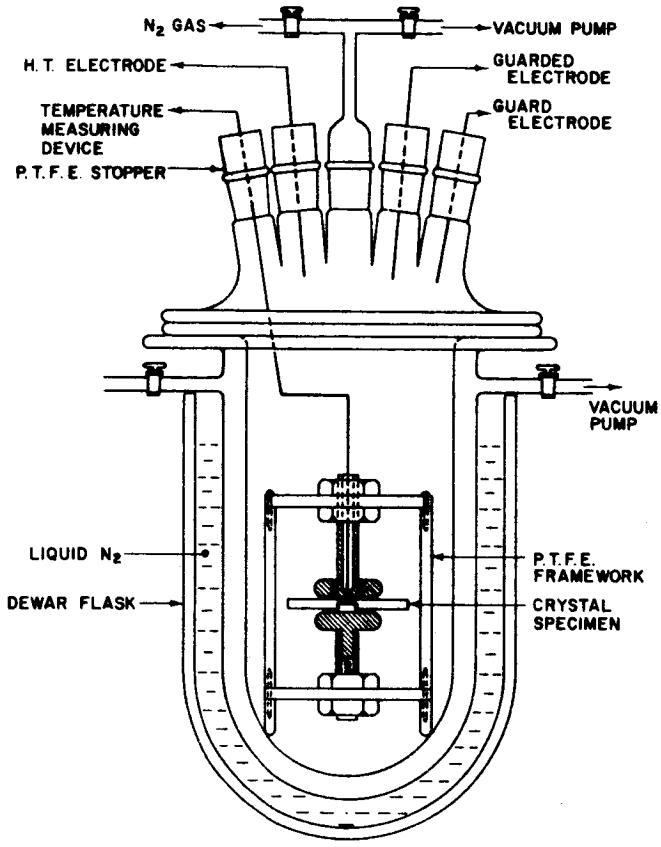

Fig. 1. Test Cell and Electrode System.

The fields were applied in ascending order of magnitude for all specimens, and the steady value reached for a given field was recorded as the conduction current for that field. The time required for the current to reach a steady value when a field is applied, and for it to decay to zero when the source was replaced by a short circuit, depends on temperature and applied field strength as shown in Figures 2 and 3, on which J_F and J_I represent final steady current and initial current respectively.

For glass it was observed that if, after it had reached a steady value, the current was interrupted for a short period, say 5 minutes, it quite quickly reached its former value when the voltage was restored. If, however, the specimen, after being electrically stressed for a substantial period, say 6 hours, were then left unstressed overnight, say 16 hours, it then showed a lower conductivity. This effect depends also on the electrode material, as shown in Figure 4. To avoid misinterpretation, only the results from the first series of tests are quoted in Figures 3, 5, and 6.

Figure 5 shows the effect of thickness of the glass specimens on conduction current for two electrode materials. Figure 6 shows the variation of conduction current with temperature for NaCl and glass for two different fields for temperatures from 140°C down to -90°C.

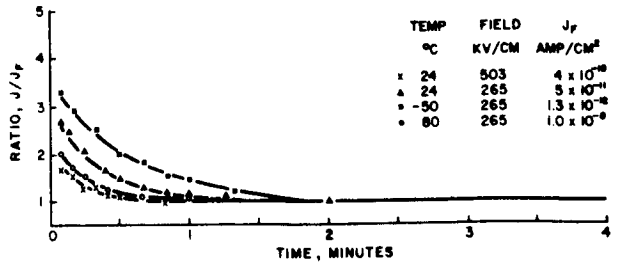

(a) AFTER APPLICATION OF D.C. FIELD
(Aluminium Electrodes)

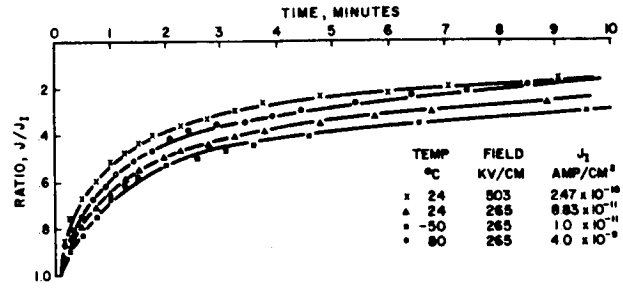

(b) AFTER REPLACEMENT OF D.C. SOURCE WITH SHORT CIRCUIT
(Aluminium Electrodes)

Fig. 2. Variation of Conduction Current of Sodium Chloride Crystal with Time.

III. Discussion

There is sufficient experimental evidence[1,2] that in glass the charge carriers are predominantly ionic, the current density being given by

$$J = \nu n e d \exp\left(-\frac{\phi}{kT}\right) 2 \sinh\left(\frac{edE}{2kT}\right) \qquad (1)$$

where d is the distance between interstitial sites, and other symbols have their usual meaning. For both glass and NaCl, the time effects of Figures 2 and 3 are so long that it seems unlikely that they are caused by displacements of an elastic nature. For glass, it has been established that Na^+ ions accumulate near the cathode and are deficient near the anode causing space charge polarization. For alkali halides, the decay has been attributed both to the formation of space charge caused by the trapping of conduction electrons at singularities by von Hippel[3] and to the electrical removal of impurities with low activation energy by Afanaseva, Vinogradov, and Konorova[4]. Konorova[5] reports that for KBr, pulse measurements can yield current values 10^5 or 10^6 times greater than steady state currents, and that the former have a field dependence satisfying the field emission equation, which is not the case for the latter. This provides further evidence of space charge effect, as does the observation that for both glass and NaCl reversing the polarity of the applied field gives rise to a great increase in initial current. It would be expected that the time required for space charge processes to reach dynamic equilibrium would decrease with increasing field or

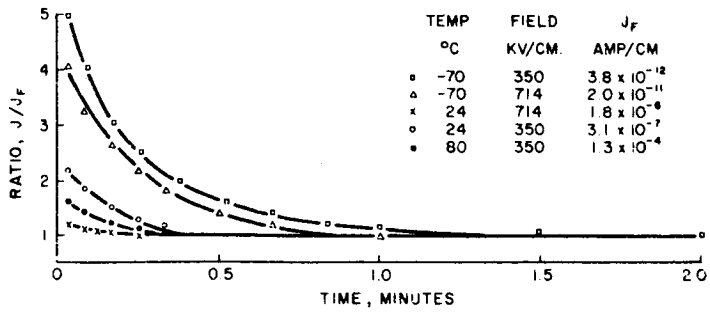

(a) AFTER APPLICATION OF D.C. FIELD
(Aluminium Electrodes)

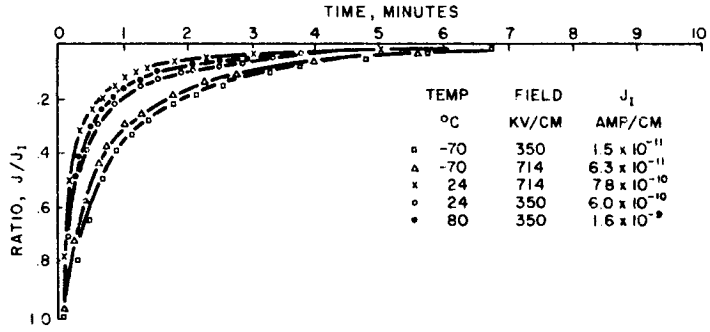

(b) AFTER REPLACEMENT OF D.C. SOURCE WITH SHORT CIRCUIT
(Aluminium Electrodes)

Fig. 3. Variation of Conduction Current of Glass with Time.

temperature as both cause faster charge movement. The time required for charging should be less than for discharging, as the latter process in the absence of applied field depends mainly on diffusion rate.

The potential distribution between electrodes depends on applied field, thickness of specimen, and dissociation and recombination rates[6]. It is possible that for the same applied field, the thicker the specimen the greater the trapped space charge and so the greater the field distortion. In fact, current decrease for increasing thickness was noted for glass (Figure 5).

The current in glass also depends on electrode material (Figure 4). Silver electrodes give higher conduction currents than copper or aluminum, possibly because the univalent Ag^+ ion can migrate into glass more easily to replace the univalent Na^+ ion. The prestressing effect (Figure 4) is likely to be caused by irreversible changes in the polarization layer.

For both glass and NaCl the relationship of ln J vs $\frac{1}{T}$ fall into two distinct regions as shown in Figure 6. The low temperature activation energy is probably associated with structure sensitive properties, which at the higher temperatures become dominated by the bulk properties of the specimens. The potential barriers, which would be expected to decrease with increasing applied field, are calculated to be:

Material	Electric Field kv/cm	High Temp. eV	Low Temp. eV
Glass	350	0.97	0.41
	714	0.89	0.32
NaCl	265	0.80	0.30
	503	0.79	0.27

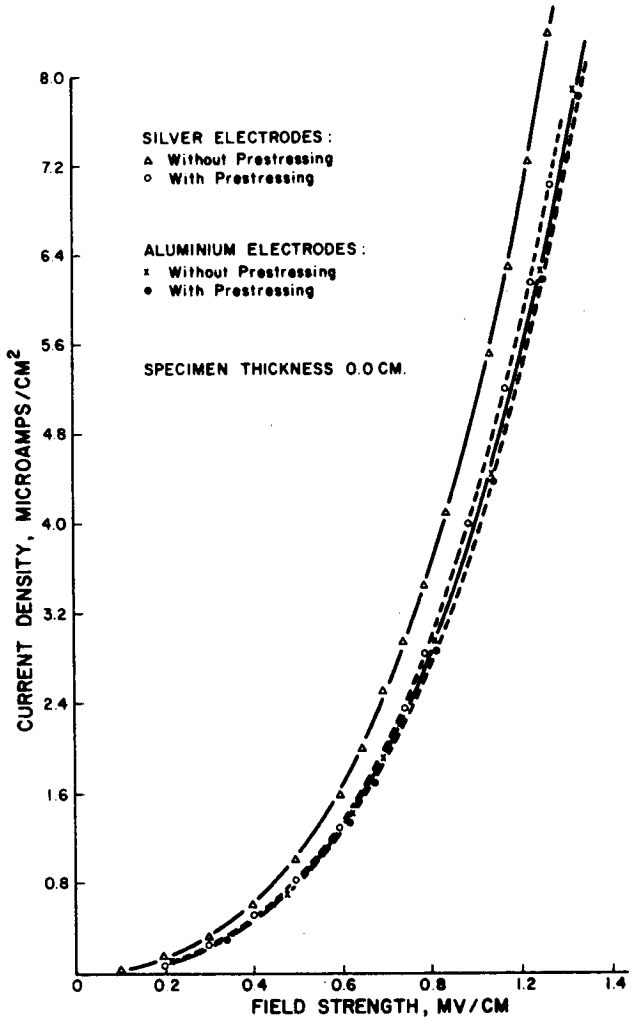

Fig. 4. The Effects of Electrode Material and Electrical Prestressing on Conduction in Glass.

On the basis of the 350 kv/cm curve for glass, the curve for 714 kv/cm calculated according to equation (1) is in good agreement with the experimental one, supporting the view that conduction in glass is ionic. On the basis of the 265 kv/cm curve for NaCl, the calculated curve for 503 kv/cm is much lower than the experimental one (Figure 6), indicating that high field conduction in NaCl is partly electronic, possibly due to field emission from the cathode[5]. The effective field at the cathode may be much higher than the average field owing to electrode surface irregularities and possible layer effect, thus assisting electron emission.

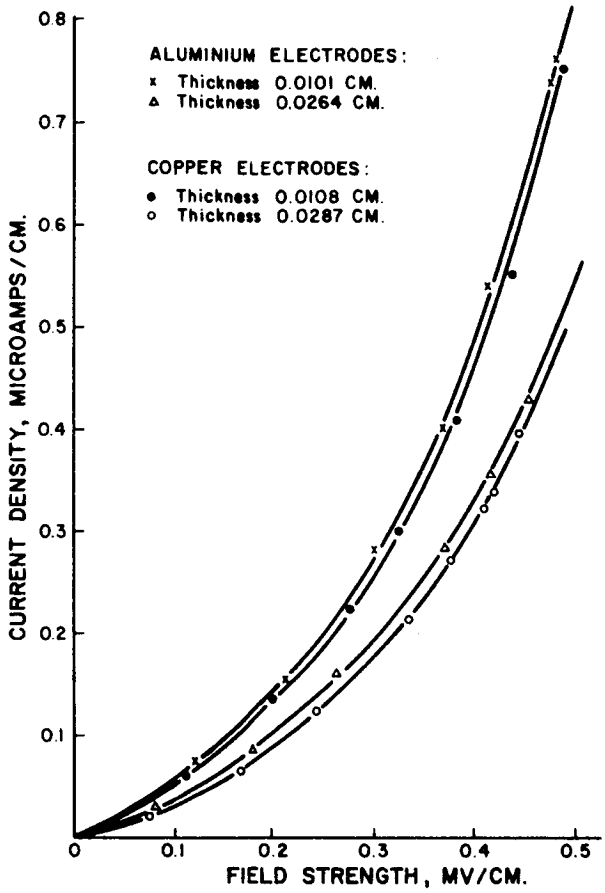

Fig. 5. The Effect of Thickness on Conduction in Glass.

References

1. Vermeer, J., Physica, Vol. 22, p. 1257, 1956.

2. Sutton, P. M., Progress in Dielectrics (Heywood), Vol. 2, p. 115, 1960.

3. von Hippel, A., Physical Review, Vol. 54, p. 1096, 1938.

4. Afanaseva, E. A., Vinogradov, V. S., and Konorova, E. A., The Bulletin of the Academy of Sciences of U.S.S.R., Vol. 24, No. 1, p. 66, 1960.

5. Konorova, E. A., The Bulletin of the Academy of Sciences of U.S.S.R., Vol. 24, No. 1, p. 58, 1960.

6. Proctor, T. M. and Sutton, P. M., Journal of Chemical Physics, Vol. 30, p. 212, 1959.

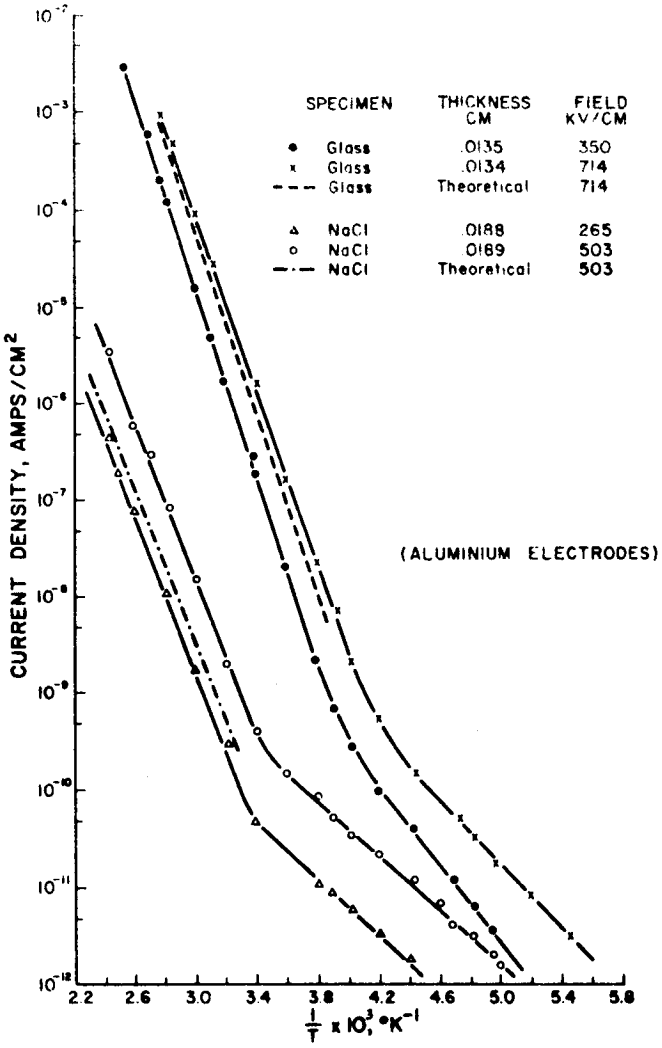

Fig. 6. Variation of Current Density of Glass and Sodium Chloride Crystal with Temperature.

DIRECT-CURRENT CONDUCTIVITY OF POLYETHYLENE AT HIGH FIELD-STRENGTHS

Günther Stetter

Technische Hochschule Munchen
Munich, Germany

The radiation induced conductivity of polyethylene has been studied quite thoroughly, mostly under field-strengths below 10^4 V/cm[1,2,3,4]. These measurements concern the direct current conductivity without irradiation at field-strengths up to 10^6 V/cm.

Measurements were made with various commercial polyethylene foils. The results reported refer to a linear low pressure polyethylene which has a relatively high conductivity and which showed the described effects particularly well. The electrodes were either evaporated tin layers or mercury electrodes.

The curves in Figure 1 show the current through a 50 μ sample with mercury electrodes as a function of the reciprocal absolute temperature. The temperature was steadily increased from room temperature to 115° C with a constant gradient of 10° per hour. The sample was connected to the source throughout the experiment.

The field strength dependence of the conductivity of polyethylene was also studied thoroughly under various conditions. Figure 2 shows the current as a function of voltage in a logarithmic scale for three temperatures. The values were measured 20 minutes after applying the voltage to a 50 μ sample with evaporated tin electrodes in high vacuum. One can see that in both cases the slope of the curves diminishes at high current densities, so that the behavior is no longer governed by equations (1) and (2). We assume that this kind of saturation is probably caused by space charge polarization near the electrodes. This becomes clearer by studying the current as a function of time.

In the normal conductance phenomenon in polyethylene immediately after connecting the sample with the voltage source, there is the exponential decrease of current due to the dielectric polarization of the material. After this, at room temperatures and low field strengths, the current does not change into a constant conductance current but continues to decrease according to $i \sim t^{-n}$ (t = time, $n \approx 1$) for a certain period of time until it finally reaches an asymptotic value.

This current is certainly also a polarization current since it reappears with opposite sign when the electrodes are short-circuited.

According to recent investigations it is connected with dipole orientation[5,6]. The behavior was principally described by Wagner[7] as early as 1923 and has been found with many high polymers[8].

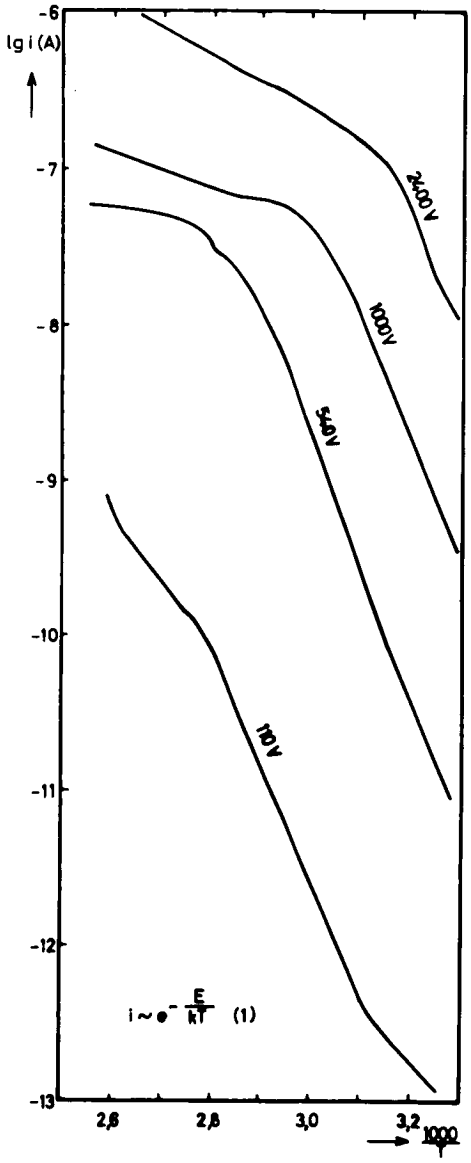

Fig. 1

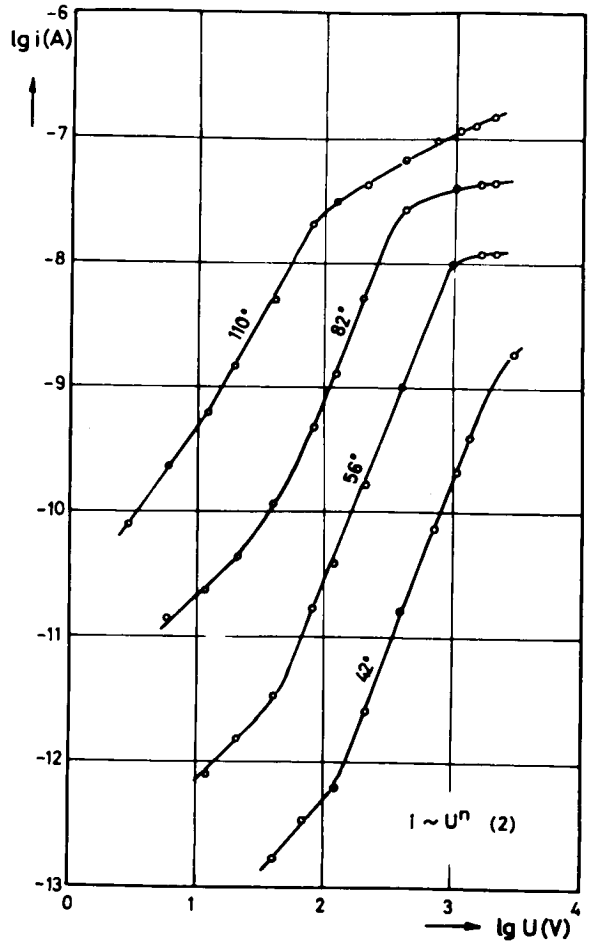

Fig. 2

With such behavior it is difficult to define any definite conductivity. According to German DIN standards the current is to be measured after 60 seconds while in the scientific literature the asymptotic value of the current is used almost universally.

Figure 3 shows the current as a function of time with the voltage as a parameter at 82° under the same conditions as in Figure 2. The measurements were carried out in high vacuum with tin electrodes. In this logarithmic diagram one can observe that the asymptotic value is only a fiction. The current is not constant over a longer period of time, but rather increases slightly with time (122 and 206 V). This increase lasts for a considerable time at moderate field strengths and is not very large. With increased voltage or temperature, that is, with increased current

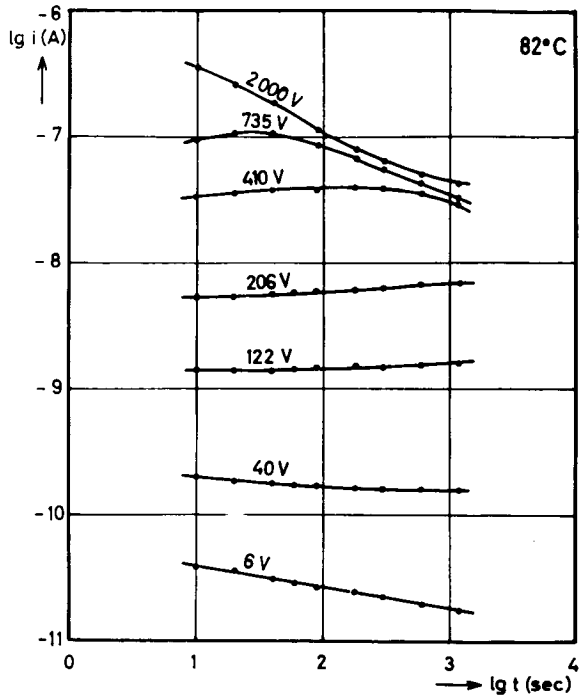

Fig. 3

density, the time scale is virtually compressed so that the current reaches a maximum within the interval of observation and a new distinct decrease of current becomes visible.

The fact that this behavior is well reproducible has been shown by measurements in a room atmosphere and with mercury instead of tin electrodes.

A comparison of the various measurements which were made shows two characteristic phenomena: Equal time dependence appears at equal current densities, no matter whether they are due to high voltage or high temperature. Furthermore, the maximal current or beginning of the second decrease occurs after the passage of approximately equal charges in the measuring circuit. This also explains why the current voltage curve seems to saturate in observations after a fixed time - as in Figure 1 on field-strength dependence. If one constructs a current voltage plot from the maximal values of the current versus time plots - that is for corresponding physical states of the sample, as we think - one obtains no deviation from the E^n behavior in the range of voltage studied and also no deviation from the exponential temperature dependence.

Finally, we shall sketch an observation which seems to be connected with the second decrease of the current with time. It concerns the transient currents which flow when the electrodes of the sample are short-circuited after application of the voltage. When the voltage and temperature were too low for the current to reach its second decrease, this back current is normal; that is, it diminishes according to t^{-n}. However, if the primary current had passed its relative maximum, this picture changes. The back current diminishes much faster and intersects the curves for lower voltages. It may even happen that the back current changes its sign. Then the discharge current has the same direction as the charging current.

Figure 4 illustrates such anomalous back currents. For the lowest field-strength E_1 and E_2 the back current is normal. The curve for E_3 has already intersected the E_2 curve, but retains its direction. The curves representing the discharge current after the application of the field strengths E_4 to E_6 show the passage to the anomalous direction, which happens sooner and sooner.

We conjecture that the second decrease of the charge current is caused by the build-up of space charge and thus a decrease of the effective field strength

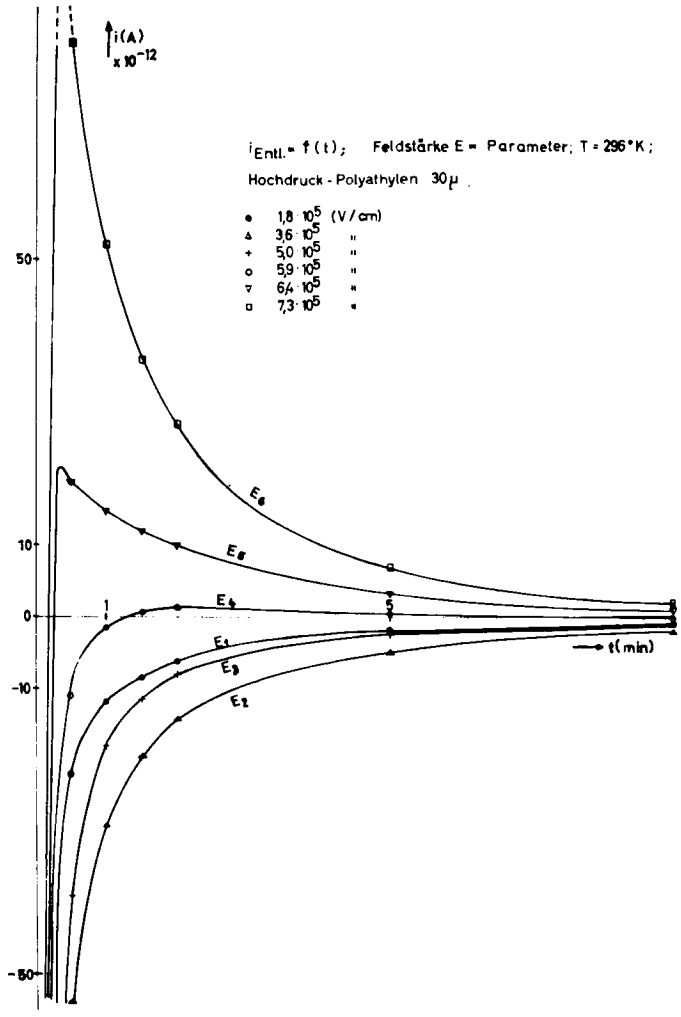

Fig. 4

throughout the sample, as other explanations for the inversion of the back current but strong field distortions are hardly conceivable. Furthermore, it has been proven that the currents at high field-strengths or temperature are nearly independent of sample thickness. This suggests that the space charges are located near the electrodes.

Since we believe that the back current inversion may supply further insight into the mechanism of conduction within polyethylene and other high polymers, further investigations of this phenomenon are in progress.

References

1. Ramsey, N. W., Nature 172, 214 (1953).
2. Fowler, J. F., Proc. Roy. Soc. A236, 464 (1956).
3. Meyer, R. A., J. Appl. Phys. 27, 1012-18 (1956).
4. Wintle, H. J., Polym. 2, 444 (1961).
5. Herwig, H. V. and Jenckel, E., Ztschr. f. Chem. 63, 360 (1959).
6. Sozin, B. I., Kunststoffe, Moskau, Nr. 6, 4 (1961).
7. Wagner, K. W., Ann. Phys. 40, 817 (1913).
8. Munick, R. J., J. Appl. Phys. 27, 114 (1956).

IRRADIATION OF POLYETHYLENE AND ELECTRICAL CONDUCTIVITY
THE BEHAVIOR OF CARRIER TRAPS IN POLYETHYLENE UNDER GAMMA-RAY IRRADIATION

Kichinosuke Yahagi and Kenichi Shinohara

Waseda University
Tokyo, Japan

The Institute of Physical and Chemical Research
Tokyo, Japan

As one of the studies of irradiated effect on polymer insulator, a study of electrical conductivity under irradiation of gamma-ray is important in researching of conduction mechanism and its technical application. It was already shown by Fowler[3] and others[4] that the induced current increased in two or three orders of magnitude under irradiation but the kind of traps or trapping process of charge carriers were scarcely referred to in their papers.

At this conference, we are going to report the trapping process of induced conductivity and the kinds of traps in polyethylene.

The films of Sumikathene (low-density polyethylene) and Marlex (high-density polyethylene) (each thickness 0.5 mm) were coated with silver paint in the form of collecting electrode and a guard ring. High energy electrons from a Van de Graaff generator were irradiated intermittently on these which were put on an Al boat floated on a liquid nitrogen bath. Total irradiated dose was about 3×10^8 rads. After electron beam irradiation, the films were applied by dc voltage 90 v from a battery and then gradually warmed at the rate of 2 or 3 °/min. The conduction currents were rapidly increased in corresponding temperature ranges shown in Figure 1. The conduction current never showed a peak value on the specimen on which its peak was detected previously by warming and again cooled down to 77°K. Charge carriers, generated by irradiation and frozen at 77°K, might be liberated with warming. Ions as charge carriers, if it may be possible, are impurities in specimen and ionized monomers,etc. Whether the charge carriers may be electrons or ions, those increases of conduction current in two or three orders of magnitude seem to be accompanied with the molecular motions of polyethylene. As one of the similar phenomena, there is an observation of ESR spectrum of irradiated polyethylene which means the investigation of free radicals generated. Lawton and others[1] show the change of free radicals generated by irradiation at 77°K and measured at 77°K with ESR spectrum in which specimen was warming up to an arbitrary temperature and cooling down to 77°K. This change of free radicals with temperature may be accompanied with molecular motions. The three decay ranges may be found in this characteristic. One of them found at about 140°K seems to be in this characteristic. One of them found at about 140°K seems to be corresponding to γ dispersion of molecular motion, second region of decay at about 200°K may be explained by Lawton as a result of the oscillation in imperfect crystalline region, and third

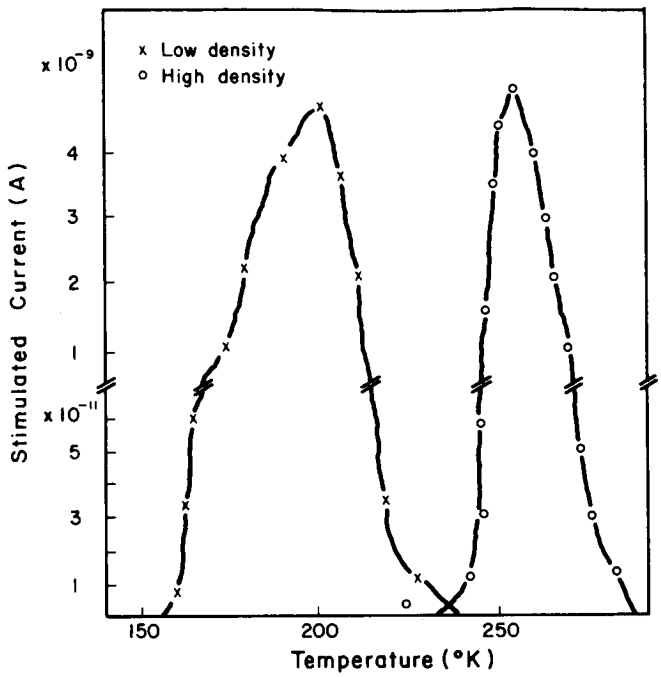

Fig. 1. Stimulated Current in Polyethylene After Irradiation of High Energy Electron ($3x10^8$ rads).

region of decay at about 250°K will correspond to segmental motions of main chains in amorphous region. It may be considered that both decay of radicals and the increase of currents appeared as a result of same molecular motions. For example, in Sumikathene (low-density polyethylene), the rapid increase of conduction current was observed in the corresponding range at about 200°K as shown in Figure 1. Corresponding to the decay region at about 200°K, the peak value of conduction current in Marlex (high-density polyethylene) is observed as in Figure 1.

In these phenomena, it may be considered that the trapping sites of charge carriers are produced in imperfect crystalline regions or in pseudo-crystalline region between crystalline part and amorphous part. In low-density polyethylene, traps may be shallow ones produced in imperfect crystalline region in addition to impurities in specimen. Therefore, most charge carriers may be liberated by the oscillation of imperfect crystalline region at about 200°K as mentioned above. In high-density polyethylene, since traps may be deeply in pseudo-crystalline region as well as in imperfect crystalline region, charge carriers may be liberated with segmental motions of main chains in amorphous regions at about 250°K. Tal'roze[2] showed the similar behavior in a paraffin crystal; conduction currents rapidly increase with increasing temperature after irradiation at 77°K. He suggested the behavior may have appeared as a result of annihilation or radicals, because radicals are just decaying at the temperature showing peak conduction currents. In polyethylene, above consideration is also possible enough, because the energy of radical annihilation is about 4 eV but the average energy level of traps is about 1.5 eV. In addition, the oxidation of radicals would occur in this specimen irradiated in air.

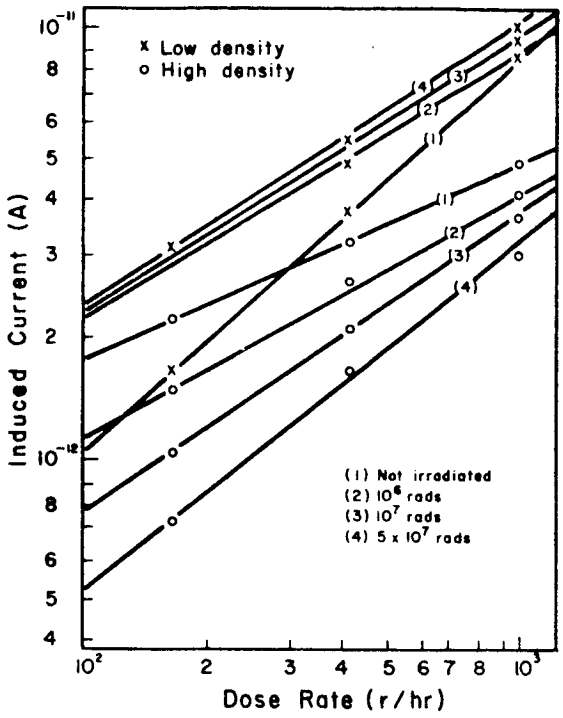

Fig. 2. Dose Rate Dependence of Induced Current in Polyethylene after Irradiation of Electron Beam.

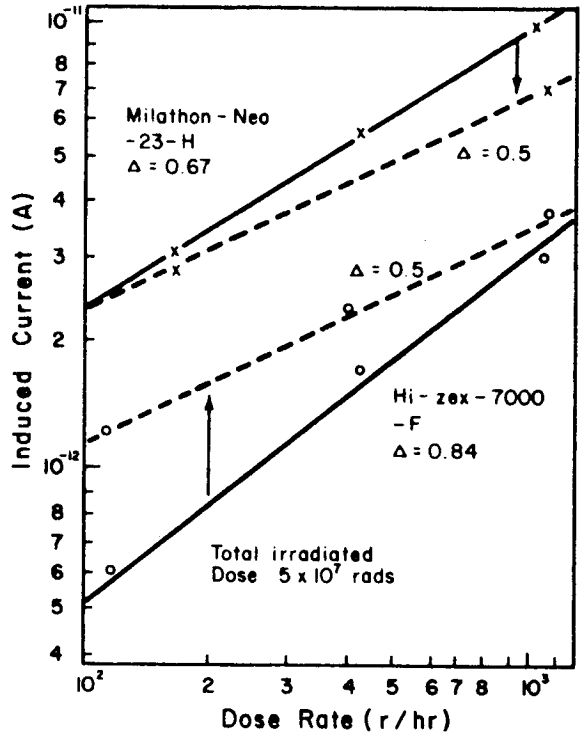

Fig. 3. The Effect of Thermal Treatment of Induced Current in Polyethylene Under Irradiation of Gamma-ray.

Generally, it is considered that in low-density polyethylene shallow traps may be produced by irradiation, but deep traps produced in high-density polyethylene. Whether traps are shallowly distributed or deeply distributed could be examined with plotting the relation of (induced current) α (dose rate)$^{\Delta}$ under irradiation of gamma-ray. Figure 2 shows the dose rate dependence of induced current under gamma-ray irradiation after electron beam irradiation. These experiments were always carried out under vacuum and room temperature conditions. In Hi-zex, value of Δ increased with dose of electron beam irradiation, but in Milathon it became about one half. From these experiments, it would be seen that deep traps are produced in high-density polyethylene and shallow traps produced in low-density ones. Figure 3 shows also the change of dose rate dependence of induced current due to heat treatment. Full line shows the dependence of the Hi-zex film irradiated to the dose of 5×10^7 rads and the dushed line, the dependence of the same sample after it was heated to 130°C in vacuum and cooled slowly to room temperature. The value of Δ changed from 0.85 to 0.5 and the magnitude of the induced current increased. Similar behavior was observed also in the samples irradiated to 10^6 and 10^7 rads. The above phenomena may be explained if it is postulated that some kind of carrier traps (electron traps), to be destroyed by that heat treatment, may be produced by high energy electron irradiation. One of them may be allyl type radicals. These radicals produced in polyethylene by irradiation are known to be quite stable at room temperature. It is shown that some

allyl radicals possess positive electron affinity of +0.24 eV(cal.) or +2.1 eV(obs.)[5]. If allyl type radicals produced in polyethylene have positive electron affinity, they may serve as electron traps.

References

1. Lawton, E. J., et al., J. Chem. Phys., 33, 395 (1960). Kasiwabara, H., Rept. Prog. Polym. Phys. Japan., 5, 283 (1962).
2. Tal'roze, V. L. and Frankevich, E. L., Dokl. Akad. Nauk. S.S.S.R., 129, 858 (1959).
3. Fowler, J. F., Proc. Roy. Soc., A236, 464 (1956).
4. Yahagi, K. and Danno, A., J. Appl. Phys., 31, 734 (1960); Yahagi, K. and Danno, A., J. Appl. Phys., 34, 804 (1963).
5. Hush, N. S. and Pople, J. A., Trans. Faraday Soc., 51, 600 (1955).

EFFECT OF HIGH-ENERGY RADIATION ON ELECTRIC CONDUCTION OF POLYETHYLENE

M. Ieda, M. Kosaki, Y. Yamada, and U. Shinohara

Nagoya University
Nagoya, Japan

I. Introduction

Although a number of investigations of the effect of ionizing radiation on physical properties of polymeric materials have been carried out, only a few investigations have been reported on the electric conduction in polymers after irradiation[1]. In this study, measurements on the electric conduction of polyethylene (PE) and other crystalline polymers after exposure to high-energy radiation fields have been made.

In the previous paper[2], the authors pointed out that a peculiar phenomenon appears in the volume resistivity (ρ) - temperature (T) characteristics of irradiated PE. In order to clarify the electric conduction, including these peculiar phenomena for the irradiated PE, experiments have been carried out concerning the effect of the kind of radiation source, the degree of crystallinity in PE, the size of the radiation dose and the atmospheric conditions under irradiation.

II. Experimental Results and Discussion

Several kinds of PE different in density of about 0.5 mm thickness were irradiated by gamma-rays from Cobalt 60 or high-energy electrons (2 Mev) in air or in vacuum with various radiation doses. All measurements of the electric current across specimens were made in air, after taking specimens out of the radiation field, over the temperature range 20 $\sim$ 170°C. The magnitude of the current was taken to be the current observed about 10 minutes after the voltage application of 97 volts.

Figure 1 shows (ρ - 1/T) characteristics of the low density PE (DYNH-3) irradiated by gamma-rays in air. At room temperature ρ of the irradiated PE decreases with increasing radiation dose and the (log ρ - 1/T) curve gives a linear relation below 60°C. Above 60°C, the decrease of ρ with temperature is less rapid until a rapid increase of ρ appears near the melting point of the crystalline parts (m.p., 110°C for DYNH-3); the authors call it "a jumping phenomenon of ρ." This phenomenon is clearly observed in the PE irradiated with a radiation dose of more than $10^3 \sim 10^4$ rad.

Figure 2 gives a result on the high density PE (Marlex 50) irradiated by electrons in air. As shown in the figure, the jumping phenomenon of ρ appears, but the (ρ - 1/T) curve differs a little from what is obtained for the low density one mentioned above. That is, (log ρ - 1/T) relation satisfies a clear linearity over a comparatively wide range of the temperature up to near the m.p. (137°C for Marlex 50) and the rapid increase of ρ occurs within a narrow temperature range. These tendencies are also observed in gamma-ray irradiated Marlex 50. However, it should be noted that

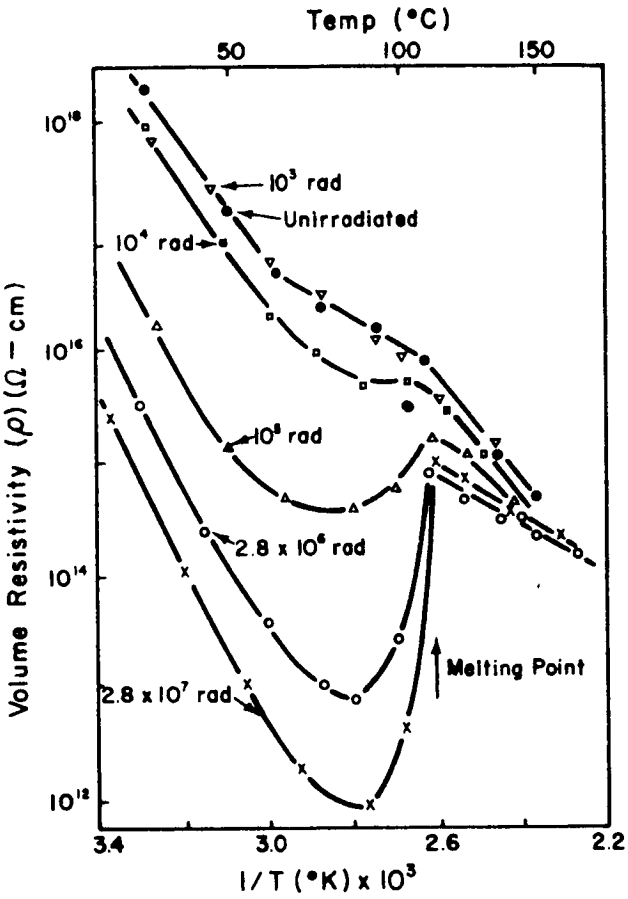

Fig. 1. Temperature Dependence of Volume Resistivity of Gamma-ray Irradiated Low Density Polyethylene (DYNH-3).

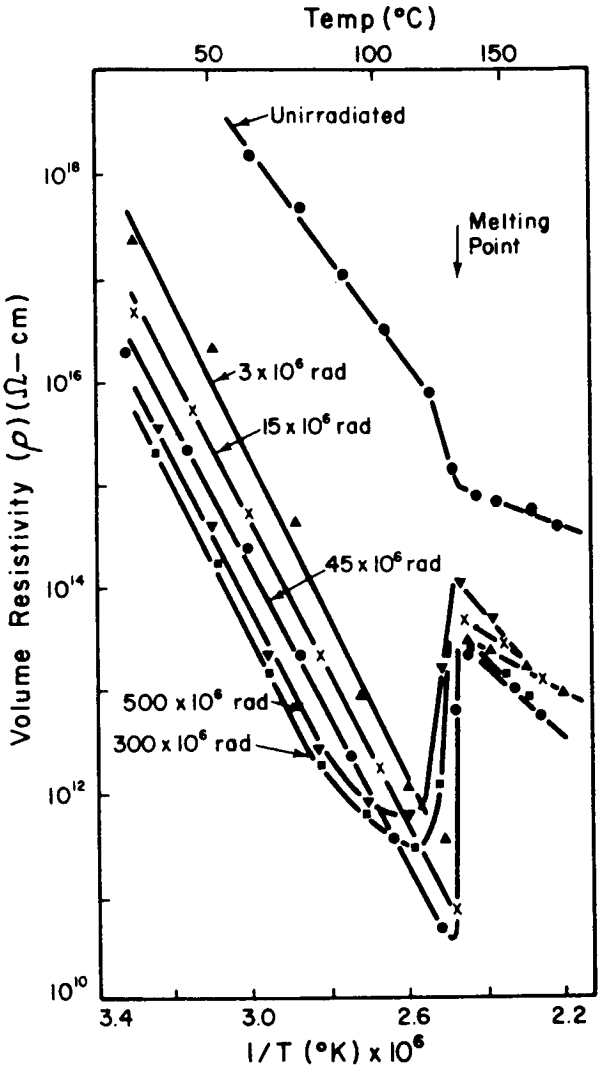

Fig. 2. Temperature Dependence of Volume Resistivity of Electron Irradiated High Density Polyethylene (Marlex-50).

the jumping phenomena observed in specimens irradiated with the large dose of $(3 \sim 5) \times 10^8$ rad, which seems to cause some degradation of the crystalline regions[3], occur within a little wider temperature range than those in specimens with rather small radiation doses. They resemble those of the irradiated low density PE. (See Figure 1 and Figure 2).

On the other hand, M. G. Gubler and A. J. Kovacks[4] indicated that the melting of crystalline parts in a low density PE is observed over a wide temperature range, although the most of the melting occurs at a so-called melting point, while in a high density PE melting occurs over a narrow temperature range. From the comparison of these results with ours, it seems that the appearance of the jumping phenomenon is similar to that of the change of crystallinity with temperature. From these considerations and the experimental results, it is suggested that the jumping phenomena of ρ are

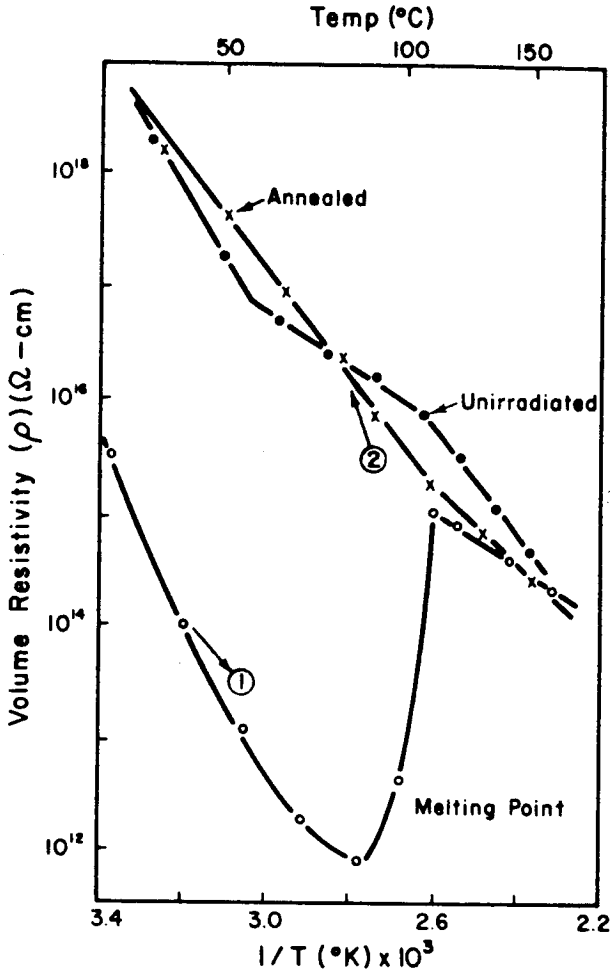

Fig. 3. Effect of Annealing on Temperature Dependence of Volume Resistivity of Gamma-ray Irradiated DYNH-3 with 2.8×10^7 rad. Curve 1 Corresponds to the First Heating Process. Curve 2 Corresponds to the Cooling Process.

closely connected with the melting of crystalline region. The $(\rho - 1/T)$ characteristics of $(3 \sim 5) \times 10^8$ rad irradiated Marlex 50 may be explained by the consideration that some melting occurs below the m.p. due to degradation of crystallinity caused by large radiation doses.

The $(\rho - 1/T)$ characteristics of the irradiated specimen heated once above the m.p. are different from those obtained in the first heating process and the jumping phenomenon never appears. This result is shown in Figure 3. Moreover, the decreased ρ and the increased activation energy induced by irradiation are almost recovered to those of the unirradiated material. However, if the heating of the irradiated sample is stopped at a temperature below the m.p., subsequent cooling and reheating will give almost the same $(\rho - 1/T)$ curve as the first heating process. These facts also support the existence of the close relation between the jumping phenomenon and the melting of crystalline region in PE.

Within a temperature range, where little melting has taken place, values of the activation energy for electric conduction of unirradiated DYNH-3 and Marlex 50 are both about 24 kcal/mol and those of irradiated samples are $30 \sim 35$ kcal/mol independent of the radiation dose. That is, the temperature dependence of electric conduction may not be dependent on the difference of crystallinity in PE, unless the crystallinity is changed with increasing temperature.

Moreover, the so-called "cleaning up phenomenon of charge carriers" was observed; the decreased ρ caused by irradiation will show some degree of recovery due to the application of a high electric field across the specimen which means a large number of electric charges passing through the specimen.

In Figure 4, the $(\rho - 1/T)$ characteristics of Marlex 50 irradiated by the gamma-rays in vacuum are shown. The jumping phenomenon is also observed as in air. The atmospheric condition under irradiation seems to have little effect on the jumping phenomenon.

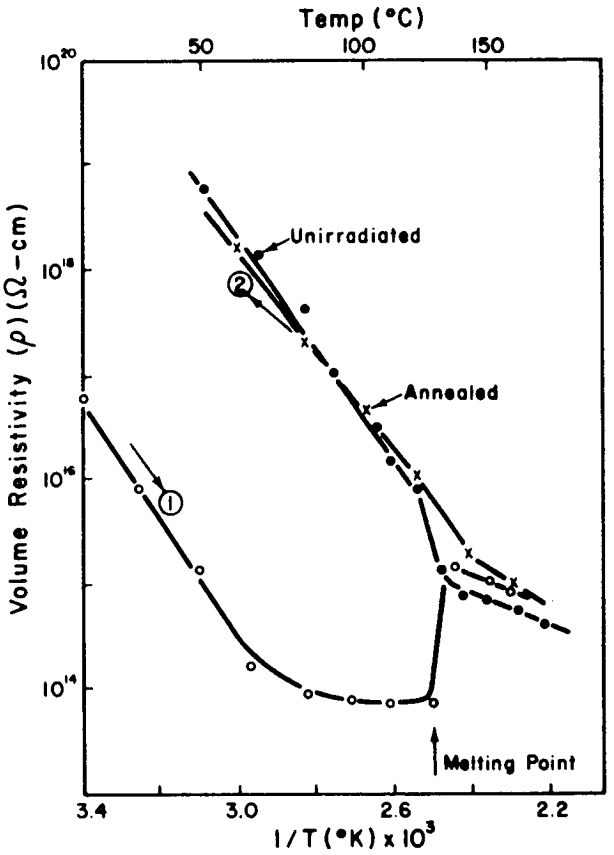

Fig. 4. Temperature Dependence of Volume Resistivity of High Density Polyethylene (Marlex-50) Irradiated in Vacuum with 5×10^6 rad Gamma-ray.

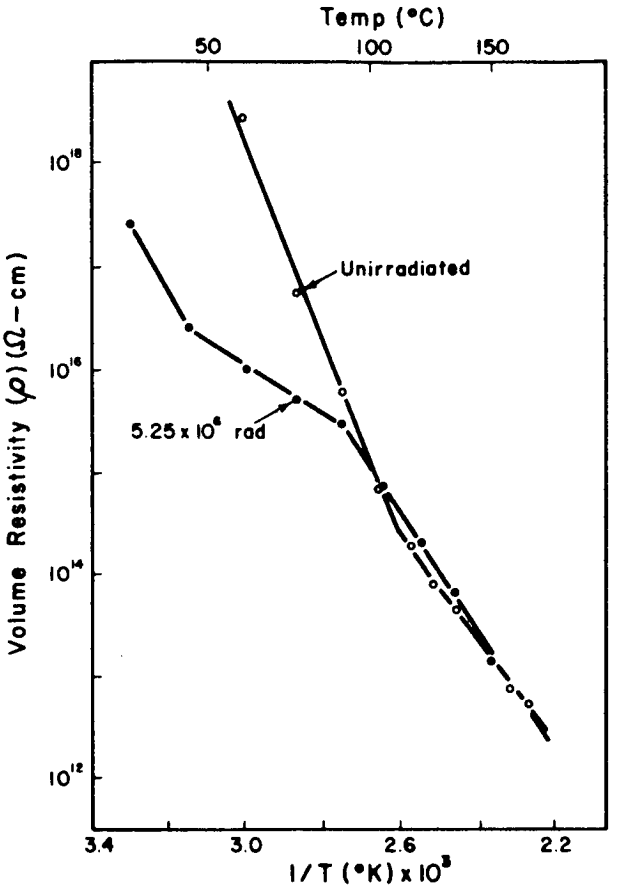

Fig. 5. Temperature Dependence of Volume Resistivity of Gamma-ray Irradiated Polypropylene.

Figure 5 gives the variation of ρ as a function of $1/T$ in a polypropylene (PP), which is said to be degraded by irradiation. Near room temperature, ρ of irradiated PP is decreased and the value of the activation energy is almost unchanged. The variation of ρ with temperature changes at about 50°C and the (ρ - $1/T$) characteristics above 100°C almost agree with that of unirradiated sample. No peculiar phenomenon is observed near m.p. (165 ~ 170°C) as was true for irradiated PE. When irradiated PP is heated above 100°C, which is far below m.p., its (ρ - $1/T$) characteristic is the same as that of unirradiated PP.

From the various experimental results for the irradiated PE, it may be suggested that a large number of charge carriers created in amorphous parts by ionizing radiation recombine within a very short time after irradiation because of rather free molecular motion in amorphous parts, while those created in crystalline region recombine slowly even after irradiation because in crystalline region the charge carriers and the vacant points which act as recombination centers are not able to move easily.

Those charge carriers are captured by the trapping centers, which are to be on the surface of crystalline parts, and their thermal release contributes to the electric conduction of the irradiated PE. The jumping phenomenon of σ may be explained by the disappearance of charge carriers due to the recombination with the vacant points associated with the melting of crystalline region. Crosslinks produced in PE may not be an important decisive factor controlling its electric conduction and, qualitatively, the phenomena mentioned above may be explained by ionic conduction.

From the behavior of the electric conduction in the irradiated PP, it may be deduced that, the recombination process can occur before the melting of crystalline region if irradiation causes degradation.

Finally, it is concluded that the crystalline region plays an important role in the electric conduction of irradiated crystalline polymers. Further investigations concerned with the chemical nature of trapping centers and quantitative considerations are now in progress.

III. Acknowledgments

The authors wish to express their thanks to The Japan Atomic Research Institute, The Government Industrial Research Institute of Nagoya, and Sumitomo Electric Ind., Ltd. for the irradiation of specimens.

References

1. Warner, A. J., 1951 Annual Report, Conf. on Elec. Insul., NAS-NRC, 26 (1952).
2. Ieda, M., et al., J. Phys. Soc. Japan, 18, 1103 (1963).
3. Charlesby, A., Atomic Radiation and Polymers (Pergamon Press Ltd. 1960).
4. Gubler, M. A. and Kovacks, A. J., J. Polymer Sci., 34, 551 (1959).

THE DIELECTRIC PROPERTIES OF SOME POLY(FLUOROALKYL VINYL ETHERS)

H. Sorkin, W. W. Graessley*, J. A. Manson, and J. H. Zufall

Air Reduction Company, Inc.
Murray Hill, New Jersey

Although much research has been done on poly(vinyl ethers) in the last decade, little attention has been paid to halogenated vinyl ether polymers, and even less to the dielectric properties of such materials. We recently undertook such a study and wish to report on some of our findings at this time.

Trifluoroethyl vinyl ether, trifluoroisopropyl vinyl ether, pentafluoropropyl vinyl ether, and heptafluorobutyl vinyl ether were polymerized under a variety of conditions. The monomer structures are shown in Figure 1. All the polymers were clear, colorless, amorphous, rubbery materials.

$CH_2=CH-O-CH_2CF_3$	$CH_2=CH-O-CH_2CF_2CF_3$
trifluoroethyl vinyl ether (TFEVE)	pentafluoropropyl vinyl ether (PFPVE)
$CH_2=CH-O-\underset{\displaystyle CH_3}{\underset{\vert}{C}}H-CF_3$	$CH_2=CH-O-CH_2CF_2CF_2CF_3$
trifluoroisopropyl vinyl ether (TFIPVE)	heptafluorobutyl vinyl ether (HFBVE)

Fig. 1. Monomers used in this Study.

Figure 2 shows the relationship between dielectric constant and frequency. The dielectric constant of poly(trifluoroethyl vinyl ether) reaches a value of 18.5 at 100 cps and possesses low losses ($\tan \delta \leq 0.01$).

At the other extreme, the dielectric constant of poly(trifluoroisopropyl vinyl ether) at 100 cps is only 4. This is particularly interesting in view of the fact that the monomer (TFIPVE) has a dielectric constant of 10. The dielectric constant of monomeric trifluoroethyl vinyl ether (TFEVE) is 9.

These observations may be explained in terms of orientation of the polar groups. At low frequencies these groups are readily able to follow the field, but as the frequency is raised there is insufficient time for this orientation to occur and the dielectric constant decreases. The dielectric constant is also temperature

*Present address: Department of Chemical Engineering, Northwestern University, Evanston, Illinois

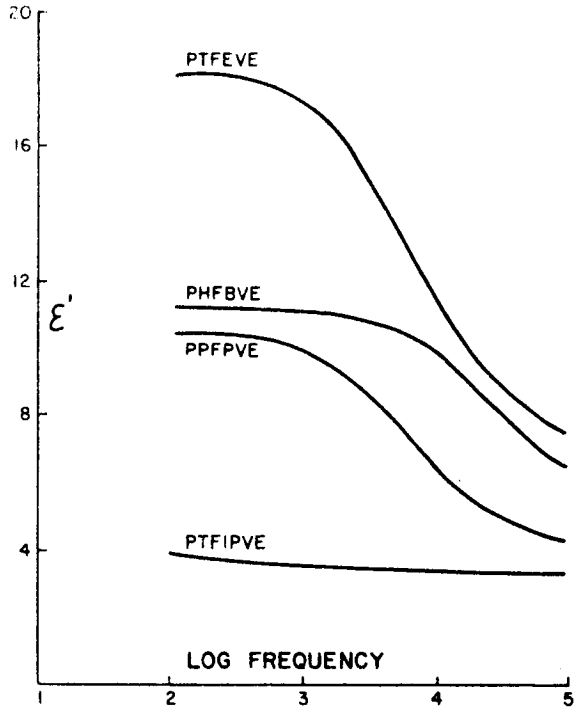

Fig. 2. Dielectric Properties of Fluoroalkyl Vinyl Ether Polymers. Temp. 23°C.

dependent: a rise in temperature results in shifting the curves toward higher frequencies. If the temperature is lowered the dielectric constant drops quickly and levels off at -10°C for poly(trifluoroethyl vinyl ether). This temperature corresponds to the glass transition temperature (the temperature at which segments of the backbone chain begin to rotate). Poly(trifluoroisopropyl vinyl ether), on the other hand, has a glass transition temperature of about 21°C and even at temperatures well above this, never develops a large dielectric constant. We believe that branching in the side chain produces steric hindrance to rotation even at elevated temperature.

The high static dielectric constants can be explained by the dual effect of a flexible fluorinated ether side chain: a glass transition temperature below room temperature, and freedom of the polar side chain from constraints of the main chain.

SIMULTANEOUS DIELECTRIC CONSTANT AND VOLUME MEASUREMENTS ON LIQUIDS AT HIGH PRESSURES

Norman L. Brown*

National Bureau of Standards
Washington, D. C.

In connection with an investigation of dielectric relaxation in liquids in relation to existing theories of free volume, a dilatometer was needed which would allow measurements of volume to about ±0.1 per cent at pressures up to 2000 kgm/cm^2 and temperatures down to about -150°C. Also required was a three-terminal liquid dielectric cell capable of being used at these pressures and temperatures with a minimum of corrections to its geometrical capacitance. Since the prospect of having to measure complex dielectric constant and volume of liquid samples in two completely separate series of experiments was not attractive, it was decided to combine the dilatometer and dielectric cell into one unit to enable the two properties to be measured simultaneously.

The dilatometer, which is shown partially disassembled in Figure 1, is similar to Bridgman's[1] bellows dilatometer, but with the piston-cylinder guide outside the bellows to allow a capacitance cell to be placed inside. Basically it is a bellows whose deflection is maintained axial by piston-cylinder arrangement. The liquid sample is placed inside the bellows through the filling tube, shown closed with a tapered pin in the illustration[2], and the whole assembly is immersed in the pressure transfer fluid inside a bomb. The piston is provided with grooves and the cylinder with holes to allow the hydraulic fluid free passage through the assembly. Thus, with all parts under only hydrostatic pressure, changes in volume of the liquid sample will be evidenced by displacement of the piston within the cylinder. (All metal parts, with the exception of the three Kovar seals through which the electrical leads are taken from the capacitance cell, are of the same material, in this case 316 stainless steel, to avoid problems of differential thermal expansion). Piston displacement is measured by a modification of the method used by Bridgman. In his device length changes were determined by measurement of the resistance of a manganin wire between one end, which was fixed to one end of the bellows, and a sliding contact fixed to the other end of the bellows. This involves knowing the resistivity of the wire as a function of temperature and pressure. The calibration requirements can be simplified, however, by measuring instead the ratio of the potential drop between the sliding contact and one end to the total potential drop along the wire. This ratio is independent of

---

*Present address: Bureau of Commercial Fisheries, Technological Laboratory, College Park, Maryland

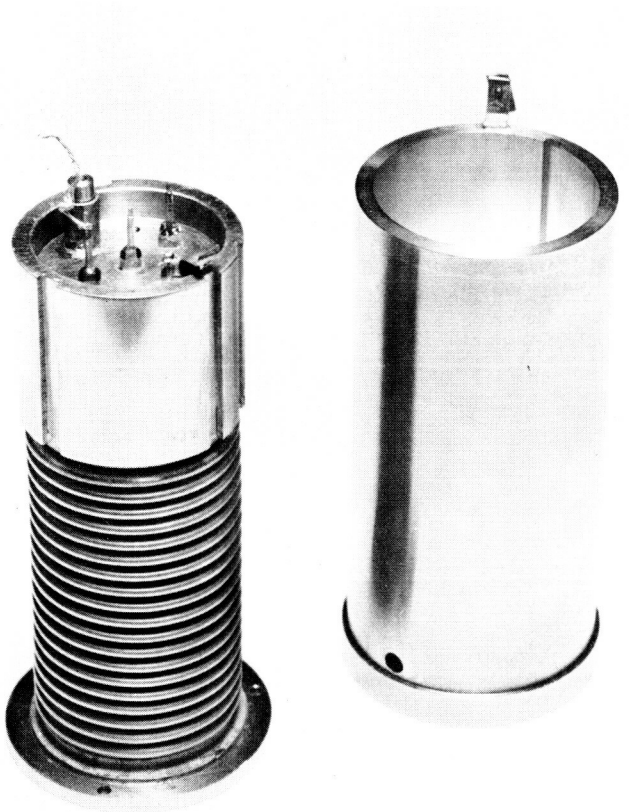

Fig. 1. Bellows Dilatometer Partially Disassembled.

resistivity, provided it is uniform over the length of the wire, and is simply the ratio of the two lengths, for wire of sufficiently uniform cross-section. If the total length of the wire (between the fixed potential contacts) were made equal to the effective length of the bellows, (i.e., sample volume divided by effective area of the bellows) at atmospheric pressure, for example, then the voltage ratio at any pressure divided by the ratio at atmospheric pressure would be directly the relative volume of the sample, because the effective area of the bellows remains constant with deflection. This scheme would of course involve corrections for volume changes with temperature at constant pressure.

A somewhat simpler scheme uses a voltage divider of arbitrary length and, with the slider fixed to the piston, a calibration of voltage ratio versus piston displacement from a fiducial position is made. This displacement is directly proportional to volume change. Such a device is illustrated in Figure 2. The wire is mounted on a piece of 316 stainless steel and insulated from it by a film of Teflon, and the mount is fastened to the cylinder in the groove which is visible in Figure 1. With the piston and cylinder assembled, a matching groove in the piston then faces the wire so that it is isolated from the metal parts along its entire length, except where it makes contact at the bottom of the mount. The helical spring is designed to keep the wire in slight

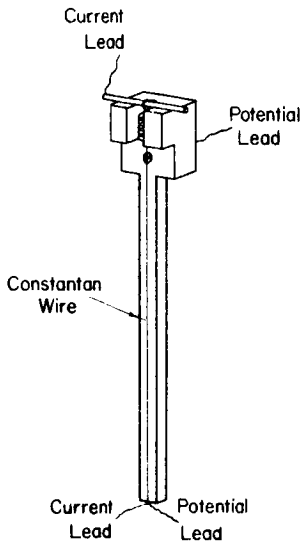

Fig. 2. Voltage Divider Used to Determine Piston Displacement.

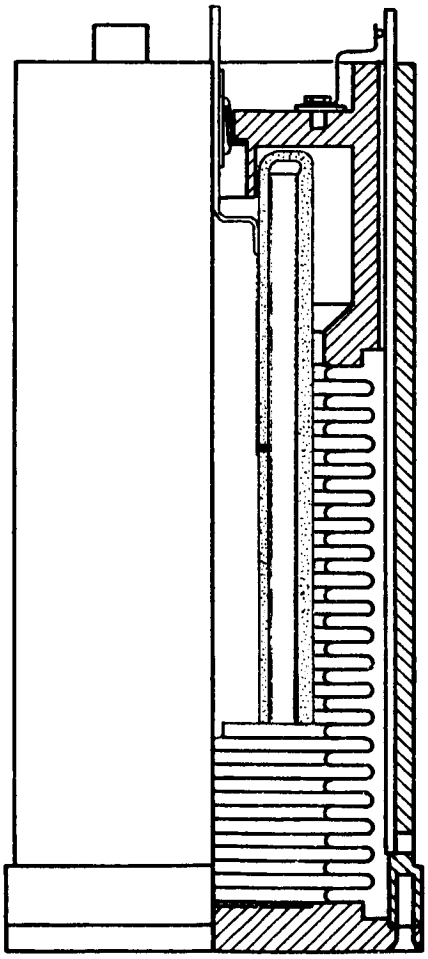

Fig. 3. Capacitance Cell Mounted in Dilatometer.

tension to compensate for the differential thermal expansion between the wire and the mount, and the spring and its anchor pin are insulated from the mount by a film of Teflon. The completed device provides measurements of volume accurate to ±0.1 per cent[3].

The capacitance cell is a three-terminal gold-plated fused quartz coaxial cylindrical capacitor which is self-supporting and is immersed in the liquid sample and thus is subject only to hydrostatic pressure. Figure 3 shows how the cell is mounted inside the dilatometer. The cell is constructed of two tubes of fused quartz attached at the ends with bridges of the same material. The outer surface of the inner tube is gold-plated[4] with a "low" electrode and two guard electrodes, and the inner surface of the outer tube is plated with the "high" or unguarded electrode. (The inner tube was first coated uniformly and then the three electrodes delineated by scratching the metal film with a tungsten carbide point). The two guard electrodes are connected by a gold stripe which runs from end to end on the inner surface of the inner tube. Connection to the "low" electrode is facilitated by drilling a small hole through the wall of the inner tube which allows the gold film to continue from the electrode through the hole and up the inner surface to the top, where a wire is soldered to it. The measuring electrode leads are hard-drawn No. 18 copper wire which is indium-soldered to the gold film, and which pass through the Kovar seals in the piston. The guard electrode is grounded to the inside of the piston.

(The third Kovar seal visible in Figure 1 is for a switching contact to warn of the approach of the bottom of the cell to the bottom of the cylinder). Although the illustrations do not show it, precautions are taken to insure continuous coaxial shielding of both electrode leads inside and outside the dilatometer, and through the bomb closure. The cell has a capacitance in air of 4.161 ± 0.001 pf. Thermal corrections to this value are much less than 0.001 pf, even at the lowest temperature used, and at 2000 atmospheres the pressure correction is about 0.2 per cent at room temperature.

In Figures 4 and 5 are examples of some of the data which have been obtained with this apparatus, using a Heise bourdon tube pressure guage[5] and a Cole bridge[6]. The circles represent measurements made with increasing pressure and the plus marks those at decreasing pressure. There is some scatter in the data for relative volume in Figure 4, but whether this can be construed as indicative of hysteresis is somewhat dubious. However, in Figure 5 the dielectric constant data do show a small but distinct hysteresis which is apparently the result of not allowing sufficient time for thermal equilibrium to be established after the adiabatic expansion cooling between points.

References and Footnotes

1. Bridgman, P. W., Proc. Am. Acad. Arts Sci. 66, 185-233 (1931).

2. This type of closure, which is copied from Bridgman's method and uses a tapered pin soldered into the filling tube after the sample is introduced, was found too inconvenient and unreliable, and has since been replaced with a screw plug and silver gasket.

3. This voltage divider has now been replaced by Dr. F. Mopsik with an earlier version which is much simpler. It consists of a fused quartz rod coated with a uniform film of platinum (Hanovia Liquid Bright Platinum 6587), and is indicated schematically in Figure 3.

4. Hanovia Liquid Bright Gold NW, approximately 0.1 ohm/square.

5. Heise Bourdon Tube Company, Newtown, Connecticut.

6. Cole, R. H. and Gross, P. M., Jr., Rev. Sci. Instr. 20, 252-60 (1949).

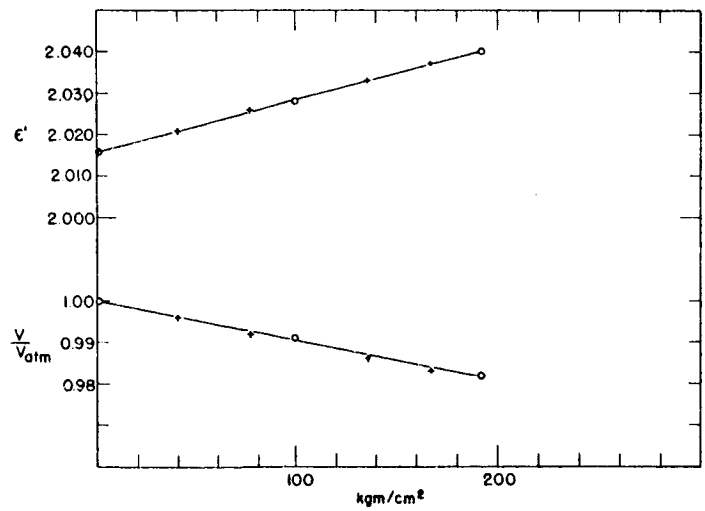

Fig. 4. Dielectric Constant and Relative Volume of Cyclohexane at 23.2°C as a Function of Pressure.

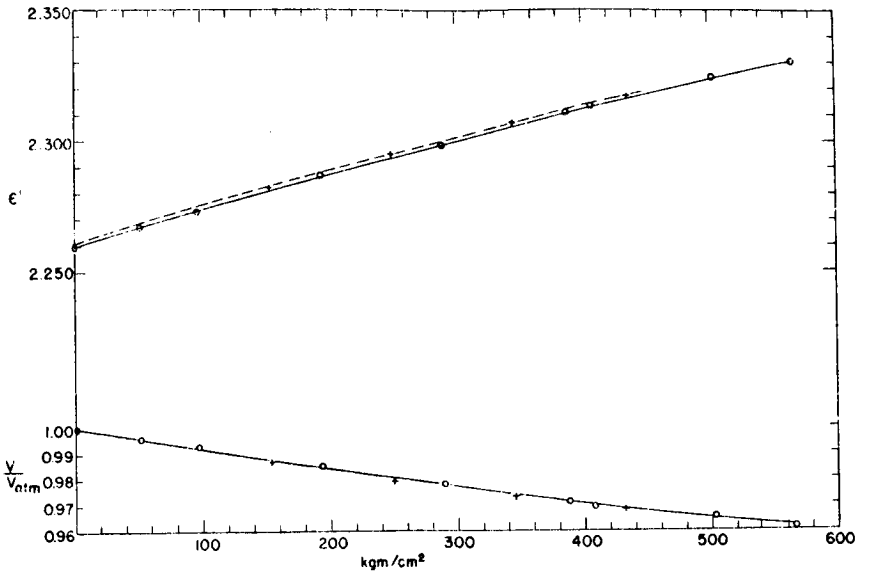

Fig. 5. Dielectric Constant and Relative Volume of Carbon Tetrachloride at 6.7°C as a Function of Pressure.

NET POSITIVE CHARGE ACCUMULATION AT DIELECTRIC SURFACES UNDER AC CORONA*

N. M. Bashara and F. M. Green

The University of Nebraska
Lincoln, Nebraska

Charges of opposite sign can co-exist in close proximity on dielectric surfaces[1]. The accumulation of charges is believed to influence the deterioration[2]. However, there is little information on the relationship between the preferential trapping of charges, the development of discharges at dielectric surfaces and the performance of dielectrics under these conditions. A recent experimental study demonstrated a relationship between pulse distribution and dielectric deterioration and an asymmetry of discharges under alternating voltage[3]. It is the latter point that will be discussed here, particularly with regard to the influence of charge trapping and accumulation.

The geometry used is a metal sphere and dielectric sheet 0.0005 inch thick having a separation of 0.002 inch from the sphere. Using photomultiplier detection and magnetic recording of the pulses a greater number of pulses having a wide distribution of magnitudes is observed on the negative half cycle (sphere negative) than on the positive half (sphere positive). Results on a specimen are tabulated in Table 1. Note that the test duration is about three hours.

	Number of Pulses				
	Total	0 to 0.5 v.*	0.5 to 1.0 v.	1.0 to 1.5 v.	>1.5 v.
Negative					
Initial	205	25 12%	50 25%	40 20%	90 43%
3 hours later	360	120 33%	40 11%	1.40 39%	60 17%
Positive					
Initial	25	25 100%			
3 hours later	160	140 88%	20 12%		

Table 1. Discharges at a Polystyrene Surface/

*The charge content of a 1-volt pulse is about 120 x 10^{-12} coulombs.

/These results are taken from Reference 3 (Bashara et al.), Figures 10 and 11.

*Supported by the National Science Foundation, G-14456.

The observed results which are illustrated by Table 1 are related to whether charges are trapped or remain relatively free at the dielectric surface. For example, if positive charges remain relatively free (untrapped) at the dielectric on the positive half cycle (sphere positive) a counter field would be created by discharges which would tend to suppress further discharges. Conversely, there would be no opposing field on the negative half cycle if the electrons are trapped by the dielectric.

To what extent these suggested mechanisms alone produce the asymmetry of the discharges observed on alternate half cycles cannot be determined easily. A carry-over of untrapped positive charge may also be of importance. That such a carry-over does exist is suggested by the following results. Small, probably reverse discharges are observed at the start (Figure 11, Reference 3) and end (Figures 10, 11, 12, and 13) of the positive half cycle. Forward discharges occur (Figure 11) at the end of the negative half cycle. (All figures refer to Reference 3).

The asymmetry in the total charge involved on alternate half cycles is believed to be real and not due to a lack of detector sensitivity. For example, assume a lower threshold of 10 mv. for the detector. A breakdown of Table 1 indicates that to realize an equal amount of charge on each positive half cycle as occurs on the negative (on the average) one would have to assume that 200 to 300 discharges of about 10 mv. magnitude each are occurring but are not detected due to the lack of detector sensitivity. This does not appear to be likely.

The asymmetry in the discharges is believed not due to cathode effects, specifically higher secondary yield from the metal sphere as compared to the dielectric. However, tests on polytetrafluoroethylene do suggest a change in cathode mechanism with time. The number of larger discharges on the negative half cycle shifts to an earlier point on the half cycle (Figure 1, Reference 3). This may be similar to observations in an electrode-less discharge[5]. The tests on polystyrene mentioned previously did not exhibit this effect. Rather, the larger negative pulses tend to occur later on the half cycle.

References

1. Thomas, A. M., British Jrnl. A. Phys., 2, 98 (1951).
2. Thomas, A. M., Jrnl IEE, 91 Part II, 549 (1944).
3. Bashara, N. M., Green, F. M., and Lederer, D. B., 64-165, IEEE Winter Meeting, Feb. 2-7, 1964. To be published IEEE Trans. Elec. Insulation, January, 1965.
4. Mason, T. H., Proc. IEE, 100 Part 2a, 149 (1953).
5. Harries, W. L. and von Engel, A., Proc. Phys. Soc. 64B, 915 (1951).

IONIZATION AND ATTACHMENT COEFFICIENTS IN PERFLUOROCARBON GASES

J. C. Devins and R. J. Wolff

General Electric Research Laboratory
Schenectady, New York

Predictions of the dependence of electric strengths of electronegative gases on molecular structure depend upon a knowledge of the relationships between the ionization and attachment coefficients and molecular structure. In this work we have measured these coefficients for a number of perfluorocarbon gases including the perfluoroalkanes $C_n F_{2n+2}$ (n = 1,2,3,4,6), octafluorocyclobutane and hexafluoropropene.

The method is similar to that used by Harrison and Geballe[1] and involves a determination of the steady state drift current due to photoelectrons and their ion products formed by collision in a uniform field gap. In such a gap the total current is given by

$$i = i_o \left\{ \frac{[\alpha/(\alpha-\eta)] \exp.\ (\alpha-\eta)\delta - \eta/(\alpha-\eta)}{1 - \gamma\,\alpha/(\alpha-\eta) \quad [\exp.\ (\alpha-\eta)\delta - 1]} \right\} \qquad \text{(Eq. 1)}$$

where i_o is the primary photocurrent produced at the cathode by irradiation with ultraviolet light; α is the number of ionizing collisions per electron per cm. drift in the field; η is the number of attaching collisions per electron per cm. drift in the field; γ is the second Townsend coefficient; δ is the length of the gap.

Since γ is generally a smaller number the fields and gaps may be easily chosen so that the denominator remains essentially unity. The current is then measured as a function of gap spacing, holding the field E, and thus α and η constant. The resulting measurements may then be curve-fit to Equation (1) to give α, η and i_o. In our work curve-fitting was accomplished using a G.E. 225 computer. The gap was varied from 0.03 to 3.0 cm., and the pressures ranged usually from 1 to 10 torr. Measurements on CF_2Cl_2 agreed satisfactorily with those of Harrison and Geballe[1].

Earlier work[2] with a large number of non-attaching gases has shown that the functional relationship between α/P and E/P (where P is pressure) may be written to a good approximation over the range of interest to breakdown as

$$\alpha/P = Ae^{\frac{-BP}{E}} \qquad \text{(Eq. 2)}$$

The constant, B, for these gases, was related to the Ramsauer cross section, Θ, by the equation

$$B = \rho\Theta\epsilon_i^{3/2} \qquad \text{(Eq. 3)}$$

where ϵ_i is the ionization potential of the molecule. The number ρ was found to be a constant for the hydrocarbons. It is a measure of the probability that collision will

lead to electronic excitation of the molecule. Finally it was observed that Θ could be written as the sum of cross sections for each pair of bonding electrons in the molecules, i.e.,

$$B/\epsilon_i^{3/2} = \Sigma_k n_k \Theta_k \qquad \text{(Eq. 4)}$$

Figure 1 shows that equation (2) is fairly well satisfied for the perfluoralkanes, although some curvature is present for low E/P in C_2F_6 and C_6F_{14}. Similar curvature has been observed in hydrocarbons. Values for the cross sections, $B/\epsilon_i^{3/2}$, are obtained from the slopes of these lines and are plotted against the number of carbon fluorine bonds in Figure 2. The corresponding plot for the hydrocarbons[2] is also shown in the figure. It is clear that for both, the cross section for the C-C bonds is essentially zero, since the intercepts are zero. The value of ρ is very nearly constant for both. The smaller slope for the fluorocarbons indicates either that the cross section for the carbon-fluorine bond is lower than that for the carbon-hydrogen bond or that ρ is smaller for the fluorocarbons. The former seems less likely since each fluorine atom has six additional non-bonding electrons which would be expected to contribute to electron scattering.

Values of η/P are plotted against E/P in Figure 3. Not only does the functional form vary from one gas to the next but little uniformity in the dependence of magnitudes on chain length can be detected. There is an increase in η/P with increasing chain length from CF_4 through C_3F_8. C_4F_{10} has generally lower values for η/P than the two lower members of the series, while C_6F_{14} is much higher than any of the others. It is clear that the relationship between attachment coefficients and molecular structure is much more complex than has been found for the corresponding ionization coefficients.

Measured sparking potentials[3] for these gases may be compared with those calculated using our values of α and η, using the fact that breakdown will occur for fields at which the denominator in equation (1) becomes zero, and fitting at one point to obtain γ. Such a comparison is shown in Figure 4. Agreement is reasonably good for the three lower members of the series and for C_6F_{14}, but is inadequate for C_4F_{10}. Since sparking potential measurements were made at higher pressures (60 - 600 torr), and since pressure dependences for η/P have been occasionally observed[4], evidence for a pressure effect in C_4F_{10} was sought. Figure 5 shows the dependence of the coefficients for C_4F_{10} on pressure at E/P = 125 volt cm^{-1} $torr^{-1}$. A decided decrease in $(\alpha-\eta)/P$ with increasing pressure is observed and may be attributed to a corresponding increase in η/P. The effect will account quantitatively for the discrepancy between measured and calculated sparking potentials in C_4F_{10}.

The pressure effect may be explained in terms of a metastable parent negative ion in which the kinetic energy of the attaching electron is converted to vibrational energy, leading to an increased lifetime. If a collision with another molecule

occurs within this lifetime permanent stabilization will occur; otherwise dissociation into an electron and molecule will occur with no net attachment. Applying unimolecular kinetics to our data a lifetime of 10^{-7} seconds is calculated assuming every collision results in stabilization. This value is consistent with the finding[5] of a very small $C_4F_{10}^-$ peak in the mass spectrum. With smaller molecules than C_4F_{10} the number of vibrational modes and thus lifetime is presumably too short for collisional stabilization over the pressure range covered, while with C_6F_{14} stabilization is complete over the whole pressure range. A large $C_6F_{14}^-$ peak has been observed[5] in the mass spectrum of $C_6F_{14}^-$, though none in molecules smaller than C_4F_{10}.

Some insight into the nature of the processes responsible for the dependencies shown in Figure 3 may be obtained from mass spectrometry. F^- is heavily predominant in all the gases below C_4F_{10} with the parent ion of importance in C_6F_{14}. In Figure 6 we have plotted maximum relative cross sections obtained from ion abundances against η_{C-F}. The similarity between these results and those shown in Figure 3 is apparent, though a more quantitative comparison must await a determination of the electron energy distributions in the discharge.

The authors are indebted to Wright-Patterson Air Force Base for support of this work.

References

1. Harrison, M. A. and Geballe, R., Phys. Rev., 91, 1 (1953).
2. LeBlanc, O. H. and Devins, J. C., Nature, 188, 219 (1960).
3. Crowe, R. W. and Devins, J. C., Unpublished results.
4. Chanin, L. M., Phelps, A. V., and Biondi, M. A., Phys. Rev., 128, 219 (1962).
5. Greenhaus, H. L., Private communication. To be published.

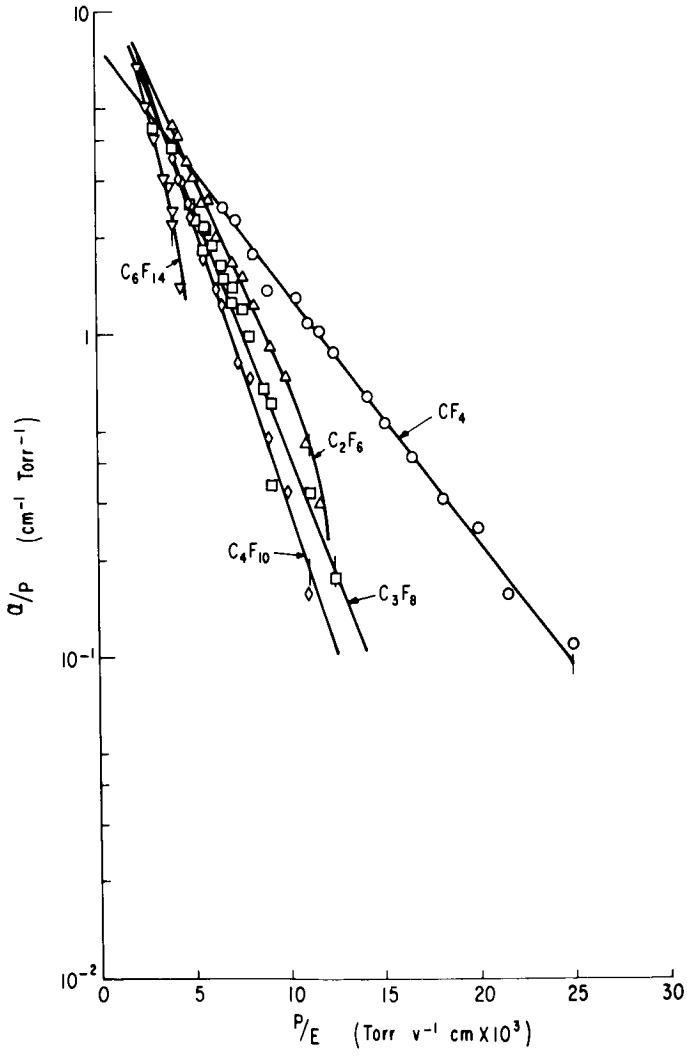

Fig. 1. Dependence of Ionization Coefficients on P/E for the Perfluoroalkanes.

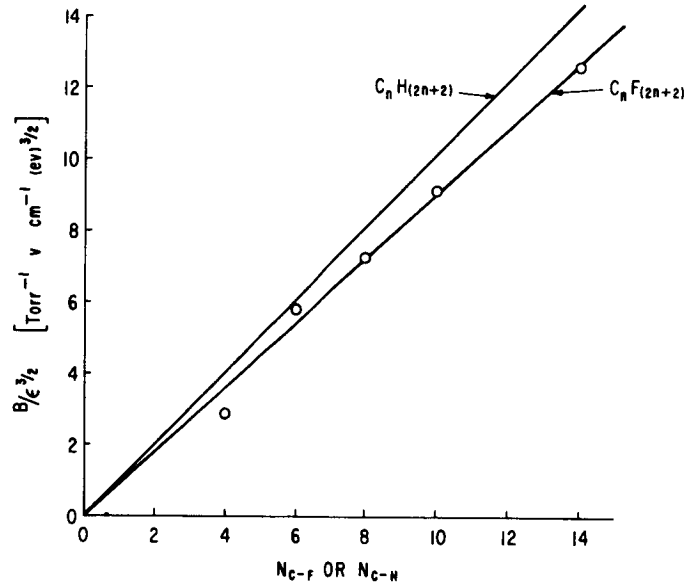

Fig. 2. Relationship Between Cross Sections and Number of Carbon-fluorine or Carbon-hydrogen Bonds in the Alkanes.

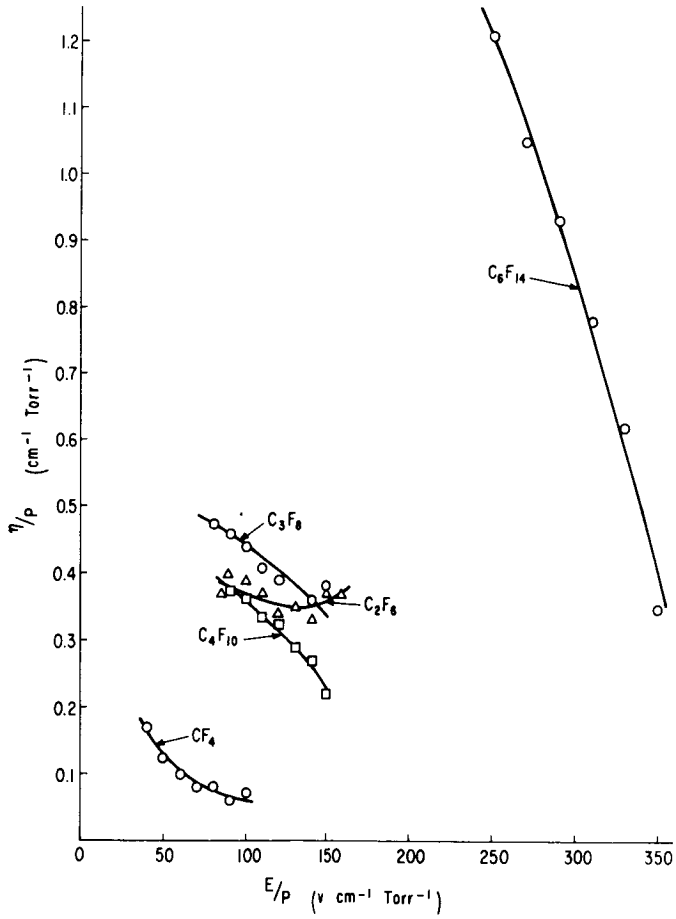

Fig. 3. Dependence of Attachment Coefficients on E/P for the Perfluoroalkanes.

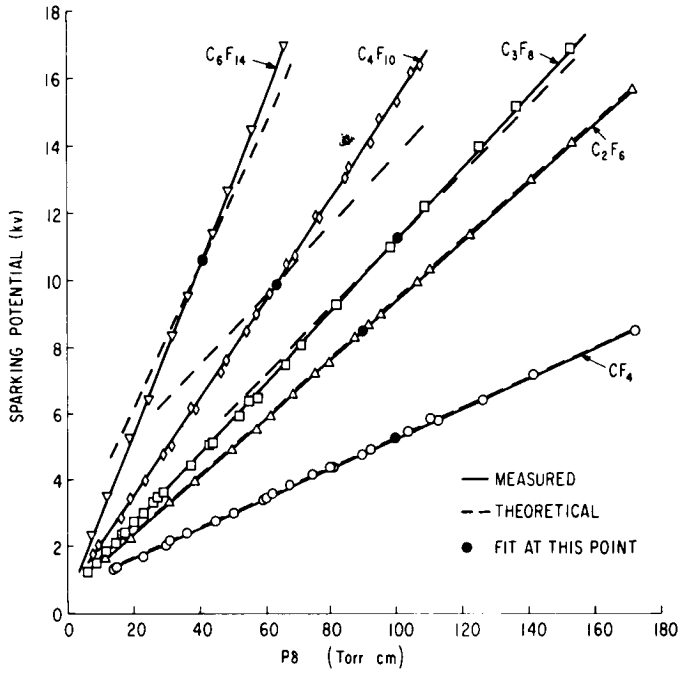

Fig. 4. Comparison of Measured and Calculated Sparking Potentials for the Perfluoroalkanes.

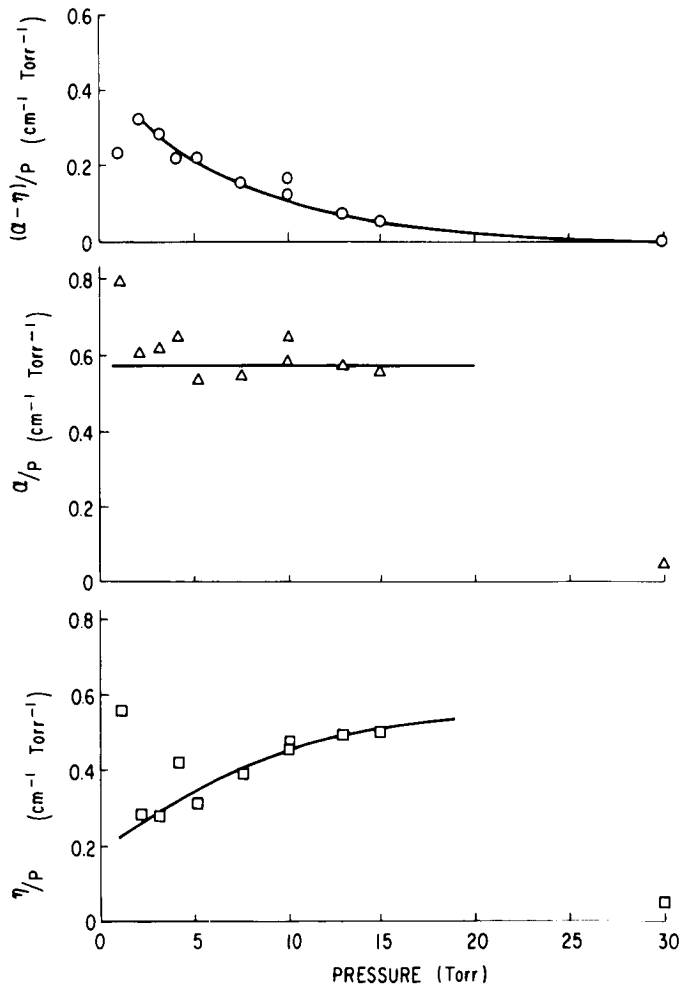

Fig. 5. Dependence of α/P, η/P and $(\alpha-\eta)/P$ on Pressure for C_4F_{10} at E/P_1 of 125 volt cm^{-1} torr^{-1}.

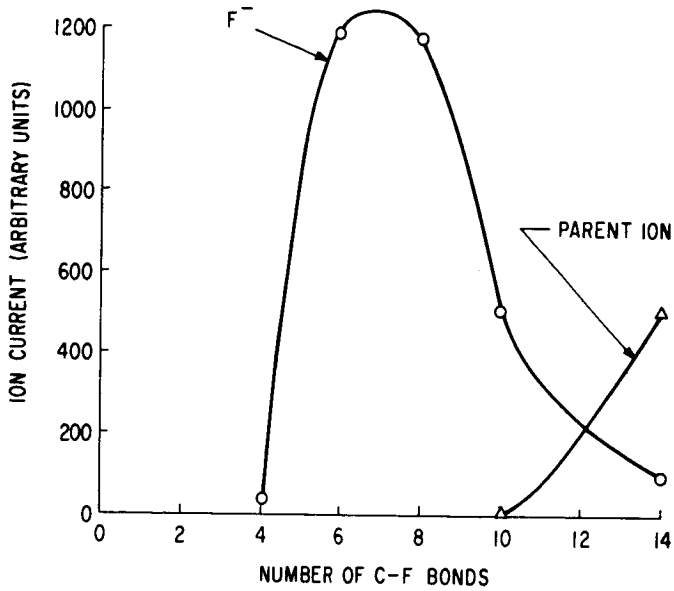

Fig. 6. Maximum Relative Cross Sections for Negative Ion Formation as a Function of Chain Length in the Perfluoroalkanes.

INSULATING FILMS OF BORON NITRIDE ON COPPER SUBSTRATES

R. R. Haberecht, R. J. Patterson, and R. D. Humphries

Texas Instruments Incorporated
Dallas, Texas

I. Introduction

The investigation of insulating BN films on copper substrates was undertaken to determine the possibility of utilizing the excellent dielectric characteristics of thin BN films in combination with copper conductors. Films 1/2μ in thickness have been deposited on copper foils and their dielectric properties have been evaluated.

Two problems are encountered in preparing these films on copper substrates:

(1) The deposition temperatures must be sufficiently low to prevent detrimental effects on the copper while maintaining good insulation integrity of the film.

(2) A strong adhesive bond must be created between the BN and the Cu substrate.

II. Sample Preparation and Description

BN films are deposited by the chemical pyrolysis of beta-trichloroborazole vapors in a low pressure flowing reactor system. Vapors of β-TCB are fed to the surface of a resistively heated copper foil. BN is deposited and volatile by-products are pumped away. The upper temperature limit imposed by the m.p. of the Cu substrates limits the rate at which the film is formed; also, at the lower deposition temperatures, film properties are affected. Temperatures between 900° - 1000°C were used to prepare the films evaluated.

In these films no X-ray diffractions were observed, indicating only small hexagonal layers randomly arranged. The smaller molecule would be expected to be more mobile and subject to a greater polarization. Sites for bonding impurities, especially H and Cl, are more abundant[1].

Bonding the deposited films to the copper substrate was accomplished by a surface degenerative process, involving a graded modification of the Cu surface characteristics by diffusing foreign metallic elements into the copper surface. In a conventional vacuum evaporator a thin layer of manganese was applied to the cold Cu surface. The Cu-Mn was heated to red heat in one atm N_2 until diffusion had taken place. Subsequently, the excess Mn was removed by a high vacuum evaporation. The metal surface characteristics were sufficiently modified to provide an adhesive bond to the BN film.

Surfaces prepared in this way were then coated with BN. A .002" Cu foil coated with 0.5μ BN could be bent double without crazing of the insulation.

III. Dielectric Testing

Aluminum counterelectrodes were evaporated onto the BN film and samples were cut from the foil for evaluation. These samples were placed in a jig and heated in a controlled ambient. Stabilization of the samples occurred during a bake at 125°C for a minimum of one hour in dry nitrogen. Where applicable, all measurements conformed to the requirements of ASTM procedures. A General Radio bridge 716C was used for the capacitance and dissipation factor measurements. Dielectric breakdown determinations were made using a 1/4-inch diameter brass probe in direct contact with the film. Voltage was applied at 500 volts per second.

IV. Dielectric Characteristics

In Table 1, the dielectric properties of 0.5μ-thick BN films on copper are compared to films deposited at 1400°C on molybdenum.

Table 1

DIELECTROC PROPERTIES OF 1/2μ THICK BN FILMS ON METAL SUBSTRATES

	Mo	Cu
Dielectric Strength, vpm		
25°C	5000	3900
125°	3800	2900
175°	3400	1500
250°	3000	-
Dielectric Constant, 1 kc		
25°C	4.4	5.7
125°	4.4	4.5
175°	4.4	4.4
250°	4.4	4.4
Dissipation Factor, 1 kc		
25°C	.003	.011
125°	-	.0045
175°	-	.0056
250°	-	.011
Resistivity, Ohm cm		
25°C	7.5×10^{17}	7.5×10^{17}
125°	1.3×10^{16}	3×10^{14}
175°	3.0×10^{15}	2.0×10^{13}
250°	6.0×10^{14}	-

Dielectric strengths (dc) of the BN-Cu samples are lower than those on Mo. Above 150°C the strength diminishes rapidly. The dielectric constant and dissipation factor for the BN-Cu samples are higher than those for films on Mo. A temperature dependency is also observed. The temperature dependency of resistivity indicates a single activation energy for each film, 1.26 eV for the BN-Cu and 2.44 eV for BN-Mo. Conduction may be primarily due to impurity ions in the structure.

V. Application

Boron nitride insulation on copper offers several distinct advantages for space application. Among these are size, weight, and low volatility. The films, strongly adherent to the substrate, affords oxidation protection to copper.

References

1. Krebs, H., Technical University of Stuttgart, private communication.

THERMOELECTRIC POWER OF SAPPHIRE SINGLE CRYSTALS

S. Dasgupta and John Hart*

Carleton University
Ottawa, Canada

The electrical and thermal conductivity of alumina, both polycrystalline and single crystals, have been studied extensively by several workers[1-4]. The results obtained by different investigators differ by several orders of magnitude and these divergencies have been attributed by some author[1] to many interrelated phenomena like impurity content, surface condition of the samples, contact resistance and method of measurements. The discrepancies are such that it has not been possible to establish any definite transport mechanism in alumina. The present study of thermoelectric power with improved measuring techniques may help this incoherent situation.

The problem of measuring small voltages across a very high resistance sample led to the choice of a two-electrometer circuit[5]. Figures 1 and 2 respectively show the details of the furnace and the necessary sample connections for the measurements of thermoelectric power. The samples were single crystals obtained from Linde Gas Co. and Semi-element Inc., cut from boules to a size of 7 cm x 1 cm x 5 mm parallel to the axis of the boule, the longest dimension making an angle of a few degrees with the c-axis of the crystal. Platinum-platinum rhodium (10%) thermocouples were used for the temperature measurements and the platinum leads of the thermocouples were used to measure the thermal e.m.f. of the alumina-platinum system.

In Figure 3, curves 1 and 2 represent the absolute thermoelectric power for a crystal obtained from Linde at pressures 15×10^{-4} and 35×10^{-4} cm respectively, changing from a negative value at the lower temperature to a positive value at the higher temperature in each case. When the pressure was reduced to 0.6×10^{-4} cm (curves 3 and 4), the increase of the positive value of thermoelectric power was very rapid, attaining a maximum and decreasing slowly thereafter. The results were reproducible within the accuracy of the measurements as shown by curve 4. Curve 5 shows the results for a single crystal obtained from Semi-element, the size of the crystal was kept exactly the same as before. The measurements this time were taken first under the lowest pressure, 0.6×10^{-4} cm. Through an adjustable leak in the vacuum system, the pressure in the furnace was then adjusted to 70×10^{-4} cm. At this pressure, no stable value could be obtained for this sample even after a few days heating. Every time the sample was heated at high temperature, there was a change observed in the value of the thermal e.m.f., although the values were all the time changing from

---

*Present address: Brock University, St. Catharines, Ontario, Canada

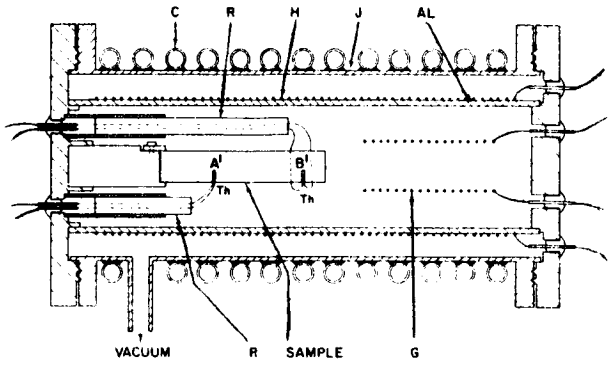

Fig. 1. Detail of Furnace.

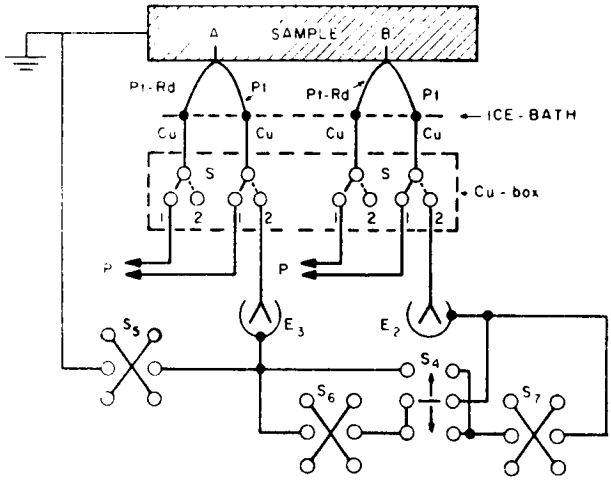

Fig. 2. Electrical Connections. E_2 and E_3 are Electrometers. PP are the Potentiometer Connections.

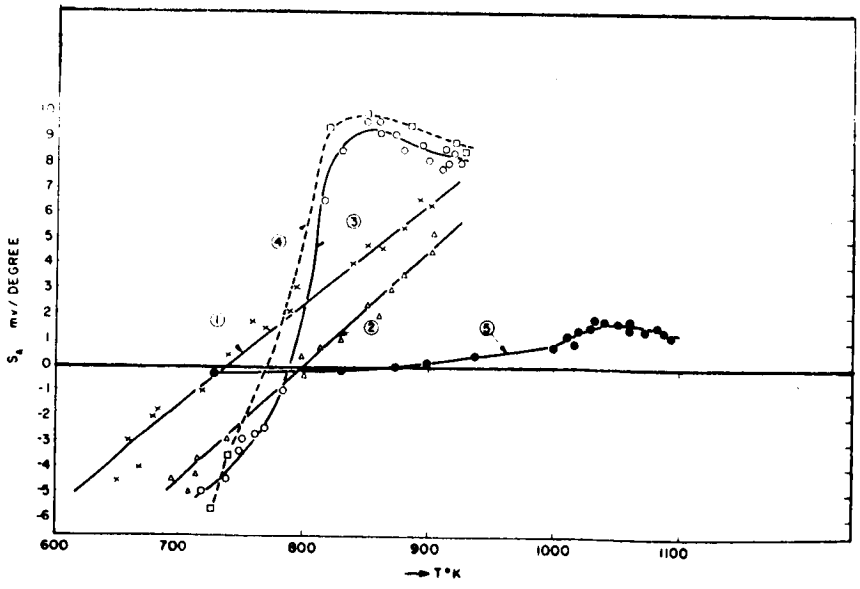

Fig. 3. The Absolute Thermoelectric Power of Sapphire Single Crystals as a Function of Temperature at Various Pressures.

negative at low temperature to positive at high temperature. The low pressure (0.6×10^{-4} cm) was then established in the furnace and the value of the thermoelectric power, though more stable this time, could not be very much reduced even after heating about 20 hours at 900°C.

Figure 4 represents the results observed in another sample obtained from Semi-elements. The sample was heated to about 900°C in vacuum (10^{-6} cm) for about 25 hours before curve A was obtained. These values were stable in this temperature range under this vacuum and further heating at the same temperature for further 6 hours did not change the value of thermoelectric power. Then dry pure argon gas was introduced in the furnace and a pressure of about 80×10^{-4} cm was maintained to obtain curve B. The original vacuum of 10^{-6} cm was then resumed in the furnace and after heating at about 900°C for about 15 hours, measurements were made giving curve C. An atmosphere of air at pressure of 10^{-4} cm was then maintained in the furnace. Measurements were made again after heating the sample at about 850°C for about 15 hours and curve D was obtained. In the next step, the vacuum of 10^{-6} cm was introduced in the furnace and the sample was heated again for about 25 hours at about 900°C; during this period the sample was flashed frequently with argon. Measurements were then made in an atmosphere of argon (10^{-4} cm), in vacuum (10^{-6} cm) and in an air atmosphere (10^{-4} cm) in succession; each time the sample was heated at about 900°C for about 20 hours in the respective atmosphere before the final measurements were taken. The results are represented in Figure 4 by A, B, and C.

The results shown by curve D, exhibit a definite indication that the presence of oxygen in the atmosphere in which the sample is heated has a great effect on the thermoelectric power of alumina. This effect is qualitatively reproducible under these pressures.

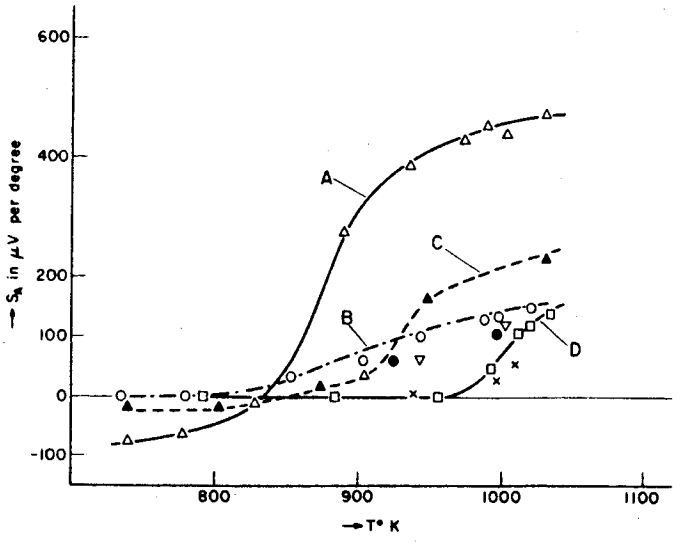

Fig. 4. The Absolute Thermoelectric Power of a Sapphire Single Crystal as a Function of Temperature in Various Atmospheres.

From the results, we believe that surface phenomena play an important role in the thermoelectric power of alumina, particularly when the atmosphere contains oxygen. It is possible that adsorption of oxygen in the surfaces caused extra discrete levels within the forbidden band to change the conduction property of the crystal. If the contribution from these levels happen to be of opposite nature to that of the conventional impurity levels, predominantly a bulk property of the crystal exhibited in curve 3, then the abrupt change of behavior of curve 3 from curves 1 and 2 will not be difficult to understand. On the other hand, like many other metallic oxides acting as semiconductors, alumina in addition to its other impurities probably contain a stoichiometric excess of one or other of the constituents. In this case there will be a changing transport property of the crystal by the changing atmosphere in its oxygen content.

In conclusion, the authors have established, not unexpectedly, that the thermoelectric power of alumina single crystals depends very much on the thermal history of the samples when the atmosphere in which they are heated contain oxygen. The amount of oxygen present in the atmosphere causes complex changes in the thermoelectric power and these changes were found irreversible in some samples. This behavior is attributed almost entirely to surface adsorption.

References

1. Cohen, J., "Electrical Conductivity of Alumina," Am. Cer. Soc., Bull., Vol. 38 (9), 441-446 (1959).

2. Pappis, J. and Kingery, W. K., "Electrical Properties of Single Crystal and Polycrystalline Alumina at High Temperature," J. Am. Cer. Soc., Vol. 44 (9), 459-464 (1961).

3. McQuarrie, M. C.,"Thermal Conductivity: Analysis of Variation of Conductivity with Temperature for Al_2O_3, BeO and MgO," J. Am. Cer. Soc., Vol. 37 (2), 91-95 (1954).

4. Kingery, W. K., "Thermal Conductivity: XII Temperature Dependence of Conductivity of Single-Phase Ceramics," J. Am. Cer. Soc., Vol. 38 (7), 251-255 (1955).

5. Fisher, G., Greig, D., and Mooser, E., "Apparatus for the Measurement of Galvanomagnetic Effects in High Resistance Semiconductors," Rev. Sci. Inst., Vol. 32 (7), 842-846 (1961).

FABRICATION OF THIN FILM INSULATION

H. L. Caswell

IBM Watson Research Center
Yorktown Heights, New York

I. Introduction

The requirements for thin film dielectrics vary appreciably from application to application with the result that a number of different materials are presently being used. It is convenient to divide these materials into two broad categories, inorganic and organic, in discussing the fabrication of dielectric films since a particular fabrication method can frequently be used for a number of different materials within a given category.

II. Inorganic Thin Film Dielectrics

Vacuum deposition is used extensively to prepare thin films of silicon oxide, magnesium fluoride, lithium fluoride, and other materials which can be evaporated from refractory metal crucibles. The characteristics of these films are strongly dependent upon deposition conditions as is illustrated by the variety of properties which can be obtained in silicon oxide films prepared by thermal evaporation of silicon monoxide. Films prepared at low evaporation source temperatures ($<1250°C$) are porous in structure, react readily with water vapor or oxygen to form Si_2O_3, and are transparent in the visible. Films prepared at high source temperatures ($>1400°C$) contain excess silicon plus a large number of defects which cause these dark brown films to be unstable and susceptible to cracking. At intermediate temperatures, light brown films characteristic of silicon monoxide are obtained which are highly stable and unreactive with water vapor and oxygen provided they are deposited at approximately normal incidence to the substrate. At higher angles of incidence a structural and stress anisotropy exists which causes films to buckle and peel from the substrate upon exposure to water vapor. Thus, thin silicon oxide films which are acceptable for many applications can be deposited reliably and reproducibly by controlling the pertinent evaporation parameters and avoiding conditions which result in instability. Without this control, a mystifying variety of properties will be observed. Although silicon oxide film properties have been studied most extensively, there is ample evidence that the same type of control is required during the vacuum deposition of thin films of other inorganic materials.

Thermal oxidization and electrical anodization are very reliable techniques for forming thin film dielectrics on materials which have coherent oxides such as silicon, aluminum, and tantalum. There is a distinct advantage in having the material to be insulated take an active role in the formation of the dielectric film since this discourages the formation of pin holes and other defects which can contribute to electrical

shorts. For example, thermal oxidation of silicon is diffusion rate limited with the result that any bare substrate area which might develop during oxidation is oxidized preferentially. These dielectric films are, therefore, in a sense "self-healing."

The extensive use of silicon for semiconductor, integrated circuits is due largely to the ease with which reliable silicon dioxide films can be thermally grown for use as circuit insulation, diffusion masks, and passivation layers. For thermal oxides the film thickness can be controlled by monitoring the furnace temperature, ambient gas, and time. In liquid or gas phase anodization where an electric field drives oxygen into the substrate, the film thickness can quite accurately be controlled by monitoring the anodization voltage.

Several other techniques have recently been reported for depositing metal oxides and glasses. These include reactive sputtering of aluminum and silicon in oxygen, chemical vapor deposition of silica, alumina-silica mixtures, and boro-alumina-silica glasses, and low temperature plasma formation of silica. These techniques are still largely in the experimental stage and further work is needed to determine their ultimate potential.

III. Organic Thin Film Dielectrics

For many years the formation of tough, tenacious, polymer films in electron microscopes due to electron bombardment of residual hydrocarbons has presented a contamination problem. More recently it was recognized that these films could be used to advantage for insulation applications where high temperature stability is not a requirement. The cryoelectronics field is an example where the plastic characteristics of polymers offer a stability to temperature cycling between room temperature and -270°C which cannot be achieved in the more brittle, highly stressed inorganic dielectrics. Several techniques have been developed for depositing polymer films in which a monomer is adsorbed on the substrate surface and cross linked by electron, ion or photon bombardment.

A very reliable method for forming polymer films involves placing the substrate to be coated on the anode of a glow discharge apparatus and striking a discharge in the presence of a polymerizable vapor. The large spread in the angle of incidence with which the gas molecules strike the substrate enables the polymer to form behind protuberances and other substrate surface defects and contributes to excellent insulation characteristics. The high energy (several kilovolts) associated with the discharge is sufficient to thoroughly fragment the gas molecules with the result that polymer films formed in a glow discharge are reported to have very similar characteristics regardless of the starting material.

Ultraviolet light has also been used to form polymer films and has the advantage that the photon energy (4-5 ev) is comparable to the energy required for polymerization and not several hundred times larger as in the case of electron beam or glow discharge polymerization. A variety of materials has been successively

polymerized including butadiene, methylmethacrylate, acrolein, and divinylbenzene. A high partial pressure of the monomer (several torr) is required to achieve a deposition rate of a few angstroms per minute.

Polymer films also have several interesting characteristics. For several metals including tin, lead, and silver the sticking probability of the metal on certain polymeric surfaces is strongly dependent upon the degree of surface polymerization. This phenomenon can be used to advantage to form electronic circuit patterns or can present a problem in instances where fine line definition is required.

IV. Conclusions

Although considerable progress has been made toward understanding the relationship between film properties and formation parameters, many technologies are still handicapped because of inadequate thin film dielectrics. Interest in field effect and tunneling devices has created a need for thin dielectrics which not only insulate at small thicknesses but also have specific surface and bulk properties. Improved fabrication techniques will have to be developed to satisfy many of these requirements.

THIN FILM ELECTRONIC COMPONENTS

David A. McLean

Bell Telephone Laboratories, Inc.
Murray Hill, New Jersey

Interest in thin films for electronic uses which has developed in recent years is based on the need for increased economy, reliability, and compactness of complex electronic systems. Research and development on thin films includes interesting possibilities for thin film transistors and diodes, but these are not discussed in this paper. The bulk of thin film activity relates to capacitors and resistors, which can be formed into passive networks and joined with discrete active devices in "hybrid" arrangements. Such arrangements may involve applique of active elements to glass or ceramic substrates containing thin films or may involve fabrication of thin film components or networks on top of a thermal silicon dioxide film on silicon wafers.

I. Thin Film Capacitors

The three forms of thin film capacitors listed in Table 1 constitute the types which have established themselves to date. They also happen to represent three methods of dielectric fabrication: evaporation (SiO), anodization (Ta_2O_5), and sintering of a glass frit. Each form has its particular attractive features. Silicon monoxide fits readily into all-vacuum circuit processing if employed with evaporated metal film or cermet resistors. Tantalum pentoxide normally requires wet processing for best results, but in return it offers highest working stress and highest capacitance per unit area. If one wishes to avoid vacuum processing entirely, then fired glasses recommend themselves. Electrode materials are usually selected to be compatible with component processing.

II. Thin Film Resistors

Resistors cover a wider range of materials as shown in Table 2 which lists the principal candidates. Processes of deposition include evaporation, sputtering, pyrolysis, and sintering. Pattern formation is normally by mechanical mask, photolithography, and silk screen.

The "cermet" types, in which we may include evaporated Cr-SiO or fired conducting glazes derive a great deal of their value from their wide range of available specific resistivities. Evaporated and sputtered types, on the other hand, depend more on thinness of the layer and on narrow lines. Precise resistor values can be achieved by a final trim starting from values below the design objective. Methods of adjustment vary with the material, and include controlled thermal oxidation, anodization, and mechanical abrasion. Anodization and thermal oxidation provide, in addition to adjustment, a protective oxide film.

Table 1

Typical Properties of Film Capacitors and Dielectrics

	Ta_2O_5	SiO(1)	Hi-K Glass(2)
Dielectric Constant	22	6.8	600
Dissipation Factor, 1 kc	0.007	0.015	
Leakage $\frac{Amps}{\mu f}$ (10 v)	$5 \cdot 10^{-9}$	$2.5 \cdot 10^{-7}$	
(75 v)	$1 \cdot 10^{-6}$	$1.5 \cdot 10^{-5}$	
TC ppm/°C	+250	+600	*
Capacitance $\frac{\mu f}{cm^2}$	0.10	0.02	0.012
Dielectric Strength, $\frac{E}{cm}$	$4 \cdot 10^{-6}$	$2 \cdot 10^{-6}$	**
Precision	±3%	+3%	

(1) Degenhart & Pratt, 1961 Transactions of the Eighth National Vacuum Symposium, p. 859.

(2) New Material. Corning Glass Works. Electronic News, Aug. 26, 1964, p. 4, p. 48.

* Max. change, -15% from -55°C to +125°C.

** Rated Voltage, 50 volts on 1.7 mils.

Table 2

Properties of Planar Thin Film Resistors

Material	Ω/□	TC ppm/°C	Best TC ppm/°C	Routine Adjustment
Nichrome	10-300	-200 to +200	±20	±1%
SnO_2	25-400	-100 to -500	-100	±1%
Cr-SiO	30-1000	-100 to +200	-50	±1%
Pd-Ag Glaze	500-10,000	-200 to -500	-100	±1%
Ta(N)	5-200	-50 to -100	-50	±0.1%
Ta(O)	50-1000	-100 to -1000	*	±0.1%

* Available in the range shown for temperature compensation.

Full evaluation of resistors requires measurements of current noise, voltage coefficient, stability and moisture sensitivity.

III. Uses

It is important that the thin film circuit elements be reproducible and well understood. For the most part, however, the interest is not in discrete capacitors

and resistors, but in arrays fabricated on substrates in such a way as to constitute complete circuits. Such arrangements have many aspects relating to the general objectives of economy, reliability, and small size. In addition, specific applications may emphasize one or more of the following factors:

1. High frequency operation.
2. Ultra-high precision.
3. In situ RC tuning.
4. Distributed parameter capability.

General References

"Thin Film Circuit Technology," A. E. Lessor, L. I. Maissel, and R. E. Thun, IEEE Spectrum, 1, 73 (1964).

"Microcircuitry with Refractory Metals," D. A. McLean, WESCON Convention Record, 3, part 6, 87 (1959).

"Tantalum Components for Microcircuitry," D. A. McLean, Proc. National Electronics Conference, 16, 206 (1960).

"Properties of Tantalum Sputtered Films," D. Gerstenberg and E. H. Mayer, Proc. Electronics Components Conference, 57 (1962).

"Properties of Evaporated Film Capacitors," F. S. Maddocks and R. E. Thun, Jl. Electrochem. Soc., 109, 99 (1962).

"The Electrical and Structural Properties of Dielectric Metal Mixtures," M. Beckerman and R. E. Thun, Trans. Eighth National Vacuum Symposium, 905 (1961).

"Properties of Evaporated Thin Films," D. B. York, Jl. Electrochem. Soc., 110, 271 (1963).

"Low Leakage Thin Film Capacitors," R. A. Rossmeist and F. M. Uno, Trans. Tenth National Vacuum Symposium, 449 (1963).

"Multilayered Thin Film Capacitors," H. J. Degenhart and I. H. Pratt, Trans. Eighth National Vacuum Symposium, 859 (1961).

"Resistive Metal Glaze and Its Product Applications," H. Casey, W. Mulligan, and J. Woods, Proc. Electronic Components Conference, 20 (1963).

"Reactively Sputtered Metal Oxide Films," L. Holland and G. Siddall, Vacuum, III, 375 (1953).

PARAMETER MEASUREMENTS IN THIN DIELECTRIC FILMS*

J. V. Cathcart

Oak Ridge National Laboratory
Oak Ridge, Tennessee

This paper attempts to summarize the advantages and limitations of ellipsometry and X-ray diffractions as methods for characterizing thin films. The results of a study of oxide films on copper crystals are used to illustrate the kinds of information that can be obtained.

In the X-ray studies[1] a standard X-ray diffractometer was employed equipped with a doubly bent LiF monochromator and a thorium-activated NaI scintillation counter as a detector. This unit was used to examine appropriate Bragg reflections from the Cu_2O films. The key requirement of the method is that the film be a single crystal or at least highly oriented. Rocking curves for such films yield a measure of the mosaic spread of the films as well as thickness data (e.g., the thickness of a film formed at room temperature on copper was shown to be 20 A). Analysis of the line contours obtained during a 2θ scan of the specimen also gives information regarding the thickness, average strain, and strain gradient in the films.

In contrast to an X-ray diffractometer, an ellipsometer[2] is a relatively little known device. It is an optical instrument which operates on the principle that when plane polarized light is reflected from a film-covered surface, in general, the components of the electric vector parallel and perpendicular to the plane of incidence undergo different phase changes and suffer different degrees of amplitude reduction during reflection. Consequently the reflected light is in general elliptically polarized. The thickness and the refractive index of the film may be deduced from the degree of ellipticity of the reflected beam.

An ellipsometer is capable of detecting changes in average film thickness of approximately 1 A. Its measurements are nondestructive and may be made from a distance. Only a relatively small specimen surface area is required, and edge effects are eliminated altogether. For these reasons the ellipsometer also lends itself to rate studies in which the growth of a film is involved.

The disadvantages of an ellipsometer are related in large measure to the complexity of the optical equations which must be used to describe the reflection process[3]. Even in dealing with the case of an isotropic film on an isotropic substrate,

---

*Research sponsored by the U. S. Atomic Energy Commission under contract with the Union Carbide Corporation.

a computer is a virtual necessity. The equations applicable to optically anisotropic systems have been worked out but have yet to be tested experimentally.

Readings taken with the ellipsometer are related to the relative amplitude reduction, $\tan\psi$, and the relative phase retardation, Δ, suffered on reflection by the parallel and perpendicular components of the electric vector of the incident light; $\tan\psi$ and Δ are in turn related to the Fresnel coefficients for reflection for the system:

$$\tan\psi \exp(i\Delta) = R^p/R^s.$$

The superscripts p and s refer, respectively, to the reflection coefficients of the parallel and perpendicular components of the E vector. R^p and R^s are rather complicated functions of a number of variables, all of which are directly measurable except n_2 and d, the index of refraction and thickness, respectively, of the film. Thus

$$\tan\psi \exp(i\Delta) = f(n_2,d). \qquad (1)$$

Since Eq. (1) contains two unknowns, it cannot be solved directly, although a graphical solution may be obtained as follows:

a) One obtains a set of $\tan\psi$ and Δ values by measuring these quantities for several films of different but unknown thickness.

b) A value is assumed for n_2 and sets of $\tan\psi$ and Δ are calculated for several film thicknesses.

c) The calculated and experimental $\tan\psi$ vs Δ curves are then compared and the calculated curve adjusted (by selecting new values for n_2) until the two curves coincide. The matching of the curves is taken as an indication that the correct value of n_2 has been chosen. Equation (1) may then be used to associate thickness values with each pair of $\tan\psi$ and Δ values.

Specific problems associated with the use of the ellipsometer are best illustrated by the results of a study of thin Cu_2O films on copper[4,5]. Both copper and cuprous oxide have cubic crystal structures and in the bulk are optically isotropic. While attempting to measure the thickness of such films on the (311), (110), (111), and (100) of a copper single crystal, we observed, however, that for the (311) and (110), a rotation of the specimen about its surface normal produced periodic changes in the apparent film thickness indicated by the ellipsometer. Maxima and minima in the apparent film thickness occurred at 90° intervals as shown in Figure 1. Examination of the (311) and (110) under a polarizing microscope confirmed the fact that the oxide on these planes was optically anisotropic. A variation in the degree of anisotropy with film thickness was also noted with a maximum in anisotropy occurring at about 300 A. No such behavior was observed for the oxide on the (111) and (100). It was possible to rationalize these facts qualitatively through a consideration of the epitaxial stresses between the oxide and the metal.

These results illustrate the possibilities of using the ellipsometer to study strain anisotropy and changes in the degree of strain anisotropy in thin films.

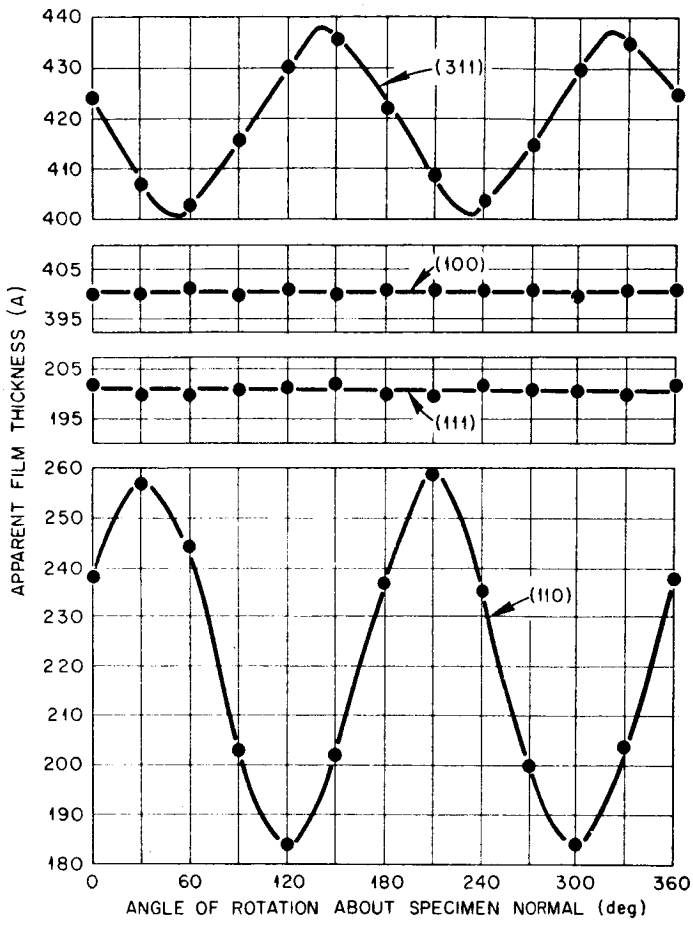

Fig. 1. Variation of Apparent Oxide Film Thickness on Four Crystallographic Planes of Copper as a Function of the Angle of Rotation about the Film Normal. After Cathcart, Epperson, and Petersen (ref. 5).

They also underscore, however, the danger of considering the oxide as a uniform, homogeneous film and emphasize the need for the development of a more realistic optical model for the films if the full potential of the ellipsometer is to be realized.

Fortunately, the application of the X-ray technique mentioned above provided considerable insight into the structural details of the films. The physical picture of the oxide as indicated by the X-ray data may be summarized as follows: In general the oxide film is subject to epitaxial forces in the plane of the surface, causing the oxide to be compressed in a lateral direction; normal to the surface there is a corresponding expansion of the lattice. A strain gradient exists in the film, which implies the existence of a corresponding gradient in the index of refraction of the oxide. Likewise, the average lattice parameter of the film varies with thickness, implying that the average index of refraction of the oxide also is a function of film thickness.

An attempt was made to utilize these findings in the formulation of a new optical model for the oxide. The film was considered to consist of m layers each of which was treated as a homogeneous, isotropic medium. The index of refraction was allowed to vary from layer to layer, and the average index of refraction of the film was assumed to change with film thickness. Applying the recursion formulas developed

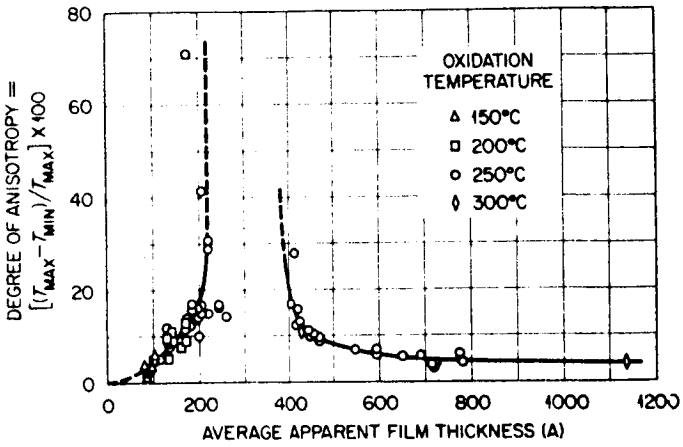

Fig. 2. Variation of Degree of Anisotropy of Oxide on the (110) of Copper as a Function of Film Thickness. After Cathcart, Epperson, and Petersen (ref. 5).

by Wolter[6] for reflection from multilayered films, ellipsometer data for oxide films on the (111) of copper were used to test the new model. Compared with the results obtained using the classical model, a better fit was achieved between the calculated and experimental tan ψ vs Δ curves, and the film thickness values were in much better agreement with those obtained from the X-ray data.

References

1. Borie, B. S., Acta Cryst. 13, 542 (1960); Borie, B. S. and Sparks, C. J., Ibid. 14, 569 (1961).

2. Winterbottom, A. B., J. Opt. Soc. Am. 38 , 1074-82 (1948); K. Danske videnskabernes Selskab Skrifter, 1955 NR 1, p. 1.

3. McCrackin, F. L., Passaglia, E., Stromberg, R. R., and Steinberg, H. L., J. Res. Nat. Bur. Std., A. 67, 363-377 (1963).

4. Borie, B. S., Sparks, C. J., and Cathcart, J. V., Acta Met. 10, 691-697 (1962).

5. Cathcart, J. V., Epperson, J. E., and Petersen, G. F., Acta Met. 10, 699-703 (1963).

6. Wolter, H., "Optik dünner Schichten," Handbuch der Physik, Vol. XXIV, pp. 461-544, Springer-Verlag, Berlin, Götingen-Heidelberg, 1956.

CONDUCTION IN THIN OXIDE INSULATORS

T. W. Hickmott

General Electric Research Laboratory
Schenectady, New York

ABSTRACT

Conduction in thin oxide films, films between 10Å and 10,000Å thick is characterized by the complexity of the current-voltage characteristics that have been observed. For insulating oxide films, conduction mechanisms proposed include tunneling, field assisted thermal emission from the metal contact (Schottky emission) or from traps, and impurity conduction. Some of the difficulties in comparing theory and experiment will be discussed. Voltage-controlled negative resistance and high conductivity can be established in the current voltage characteristics of insulating films by applying voltage to metal-insulator-metal diodes with insulator thicknesses greater than about 100Å. Phenomena such as electron emission and electroluminescence which are associated with this conducting state will be described.

CONDUCTION IN THIN ORGANIC INSULATORS*

N. M. Bashara

The University of Nebraska
Lincoln, Nebraska

Phenomenologic models have been developed which provide a qualitative understanding of the conduction in certain insulators[1-5]. Use of the models in the interpretation of the data requires a reservoir of carriers (ohmic contact) at the contacting electrode[6,7]. Ohmic contact appears to be related to the overcoming of surface states[8] which if unneutralized drastically reduce the number of injected carriers. The models appear to fit the behavior of cadmium sulphide[1], selenium[9] and anthracene[10] where sample thicknesses greater than a few microns are used.

Recently, Bashara and Doty[11,12] have reported on polybutadiene films less than 500 angstroms thick formed in a glow discharge. (Information on fabrication and test procedures as well as details of experimental results are found in the Journal of Applied Physics, December, 1964). The following are among the most significant results.

At room temperature and at fields of about 10^5 v/cm the dc resistivity is in the range of 10^{12} to 10^{13} ohm-cm where ohmic contact is established and about 10^{16} ohm-cm where it is not. The ac resistivity at fields under 10^4 v/cm is about 10^{13} ohm-cm and did not vary by more than a factor of three between ten specimens. The dc resistivity changes by 5 to 6 orders of magnitude over a temperature range of -190°C to 110°C in contrast to the ac value which changes by a factor of 4 or 5 in the same temperature range.

The current-voltage characteristic is space-charge limited. However, to achieve this mode of behavior it was necessary in all cases except one to operate at fields which resulted in field emission. It appears that tunneling through the contact barrier has occurred. Supporting this suggestion is the fact that the potential barrier near the electrodes is reduced in magnitude and narrowed as the film thickness decreases. Of general interest is the possibility that thin films make it possible to tunnel through the blocking contact thereby eliminating the need for "matching" characteristics at the metal-insulator interface to establish ohmic contact. The result would be of interest to dielectricians since the procedure to achieve ohmic contact by matching characteristics is not well understood.

The voltage and thickness dependence associated with space charge limited current was observed. Current was found to increase with voltage raised to the nth

*Supported by the Office of Naval Research. NONR3718(01).

power and was proportional to reciprocal thickness raised to 2n where n is greater than 2.

$$I \alpha \frac{V^n}{L^{2n}}$$

where I = current,
V = voltage,
L = thickness,
N > 2

In a number of specimens current starts to increase at about 3×10^4 v/cm but does not reach space charge limited operation which is characterized by the voltage and thickness dependence discussed previously. Apparently current injection efficiency is not great enough to overcome the traps.

Further evidence of space charge limited operation is provided by the following. As temperature is decreased, the current is lowered and rises more rapidly with increase in voltage. Also, the onset of an increase in current shifts to a higher voltage. Since trap occupancy is reduced at a lower temperature the Fermi level falls. The voltage must then be increased to increase the injection current so as to raise the Fermi level and restore the current to its value at the higher temperature.

References

1. Rose, A., Phys. Rev. 97, 1538 (1955).
2. Rose, A., Concepts in Photoconductivity and Allied Problems (Interscience Publishers, 1963).
3. Lampert, M. A., Phys. Rev. 103, 1648 (1956).
4. Lampert, M. A., Phys. Rev. 125, 126 (1962).
5. Lampert, M. A., Proc. IRE 50, 1781 (1962).
6. Smith, R. W., Phys. Rev. 97, 1525 (1955).
7. Kallman, H. and Pope, M., J. Chem. Phys. 32, 300 (1960).
8. Bardeen, J., Phys. Rev. 71, 717 (1947).
9. Lanyon, H. P. D., Phys. Rev. 130, 134 (1963).
10. Symposium on Electrical Conductivity in Organic Solids (Interscience Publishers, 1961).
11. Bashara, N. M. and Doty, C. T., Bulletin Am. Phys. Soc. 9, 428 (1964).
12. Bashara, N. M. and Doty, C. T., J. Appl. Phys. (to be published) December, 1964.

EXPERIMENTAL VERIFICATION OF THE WLF SUPERPOSITION TECHNIQUE

Anthony J. Bur

National Bureau of Standards
Washington, D. C.

In 1955, Williams, Landel, and Ferry[1] (WLF) analyzed the mechanical and dielectric relaxation measurements on a number of glass forming liquids. They found that in the temperature range T_g to T_g + 100K°, where T_g is the glass transition temperature, a universal equation governed the temperature dependence of the relaxation times,

$$\text{Log } b_T = \log \tau/\tau_o = - \frac{C_1(T-T_o)}{C_2+T-T_o} \quad , \qquad (1)$$

where τ and τ_o are relaxation times at temperatures T and T_o, T_o is a reference temperature approximately equal to T_g + 50K°, and C_1 and C_2 are "universal" constants. The values of b_T for a given substance where obtained by observing the frequency shift that the normalized or reduced relaxation parameters (the dynamic mechanical modulus or dielectric constant) undergo with a change in temperature and by observing the successful superposition of the data to some reference temperature[2].

The superposition of data allows an observer to expand his available experimental frequency range by changing the temperature of the sample, since lowering the temperature of the system corresponds to increasing the frequency. We have decided to test the superposition by observing how well the dispersion curve obtained from superposition agrees with the actual measurement of the curve over the entire frequency range. To do this, measurements of the real and imaginary parts of the dielectric constant, ϵ' and ϵ'', of polyvinyl decanoate have been made over a frequency range of 10 Hz to 2.5 x 10^8 Hz at 23°C. The resulting curve is shown to coincide within experimental error with the previously published[3] dispersion curve for this same sample which was obtained by a superposition of data. The polyvinyl decanoate, $[\ -CH_2C(OC{=}OC_9H_{20})H-\ ]_m$, was characterized by a weight average molecular weight M_w = 0.90 x 10^5 and by a glass transition temperature $T_g \approx$ -60°C.

The dielectric cell and the equipment used to cover the available experimental frequency range of 10^{-2} Hz to 6 x 10^8 Hz will be discussed in detail in a future publication[4]. The accuracy of the measurement of ϵ' is ±1% over the entire frequency range. The accuracy of the measurement of ϵ'' is ±2% in the frequency range 10^{-2} Hz to 10^5 Hz and ±4% in the frequency range 10^5 Hz to 6 x 10^8 Hz.

Results and Discussion

Figure 1 shows the coincidence of the directly measured dispersion curve and the data obtained by superposition. The superposed data[3] resulted from data taken at 9 different temperatures between -30°C and +32°C and over a frequency range from

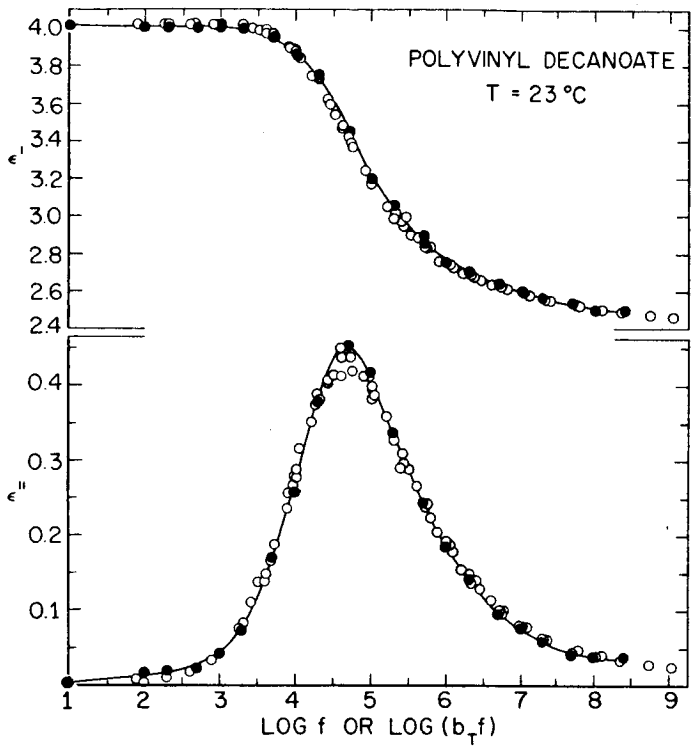

Fig. 1. The Real and the Imaginary Parts of the Dielectric Constant, ϵ' and ϵ'', Plotted Against the Log of the Frequency for Polyvinyl Decanoate at 23°C. Open Circles Represent Data Obtained by Superposition; Closed Circles Represent Data Which were Directly Observed at 23°C.

10^2 Hz to 5 x 10^4 Hz. Attention should be focussed on the frequency region between the 5th and 9th decades which is the "unattainable" region as far as the superposition curve is concerned. It is in this region that the unsymmetric character of the loss curve develops and a plot of ϵ'' vs. ϵ' yields the Davidson-Cole[5] skewed arc with the parameter $\beta = 0.40$ which is typical of glass forming substances. Thus, it may be said that we have obtained the Davidson-Cole skewed arc by a direct measurement over the entire frequency range as well as by a superposition of data from a range of temperatures. The exact molecular mechanism which gives rise to the Davidson-Cole dielectric relaxation is, as yet, unknown, and it is apparent from this presentation that a molecular model chosen to describe the Davidson-Cole dielectric phenomenon must also point out the intimate relationship between the WLF equation and Davidson-Cole equation.

References

1. Williams, M. L., Landel, R. F., and Ferry, J. D., J. Am. Chem. Soc. 77, 3701 (1955).
2. Ferry, J. D. and Strella, S., J. Colloid Sci. 13, 459 (1958).
3. Bur, A. J., Ph. D. Thesis, The Pennsylvania State University, 1962.
4. Broadhurst, M. G. and Bur, A. J., J. Research Natl. Bur. Standards (to be published).
5. Davidson, D. W. and Cole, R. H., J. Chem. Phys. 19, 1484 (1951).

DIELECTRIC SPECIMEN HOLDER FOR ELECTRONIC MATERIALS

Edwin C. Bamberger and John L. Dalke

National Bureau of Standards
Boulder, Colorado

ABSTRACT

This paper will describe a specimen holder that is used in the evaluation of the dielectric properties of electronic materials. Data for ϵ', ϵ'', and dissipation factor are obtained from the difference between the capacity and conductance of a material with known dielectric properties and that of the specimen under investigation. The design is particularly adaptable to measurements at reduced or elevated temperature. Such measurements are usually encumbered by changes in the holder's capacitance calibration with temperature. The method to be described requires no capacitance or length calibration per se. Under these measurement conditions, parameters such as extraneous capacity, inductance and resistance, leads and systems can considerably reduce errors provided that both measurements are obtained at the same temperature and frequency.

This system operates from -190°C to +200°C over a frequency range from 50 Hz to about 10 MHz. The present holder is being used as an experimental device to determine what improvements are necessary to extend the range from liquid helium temperatures to over +700°C. Such holders are being used to obtain the dielectric frequency spectrum, with temperature as a parameter, of materials such as high purity alkali-halides.

CHARGE BEHAVIOR OF AN ABSORPTIVE DIELECTRIC*

M. M. Perlman

College Militaire Royal
St-Jean, Quebec, Canada

I. Introduction

When a non-ideal dielectric such as Carnauba wax is polarized between metal electrodes in a strong electric field (region A - Fig. 1), and stored with its surfaces shielded by metal plates (region B), its surface charge is observed to decrease reverse in sign and then "grow" to a large permanent value. This is known as the electret effect.

If the surfaces are unshielded, the charge is observed to decay (region C). If at any stage of the decay, the surfaces are shielded once more (region D), the charge "grows" back to a value smaller than that at the end of region B.

Gross[1] has explained qualitatively the reversal in region B by postulating the existence of two charges of different nature, a volume polarization $P(t)$ of polarity opposite to that of the adjacent electrode, called heterocharge, and a real surface charge $\sigma_r(t)$ due to discharges in the dielectric-electrode gap, of the same polarity as the adjacent electrode, called homocharge. The net surface charge $[\, \sigma_r(t) - P(t) \,]$ is the algebraic sum of the heterocharge and homocharge.

When the dielectric is shielded in region B, the field within the sample becomes negligibly small. The heterocharge decays thermally, while the homocharge remains relatively constant, causing the observed reversal in sign of the net surface charge.

Wiseman and Feaster[2] developed a phenomenological theory of the electret effect based on the two charge theory of Gross. They were able to fit quantitatively the "growth" of the net surface charge in region B (dielectric shielded). This work studies the decay of the net surface charge in region C, (dielectric unshielded), where a time dependent internal field exists and the conductivity of the dielectric permits a decay of the real surface charge.

II. Superposition Principle, Ohm's Law and Charge Decay

The polarization response $P(t)$ of a non-ideal dielectric to a varying internal field $E(t)$ according to the superposition principle[3] is

$$P(t) = E(0)\ \pi(t) + \int_0^t \frac{dE(T)}{dT}\ \pi(t - T)\ dT \qquad (1)$$

where $\pi(t)$ is the polarization per unit applied step field.

---

*Supported by the Defence Research Board of Canada under grants 5501-08, 5501-33.

This paper is a preliminary report of an article to be published by the Journal of Applied Physics in Jan. or Feb. 1965.

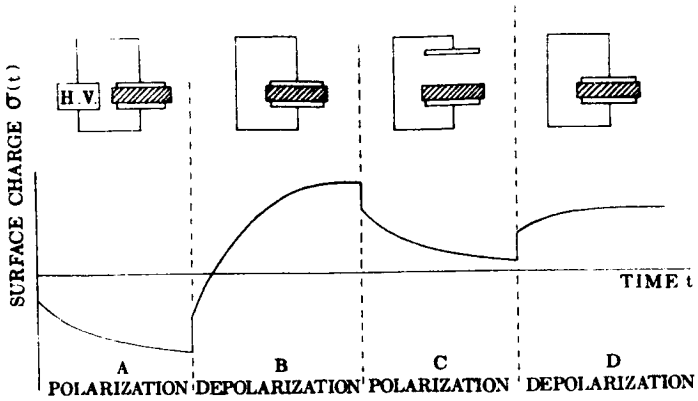

Fig. 1. Typical Behavior of the Net Surface Charge $\sigma(t)$ of a Non-ideal Dielectric Under an Applied Field in A, Shielding by Metal Electrodes in B, Unshielding in C, and Reshielding in D.

Using Maxwell's equations for a 2-layer capacitor, one can show that

$$E(t) = \frac{V + \left[\sigma_r(t) - P(t) \right] d'/\epsilon_o}{d + d'} \tag{2}$$

where V is the potential difference applied across the two electrodes; and d and d' are the thicknesses of the sample and air gap respectively.

Using Ohm's law one obtains

$$\sigma_r(t) = \sigma_{r_o} - c \int_0^t E(t)\, dt \tag{3}$$

where σ_{r_o} is the initial real surface charge and c is the volume conductivity.

Using equations (1), (2), and (3) one obtains the following integral equation for the field

$$E(0)\, \pi(t) + \epsilon_o E(t) + \int_0^t \frac{dE(T)}{dT}\, \pi(t - T)\, dT + c \int_0^t E(t)\, dt = \sigma_{r_o} \tag{4}$$

The above equation holds only if there is no net local charge within the volume of the dielectric.

Using a specific polarization function $\pi(t)$ to be determined by experiment, the integral equation (4) can be solved for the field $E(t)$ by the standard method of Laplace transform.

Using this solution and Eq. (2), the relative net surface charge in region C is

$$\frac{\sigma_r(t) - P_s(t)}{\sigma_{r_o}} = \frac{K}{K} \left[Q_1 e^{-t/T_1} + Q_2 e^{-t/T_2} + Q_3 e^{-t/T_3} \right] \tag{5}$$

where $P_s(t)$ is the component of the polarization that responds slowly to charges in the internal field; the coefficients, relaxation times, and k depend on the conductivity of the sample and the constants of the $\pi(t)$ function (Figure 2); and K is the dielectric constant of the sample.

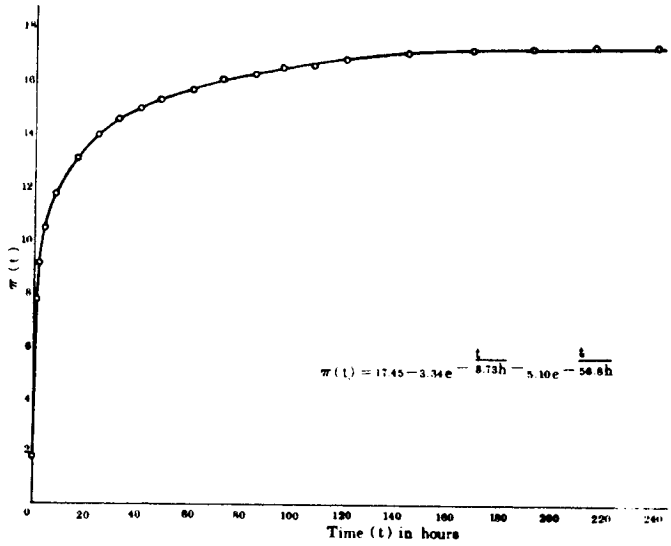

Fig. 2. Specific Polarization Function $\pi(t)$ for Carnauba Wax at 40°C, 10^{-5} Torr in Units of 10^{-11} Coulomb^2/nt-m^2.

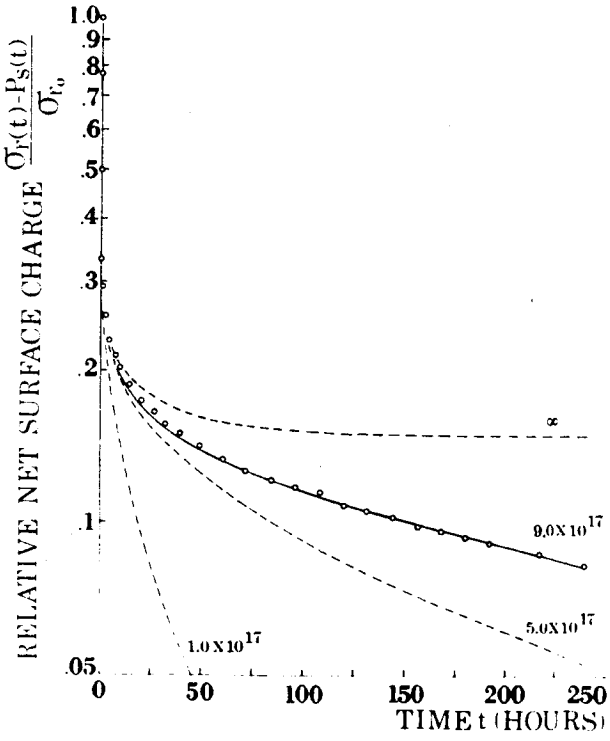

Fig. 3. Decay of the Relative Net Surface Charge of Carnauba Wax Electrets in the Unshielded State at 40°C and 10^{-5} Torr. The Open Circles are Experimental Points. The Solid Curve is a Plot of Eq. (9). Dashed Curves Show Predictions for Other Resistivities. Theory and Experiment Agree for a Resistivity of 9.0×10^{17} ohm-cm.

III. Experimental

Carnauba wax flakes were cast in molds, and then machined into disks flat and parallel to 10μ. The disks were placed in a dissectible capacitor, and charge deposited on their surfaces by an ion source. The dissectible capacitor was placed in an evacuated cylinder (10^{-5} Torr) and the cylinder placed in a constant temperature bath kept at 40 ± .05°C. The sample was unshielded to allow charge decay to take place, and measurements of surface charge were made by the standard method of induction.

The specific polarization function $\pi(t)$ was determined from charge measurements during reshielding in region D, and is shown in Figure 2. Using this $\pi(t)$, theoretical curves for a decay of the net surface charge during unshielding in Region C as given by Eq. (5) were calculated and are plotted for different resistivities in Figure 3. The open circles are experimental points.

Theory and experiment agree for a volume resistivity $9.0 \pm 0.5 \times 10^{17}$ ohm-cm and for a dielectric constant of 3.08 ± 0.12.

A more demanding test of the theory is to compare the experimental coefficients and relaxation times for the charge decay with the theoretical values from Eq.(5) for a resistivity of 9.0×10^{17} ohm-cm. This is shown in Table 1, and the agreement is considered good.

Table 1

Comparison of Experimental and Theoretical Coefficients and Relaxation Times

	Q_1	Q_2	Q_3	T_1	T_2	T_3
EXP	0.22	0.25	0.51	5.6 h	36 h	480 h
THEO	0.29	0.21	0.50	6.4 h	40 h	480 h

Preliminary measurements at 50°C indicate that the above phenomenological theory can be applied at this temperature as well. The polarization response is larger than at 40°C; theory and experiment agree for a volume resistivity of 2×10^{17} ohm-cm and a dielectric constant of 3.21.

Further measurements at elevated temperature on both charge and current are contemplated. The measurement of conduction currents should provide a determination of resistivities independent of the procedure used in this experiment.

References

1. Gross, B., Phys. Rev. 66, 26 (1944).
2. Feaster, G., Ph. D. Thesis, University of Kansas (1953); Wiseman, G. and Feaster, G., J. Chem. Phys. 26, 521 (1957).
3. Lepage, W. R. and Seely, S., General Network Analysis, McGraw-Hill, p. 424 (1952); MacDonald, J. R. and Barlow, C. A., Jr., Rev. Mod. Phys. 35, 940 (1963).

A ROGOWSKI SURFACE FOR DIELECTRIC STRENGTH TESTS

O. Milton

Sandia Corporation
Albuquerque, New Mexico

I. Introduction

A Rogowski contour has been used successfully in this study for determining dielectric strength. Random spatial distribution of dielectric breakdown in the uniform maximum field area was achieved together with an increase in the observed dielectric strength of the insulating material. This technique for determining dielectric strength avoids local increase of stress in the surrounding medium and thus prevents breakdown in locations of unknown electrical field value.

The molded plastic electrode contour used is one of a family suggested by Rogowski[1] and derived from the Maxwell transformation: $w = z + e^{z}$. Rogowski derived the expression

$$\frac{E}{E_o} = \frac{1}{(1+e^{x}+2e^{x}\cos y)^{1/2}}$$

which compares the field magnitude E, in the W plane to the field magnitude E_o, in the Z plane. The transformation maps the infinite parallel plate condenser, which cannot be achieved in practice, to a practical configuration. The advantage obtained is that the upper infinite plate has become terminated at one end, thus obtaining a practical possibility for an electrode configuration whose field is as well known as the infinite parallel plate condenser. The result is subject to the assumptions required for a two dimensional analysis. The significance of these assumptions can be minimized by judicious dimensioning of the electrode surface.

An infinite family of possible surfaces for various choice of equipotential surfaces at various electrode spacings is possible. As Rogowski shows, it is preferable to choose an equipotential surface for $y \leq \pi/2$ so that the field decreases as one goes outward along the surface. We chose $y = 0.4\ \pi$ for our equipotential surface. This choice was dictated by two considerations. One, a choice of $y = \pi/2$ would have simplified the mathematics but it represented a borderline situation in regard to reduction of field on the extremities of the contour, and two, a choice of something less than $y = 0.4\ \pi$ would have given a contour of undesirable large size. The actual curves used are shown in Figure 1. Note that the $y = 0.4\ \pi$ curve has a different curvature for each dielectric thickness, and that the curvature gets more gradual as the thickness increases. For spacings greater than about 0.100 inch the curve begins to become impractical in size.

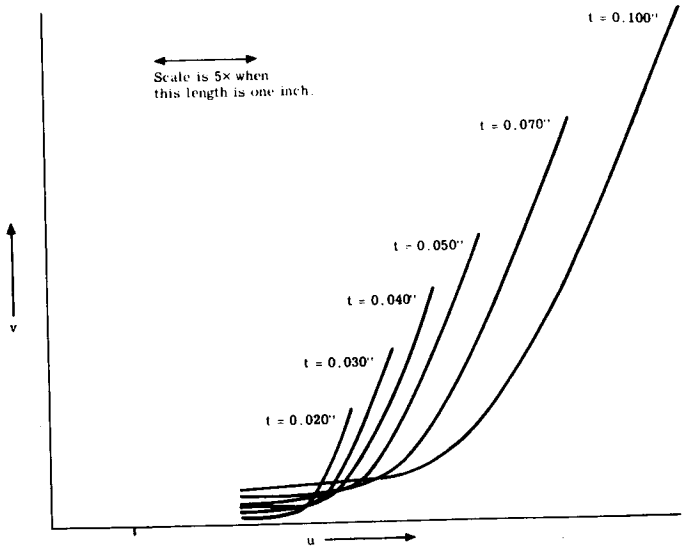

Fig. 1. Computer Plots of the y = 0.4 π Equipotential Curves for Various Thickness t.

The vector expression for the electrical field $\underline{Ew}$ at each point of the contour for each of the test shapes is

$$\underline{Ew} = \frac{P_o e^x \sin y}{A\pi(1+e^{2x}+2e^x \cos y)}\,\underline{i} - \frac{P_o(1+e^x \cos y)}{A\pi(1+e^{2x}+2e^x \cos y)}\,\underline{j}$$

P_o is the applied potential and A is a scaling factor. Occasionally a sample breaks down outside the flat maximum field area and this equation permits analysis of the field at the point of breakdown. This also allows correction of data for statistical analysis.

The variation of the field on the y = 0.4 π contour is shown in Figure 2. It can be seen that the decrease in field is exponential and falls off very rapidly as one goes outward along the contour. A six per cent field point was arbitrarily chosen as a point of termination for the contours.

II. The Experimental Technique and Materials

Several molding materials of good electrical and molding property were chosen for preliminary investigation of the use of the y = 0.4 π contour in dielectric strength testing.

A computer-controlled mill made a mold which molded or cast dielectrics to the desired shape. A stack of these test samples about 4 inches in diameter for contours of test thickness ranging from 0.020 inch to 0.100 inch is shown in Figure 3. Also shown is a plug used to plot the breakdown location and a sample that has been electroded and tested. The clear plug is inserted into the cavity of the test specimen after breakdown and the location of the breakdown noted with respect to the scribed lines. Indexing is accomplished by means of an index mark molded into the test sample.

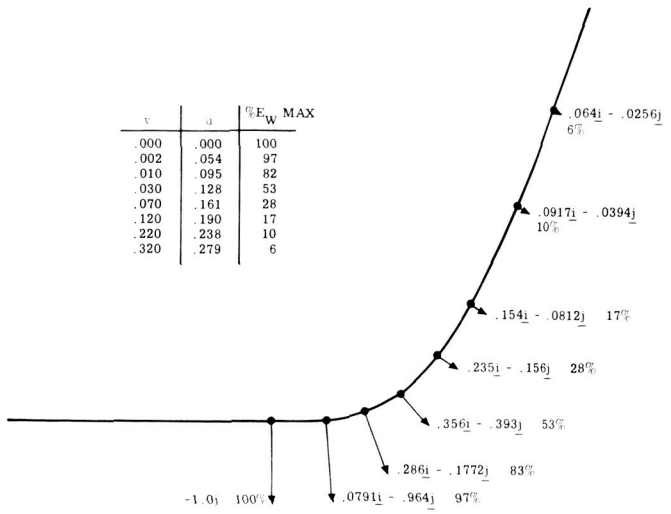

v	u	%E_w MAX
.000	.000	100
.002	.054	97
.010	.095	82
.030	.128	53
.070	.161	28
.120	.190	17
.220	.238	10
.320	.279	6

Fig. 2. Magnitude and Direction of the Field Vector on the y = 0.4 π Contour.

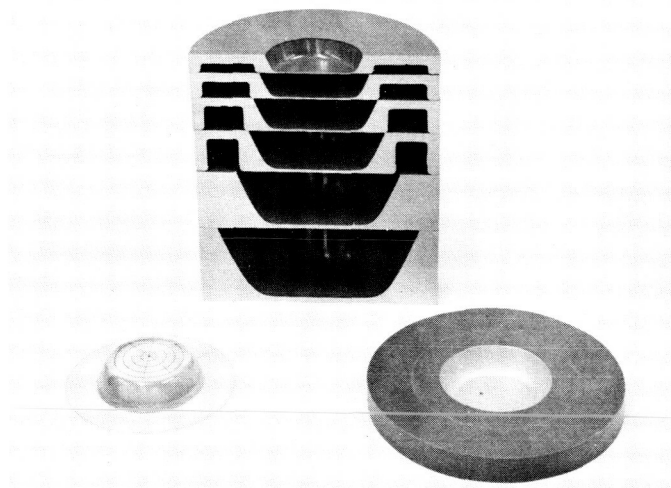

Fig. 3. Plastic Samples Molded to the y = 0.4 π Contour.

The accuracy of the contours was controlled to 3/10,000 inch. The samples were cleaned with vapor degreasing and then silver electrodes were sprayed on.

Tests were conducted with the samples in oil dielectric and heavy duty electrical generators supplying ac, dc, and pulses to 500 kv. The trapezoidal pulse used has about 20 microseconds duration and 3 microsecond rise time. The voltage was stepped up 5 kv at a time, once each second until breakdown.

III. Experimental Results

For purposes of comparison and evaluation of the significance of the results of the contour, Figure 4 shows results obtained with a typical test geometry using a cylindrical electrode of rounded edge and not recessed. The material is Diallylphthalate 52-20-30, a glass filled material. The design value for dielectric strength is about 500 v/mil for a 1/8-inch sample. The bottom curve is for ac and the top curve is for the pulse.

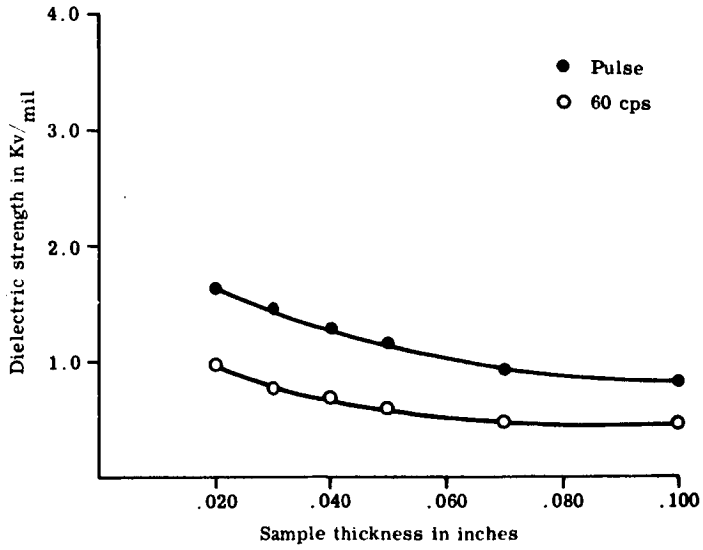

Fig. 4. Dielectric Strength vs. Thickness for Flat Samples and ASTM Electrodes. Diall 52-20-30.

For the thickness range of 0.020 inch to 0.100 inch the dielectric strength decreases from about 1.0 kv/mil to 0.5 kv/mil or the ASTM value. The pulse dielectric strength has a maximum of about 1.7 kv/mil decreasing to 1.0 kv/mil for the thicker samples. It appears to be about double the ac dielectric strength.

Values of dielectric strength obtained with the contour are shown in Figure 5. About a 70 per cent increase was obtained and the drop off with increasing thickness is not so apparent. If one applies Gumbel's extreme value statistics[2] to the data the dielectric strength is about 2.9 kv/mil regardless of sample thickness. The result is for individual sample lots of 30.

Figure 6 shows the location of the breakdown for 97 consecutive test samples of 6 different molding materials. The breakdowns are randomly located within the area of the uniform field. Only a few broke outside the flat area and these were accounted for by obvious flaws in the sample.

References

1. Rogowski, W., Die elektrische Festigkeit am Rande des Plattenkondensators. Ein Beitrag zur Theorie der Funkenstrecken und Durchfuhrugen., Archiv fur Elecktrotechnik, Vol. 12, No. 1, 1923.

2. Gumbel, E. J., "Statistical Theory of Extreme Values and Some Practical Applications," National Bureau of Standards Applied Mathematics Series 33, U. S. Government Printing Office, Washington, D. C., 1954.

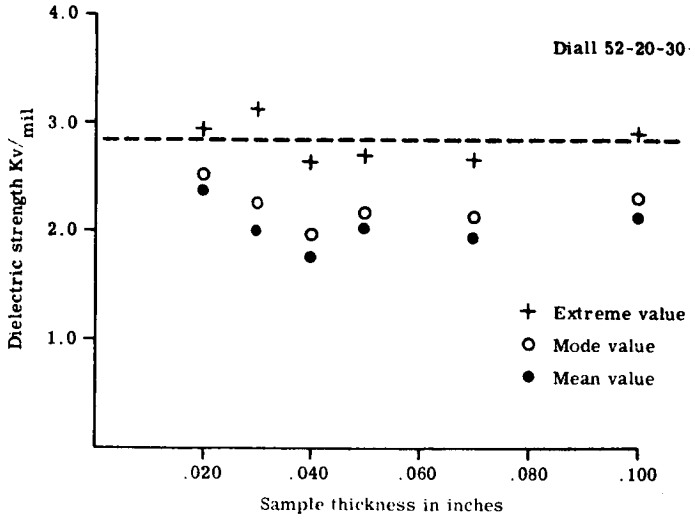

Fig. 5. Pulse Dielectric Strength Values for Six y = 0.4 π Contours.

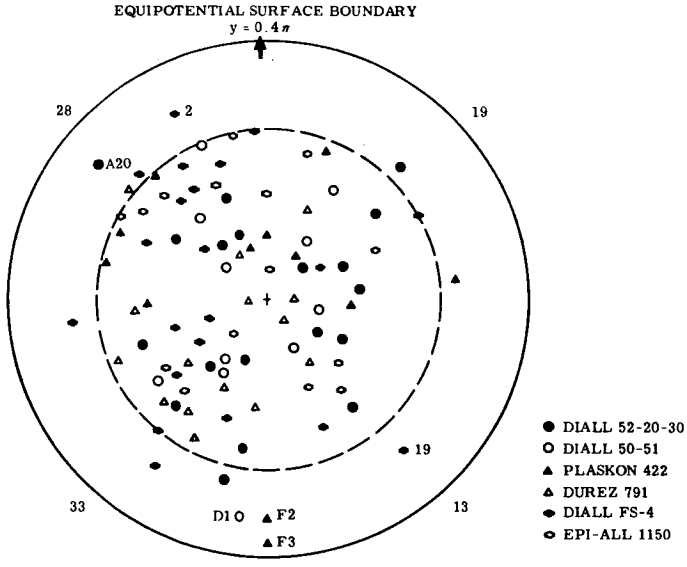

Fig. 6. Location of Punctures on the y = 0.4 π Contour.

A CONTROLLED THERMAL ENVIRONMENT FOR DIELECTRIC BREAKDOWN STRENGTH STUDIES

Lee J. Seligman

Sandia Corporation
Albuquerque, New Mexico

A small automatic temperature chamber has been developed in which it is possible to conduct dielectric breakdown strength tests and similar studies over the range of -10°C to +210°C with ±0.1°C stability. The chamber is of the fluid immersion type and was designed around a 220 kv pulse generator, although it is readily adaptable to most other types of high voltage generating equipment. Made of Pyrex, it is composed of two cylindrical vessels stacked vertically: the upper, called the test chamber, contains the specimen and the circulating temperature bath while the lower merely surrounds the high voltage bus bar with a room temperature fluid and reduces the flow of heat through this bus to the high voltage generator which has been calibrated at room temperature.

The dielectric fluid, having passed through a heat exchanger, enters the four-gallon test chamber from beneath and is forced to assume a circular flow pattern by three input tubes which protrude tangentially into the chamber. Thus as the fluid level rises, a selective heat field is developed; the outer, rapidly-rotating layers exchanging their heat with the chamber walls, the core rotating very little and retaining its temperature and that of the dielectric specimen within it.

In the system (Figure 1), the temperature chamber is supplied with a silicone dielectric fluid by a pump/heat-exchanger unit through three metal hoses, and exhausts to this unit in the same way. An auxiliary 430 W heater is shown wrapped around the set of input hoses and augments the two 500 W and 700 W submersible heaters in the heat exchanger. All heaters are singly controlled and may be operated in combination. (With all heaters on, the chamber temperature will reach +210°C in about 5 hours). When a desired temperature has been achieved in the chamber, an immersed contact thermometer actuates a relay which de-energizes the heaters in use. While this thermostatic action provides gross temperature pulsations at the pump, the

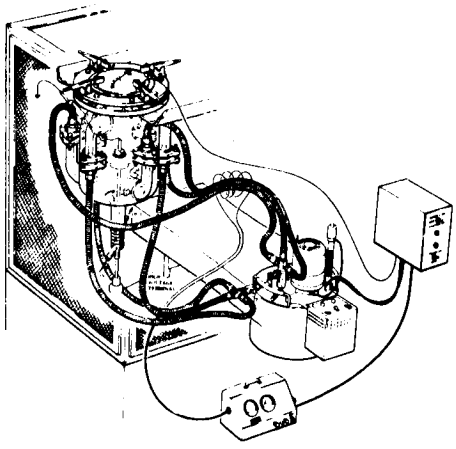

Fig. 1. Thermal Environmental Apparatus, Showing Temperature Chamber, Heat exchanger, and Control Box.

combination of its diffusive mixing action, the selective rotary flow pattern and glass wool insulation (not shown) serves to maintain the temperature at the dielectric specimen ±0.1°C.

Temperatures below ambient are achieved by passing a fluid heat sink through a submerged cooling coil within the heat exchanger. Control is provided by one heater with the contact thermometer. With the same silicone dielectric fluid, temperatures of -10°C have been reached but at the expense of bubbles and moisture condensation in the oil and of sluggish fluid flow. A dry atmosphere and a less viscous fluid would correct the latter two defects. However, the bubbling occurs at all temperatures and is a characteristic of the pump in this system.

To avoid long delay in bringing chamber and specimen to a high temperature, an automatic warmup system has been devised which starts pump and heaters at some early hour and ensures their safe operation. Should the hot fluid threaten to overfill the test chamber, for example, a floating switch shuts the entire system off, permitting the fluid to reestablish a safe level at which time normal operation resumes.

The tests performed in this environment have thus far been tests of dielectric strength, with electrodes of two types (Figure 2): an ASTM electrode combination of nickel-plated brass, and an imbedded $y = 0.4\ \pi$ Rogowski[1] contour coated with metallic paint to which the ASTM electrodes merely provide electrical contact. In both cases, positive voltage pulses of about 20 μs duration (Figure 3) were applied once per second, each successive pulse increasing in amplitude by 2.5 kv until breakdown occurred.

Using the first of these electrode configurations, Hysol epoxy 13-009[2] in flat sheets 4 x 4 square inches in area and having various thicknesses was tested to determine its dielectric strength versus thickness and temperature. The resulting surface (Figure 4) represents the mean of some 330 data and displays the expected decrease[3,4] of dielectric strength with increasing thickness and temperature in range.

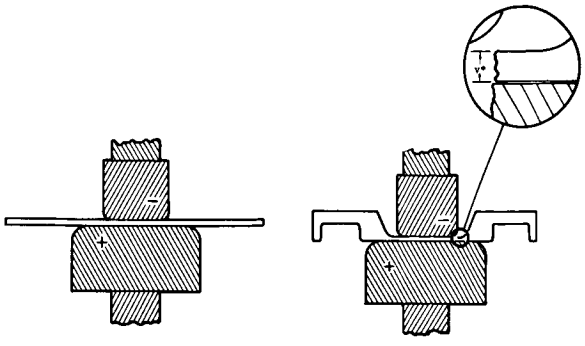

Fig. 2. Electrodes for Sheet-cast and Recess-molded Dielectrics. Top Electrode Diameter is one inch.

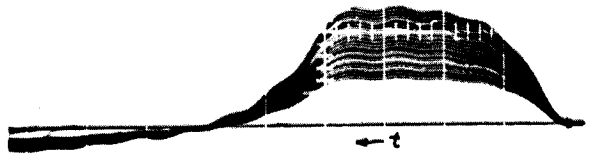

Fig. 3. Pulse Shape: 2.5 kv Increment Each Second, 5 μ sec per Division. 89 kv Breakdown.

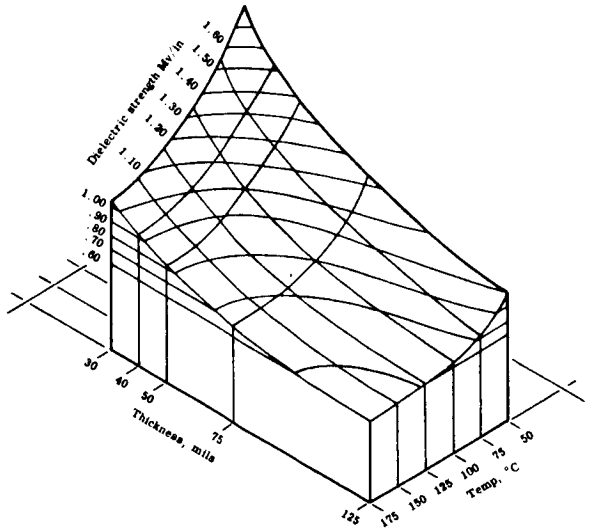

Fig. 4. Dielectric Strength of SRIR Epoxy Sheets Versus Temperature and Thickness.

In the second group, three materials were tested with the y = 0.4 π electrode: Diall 52-20-30 (diallylphthalate with kaolinite filler and reinforced with long glass fiber), Diall FS-4 (diallyl isophthalate with kaolinite filler and reinforced with long glass fiber), and Plaskon 422 (a mineral-filled alkyd molding compound). The data averaged for these tests appear in Figure 5.

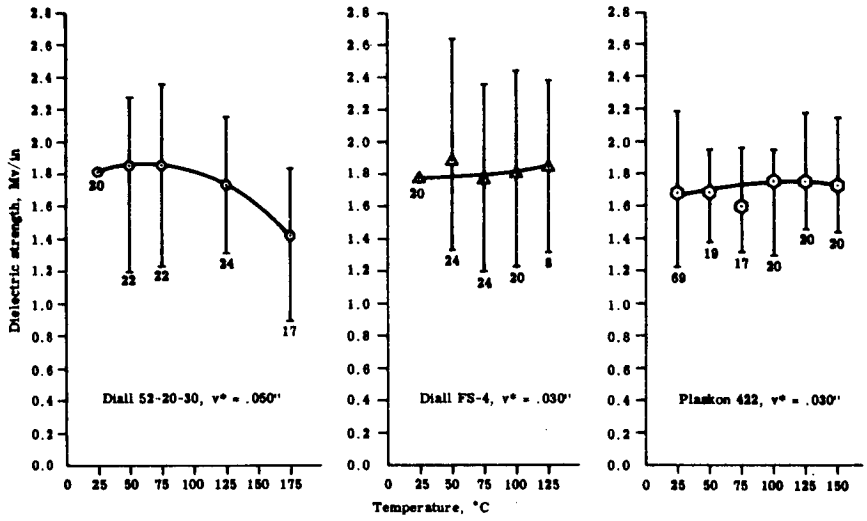

Fig. 5. Dielectric Strength Versus Temperature of Three Molded Resins with Imbedded Rogowski Contour.

References

1. Milton, O., "A Rogowski Surface for Dielectric Strength Tests," 33rd Conference on Electrical Insulation, NAS-NRC, October 1964.

2. Carroll, B. and Smatana, J., "Transparent Cold-Shock-Resistant Epoxy Casting Resin," SCR-173, Sandia Corporation, Albuquerque, April 1960.

3. Mason, J. H., "Electrical Insulation (Part I): Dielectric Breakdown," Electrical Energy, p. 68, November 1956.

4. Whitehead, S., Dielectric Breakdown of Solids, (Oxford, London, 1953), p. 39 ff.

PULSED, NON-UNIFORM FIELD ELECTRIC STRENGTH OF A HIGH POLYMER

J. L. Wentz

Sandia Corporation
Albuquerque, New Mexico

The purpose of this study was to obtain the voltage and current relations during electrical breakdown of an amorphous solid to help determine the nature of such a discharge. It was believed that such data, when compared with related pulse data by Milton, Seligman, and Allyn[1], would lead to a better understanding of the mechanisms of failure in amorphous solids. Voltage and current relations have been obtained along with a dielectric strength value of an epoxy casting resin (SRIR). The dielectric strength data are compared with data taken in a uniform field test.

A cable discharge system similar to the one used by Tucker[2] in exploding wire studies was used for some of the dielectric strength data. It consists of a dc power supply with reversible polarity; a length of charge storage cable; an adjustable spark gap with high pressure nitrogen capability, a length of delay cable; a test cell which also contains the current and voltage viewing resistors; and two high speed oscilloscopes with recording cameras. The sequence of operation is to adjust the spark gap to hold off the expected voltage when pressurized with dry nitrogen (up to 1000 psi), charge the storage cable to the desired voltage maximum (up to ±60kv) then release the pressure allowing the gap to breakdown, sending the stored charge into the second cable. A voltage pulse with a rise time of about 1 MV/μs is realized at the test cell. Pulse widths of 3 and 0.3 μs have been used.

The test sample contains 16 pins cast into a slab of the test resin with a common ground plane. Two 1 x 3 inch glass microscope slides form the flat surfaces of the sample and provide good optical properties.

A typical point may be approximated by a hyperboloid of revolution of the form, $x^2/a^2-y^2/b^2 = 1$, where the "a" constant is the gap length. A technique of rapidly determining the pin geometry is to match a photomicrograph (at 215X) of the tip to one of several hyperbola curves to find a best fit to a curve. Thereby, a value of the b/a ratio for any final gap distance found after potting can be assigned to each electrode.

The hyperbolic approximation is used since there are at least two different field solutions for this shape. One by Eyring[3] has been used extensively:

$$\left|\frac{E}{V}\right| = \frac{2k/(1-k^2)}{t \ln(\frac{1+k}{1-k})}, \quad \text{where } k^2 = \frac{x_i^2 - t^2}{x_i^2 + y_i^2 - t^2},$$

is a constant for a true hyperbola and t is the gap distance. The other equation considered[4] is

$$\left|\frac{E}{V}\right| = \frac{2}{\pi b} ,$$

and it is valid when the gap distance is equal to a. A comparison is made between the two in Figure 1 for a fixed ratio of b/a = 1/3. Since the Eyring geometry factor yielded much too high of a value, the latter expression was used in this study to compute the field. The value of V was taken from a voltage time trace during breakdown. Figure 2 shows a typical pair of traces during breakdown. These traces are for a negative signal, the positive signals are simply reciprocal images of these. The time trace is 50 ns/cm but for small gap separations, 20 ns/cm sweep times have been used. The point of breakdown is taken at the time the voltage drops and the current rises which are simultaneous within the limits of resolution of this system (provided that sweep trigger times are correlated). An analysis of the various traces indicates that breakdowns occurred within nanoseconds which confirms results of a streak camera test which showed that pre-cursers (similar to gas pre-breakdown streamers as shown by Meek and Craig[5]) in the solid formed at a velocity greater than 50 mm/μs. However, the velocity of propagation data are not conclusive and are therefore not reported at this time.

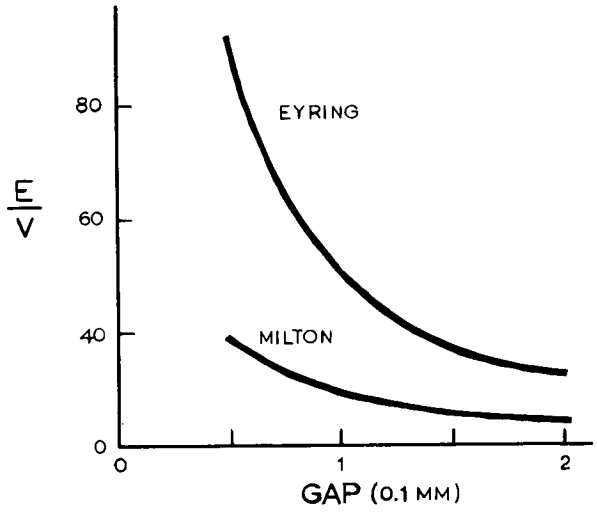

Fig. 1. Comparison of Two Field Geometry Factors for Conoidal Point Near Plane as a Function of the Gap Distance.

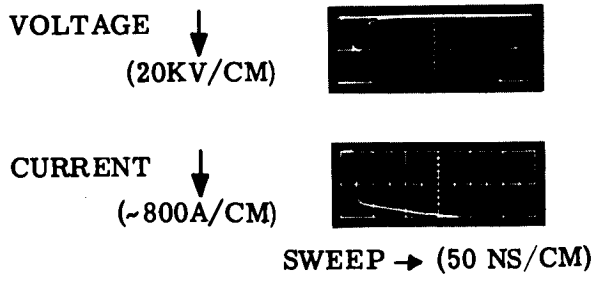

Fig. 2. Typical Traces During Breakdown in SRIR. Pin Cathode, Plane Anode. Gap = 0.25 mm.

Breakdown data are shown in Figure 3. The top graph represents data taken using the fast rise time by cable while the lower graph represents data taken using the transformer pulse[1]. Note that for fast rise times, it apparently makes no difference whether the pin is the anode or cathode. The degree of scatter on both graphs is within a factor of 2 which is quite good for most pulse type data.

The average value of 7.58 MV/cm for the pin anode data on the lower graph

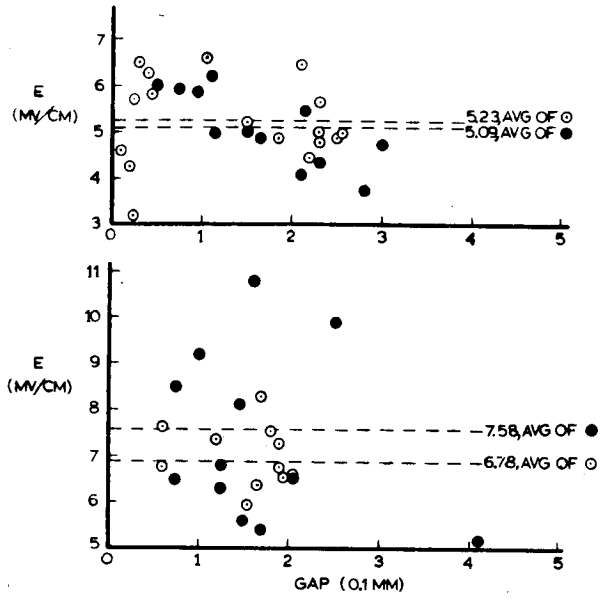

Fig. 3. Values of Dielectric Strength of SRIR Using Conoidal Points Near a Plane at the Gap Distances Shown. Rise Rate 1 MV/μs (Top) and 15 kv/μs (Bottom), Pin Anode ● , Pin Cathode ⊙ .

compares favorably with data taken on the same machine and polarity but with a Rogowski contour. These data, shown in Figure 4, were generated by Milton[4] and the ordinate represents dielectric strength in kv/mil while the abscissa is a frequency of the population after the Gumbel extreme-value statistics. The abscissa can also be made to represent ratios of areas and, if the data are interpreted to be controlled by a weak link mechanism which is proportional to sample area and if the data are extrapolated to the 1/10,000 point (off the graph), a value of 20 kv/mil (7.88 MV/cm) is obtained which is within 4 per cent of the 7.58 average in Figure 3. It should be mentioned that this extrapolation was made prior to the pin sample tests based on the fact that the ratio of the areas of the two test geometries is about 10,000 to 1!

The conclusions reached as a result of this study are: that electrical breakdown in amorphous solids occurs within a few nanoseconds when the critical field is reached and maintained, the inexpensive cable discharge system is suitable for obtaining pulsed dielectric strength data, and the small volume configuration yields data which is suitable for quantitative analysis.

References

1. Milton, O., Seligman, L. J., and Allyn, J. B., Papers No. 23, 26, 27 and 28 respectively, 33rd Annual Meeting, Conference on Electrical Insulation, NAS-NRC, Cleveland, Ohio, Oct. 11-14, 1964.

2. Tucker, T. J., "Square Wave Generator for the Study of Exploding Wires," Rev. of Sci. Instr., Vol. 31, No. 2, 165 (Feb. 1960).

3. Eyring, C. F., Mackeown, S. S., and Millikan, R. A., "Field Currents from Points," Phys. Rev., Vol. 31, 900 (May 1928).

4. Milton, O., Sandia Corporation, Private Communication.

5. Meek, J. M. and Craggs, J. D., Electrical Breakdown of Gases, Clarendon Press, Oxford, 1953.

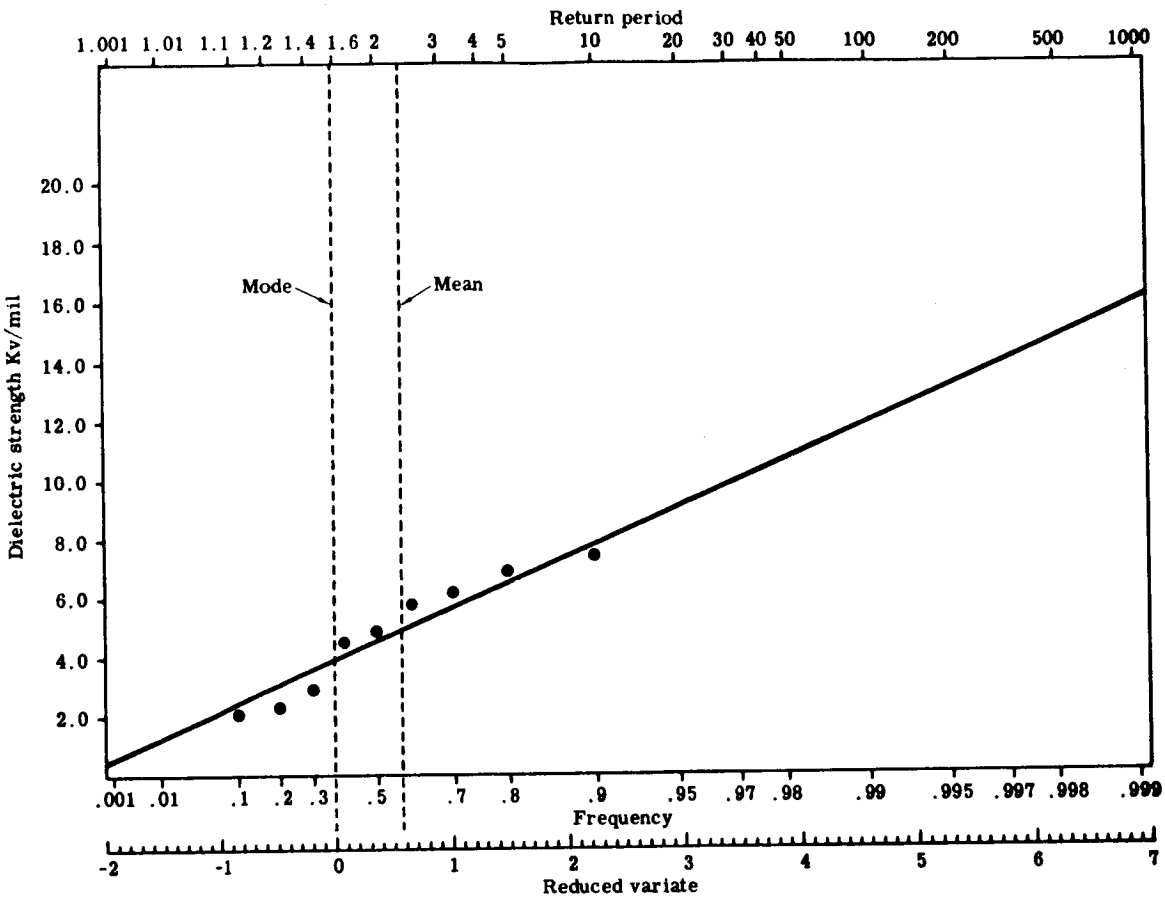

Fig. 4. Distribution of Pulse Dielectric Strengths for SRIR Epoxy. Contoured Sample, 0.030 Inch Thick with 1.11 Square Inch Area.

APPLICATION OF THE POINTED ELECTRODE IN EVALUATING PULSE LIFE OF CASTING RESINS

O. Milton

Sandia Corporation
Albuquerque, New Mexico

This paper describes a method of electrically evaluating the suitability of resins for potting pulsed transformers and circuits.

The needle point represents one of the worst conditions in practice as far as inducing breakdown is concerned and it is a simple geometry to achieve, therefore an electrically pulsed needle point is used in the test.

The work of Olyphant with a point-to-plane configuration was of especial value to us for he showed that the tree breakdown was progressive and that a void, once started, would slowly erode[1]. The time to failure was observed as the dependent variable to evaluate the resin. Tests up to 2500 hours were made without breakdown.

Since we are interested in pulse resistance, it was natural to make the number of pulses to breakdown, rather than the time to breakdown, the dependent variable.

I. Experimental Procedure

The electrode point is at the end of a conically tipped cylinder of 1/4-inch diameter. Each rod was hardened and ground under an identical machine set up, tip radius was about 7.5 microns as determined from photomicrographs at 215X magnification. The point was in the center of a block of casting resin, either a 2-inch cube or a 4-inch cube, thus allowing either one or two inches of dielectric in all directions from the tip. The electrode was electrically positive (we observed that the failure progresses faster this way than if the electrode is negative) and a counter electrode was not used. Many of the resins used for encapsulation are clear for purpose of visual inspection; thus it was possible to see the tree that forms during the test and look for flaws such as bubbles or impurities before the test starts.

The pulse used was trapezoidal in shape with a duration of about 20 microseconds and a rise time of about 3 microseconds. A 200-kv pulse applied once each second was used in the test; it was found that this voltage would break our best material down in less than 10,000 pulses. A hypodermic needle was cast into the resin in order to analyze the decomposition products formed in the course of the pulsing. Decomposition gases were collected from the needle and analyzed with a Beckman infrared spectrophotometer.

Stress patterns were observed in the test blocks with polarized light. The stress results from shrinkage of the resin during cure.

The pulse generator used in the testing, designed and built in this laboratory by J. H. Lovelace, has a 500-kv capability with variable pulse length. It steps up voltage automatically and repeats pulses at various time intervals.

II. Results

Figure 1 shows dielectric strength values for 6 casting resins of varying filler, cure schedule, hardener, or polymer system; note that, although the epoxy system changes significantly, there is not a great change in the dielectric strength result. If a selection were to be made on the basis of this data the TIR or Transformer Impregnation Resin would not be selected for pulse use when in fact it turns out to be one of the best materials studied.

MATERIAL		DIELECTRIC STRENGTH ASTM D 149	
FORMULA	CURE	SHORT TIME 1/8 INCH VOLTS/MIL	STEP BY STEP 1/8 INCH VOLTS/MIL
828 - 100 DEA - 12	15 HRS AT 165°F	513 ± 30	
828 - 60 MICA - 40 LP - 3 - 30 PIP - 3.6	15 HRS AT 110°F + 10 HRS AT 160°F	565 ± 30	
(SRIR) PART A - 100 PART B - 100	15 HRS AT 130°F 24 HRS AT 160°F	459 ± 9	
(TIR) PART A - 70 PART B - 30	15 HRS AT 140°F+ 2 HRS AT 170°F+ 24 HRS AT 200°F	397 ± 12	
ADIPRENE L - 100 - 100 MOCA - 11	4 HRS AT 160°F	405	375
828 - 100 Al_2O_3 - 300 DEA - 12	15 HRS AT 160°F	485	

Fig. 1. Dielectric Strength Values.

Figure 2 shows dielectric strength results obtained as a function of thickness for two of the systems, SRIR and Adiprene. Note that the pulse dielectric strength is greater than the ac dielectric strength and that it is a stronger function of the thickness of dielectric. In fact, the pulse dielectric strength seems to be in the neighborhood of twice the ac dielectric strength but this ratio changes with the thickness. Thus it is difficult to predict the pulse strength from the ac value for varying thickness.

Even if one had a true figure for the dielectric strength, Figure 3 shows that it would be difficult to predict the pulse life, because the pulse life of thin samples is a strong function of the voltage applied to the sample. To obtain a life of about 200 pulses the voltage must be reduced considerably. In many applications it is desirable to sustain thousands of pulses. Thus for a thin sample one could use approximately the peak ac dielectric strength as a guide, but as pointed out previously, this does not change much from one polymer to another so that material selection is still difficult.

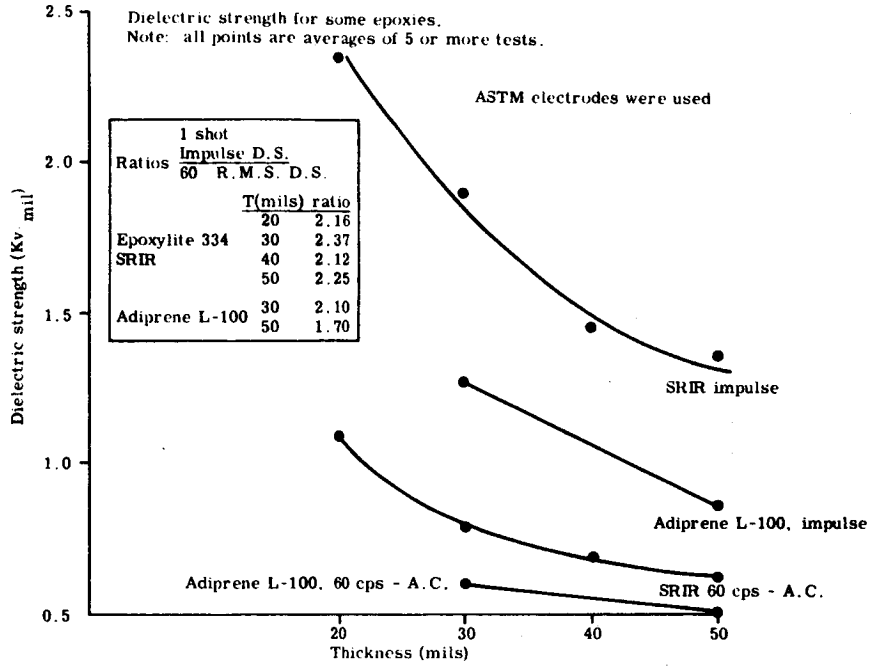

Fig. 2. Dielectric Strength Versus Thickness for Some Epoxies.

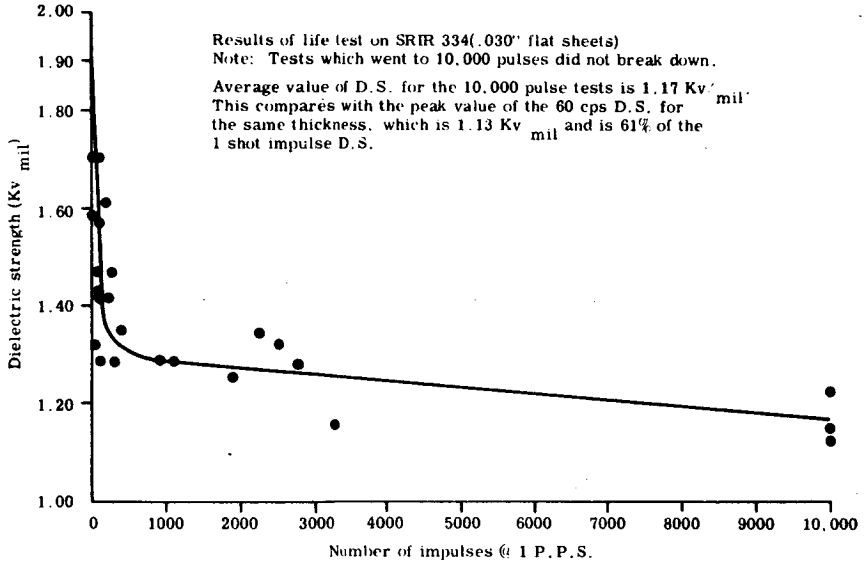

Fig. 3. Dielectric Strength as a Function of Pulse Life for SRIR.

Figure 4 shows the results obtained with the pointed electrode compared with the dielectric strength determined by ASTM D-149. The pulse life varies by three orders of magnitude and the material with the greatest pulse life does not have the greatest ac dielectric strength. The best material tested had a pulse life of greater than 4300 pulses -- often going as far as 20,000 pulses. The poorest material consistently had a pulse life of less than 5 pulses but shows a high steady state electric strength.

No.	Material	ASTM dielectric strength (v/mil)	Pulse life
1	Transformer impregnating resin (TIR)	450	>2500
2	Semirigid inspection resin (SRIR)	459	>4300
3	Adiprene L-100 Moca 6.6	300	<200
4	LTV-60	750*	<5
5	Sylgard 182	500	<20

* Data for hemispherical electrode.

Fig. 4. Pulse Life of Some Epoxies Tested in a 200 kv Nonuniform Field.

The density of the branches of the trees that grew with repeated pulsing, increased in the materials with the longest pulse life. However, the density of the tree branches could not be directly correlated with the number of pulses applied to the sample.

The experiment showed three other points. First, no correlation of breakdown path or pulse life to the mechanical stress pattern was observed. Second, the gases liberated in the tree in the test samples were found (for SRIR) to be essentially methane with a small amount of H, N, and O. It did not appear that venting of the needle reduced pulse life. Finally, comparison of the pulse life evaluation of the 5 materials agreed with results obtained from a simple pulse transformer imbedded in the 5 resins tested.

Reference

1. Olyphant, M., Jr., "Corona and Treeing Breakdown of Insulation-Progress and Problems," Insulation, March 1963.

PULSE LIFE AND DIELECTRIC STRENGTH OF A GLASS-FILLED EPOXY RESIN SYSTEM

Lee J. Seligman

Sandia Corporation
Albuquerque, New Mexico

From the appearance of dendritic tree growth, which precedes catastrophic failure of a dielectric in a non-uniform electric field, it was felt that the presence of high-strength inclusions might hinder this growth and so increase the pulse life and dielectric strength of the material. For an epoxy host material, spherical glass particles were used as they satisfied the initial criteria of a high dielectric strength material having a shape permitting analysis while contributing little opportunity for local increases in field, and were commercially available.

The spheres used varied in size from about 350 μ inches to .65 inches and were composed of such glasses as standard soda-lime and 17 per cent borosilicate. A crushed silica powder was also used. The soda-lime has been utilized almost exclusively thus far because of its ready availability.

The dielectric system to which the spheres were added was SRIR (semi-rigid inspection resin), a clear polyol-modified, acid anhydride-cured epoxy resin[1]. The desired mixture was cast in a cubic mold 2 inches on a side having at its center the tip of a conical electrode, the other end of which protruded from one face for connection to the high voltage pulse generator. This geometry may be seen in Figure 1, which

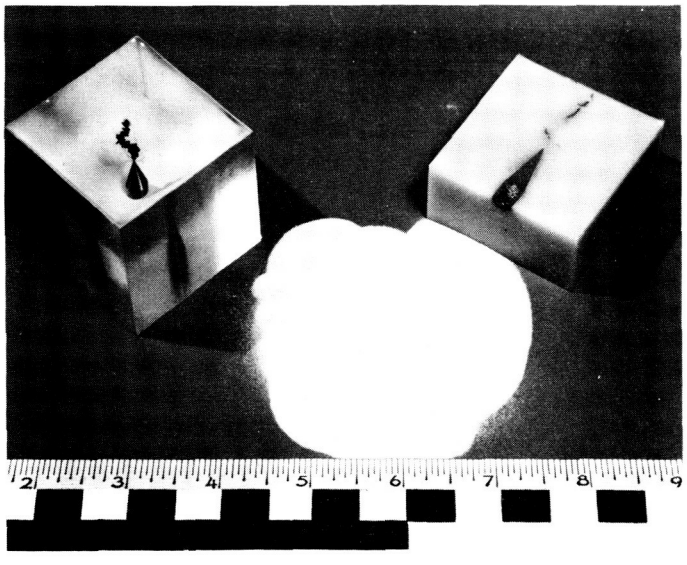

Fig. 1. An Unfilled Epoxy Specimen, the Filler Material, and a Cut-away View of a Typical Filled Dielectric.

shows also the pattern assumed by the breakdown arc, in both the unfilled and the filled resin. For the smaller spheres, a loading ratio of 2 parts glass to 1 part resin by weight was about as dense a packing as could be obtained before the mix became so thick it could not be properly evacuated prior to cure, and the very smallest required a 1:1 mixture. To prevent the larger spheres from settling out, the ratio had to be increased.

The finished specimens were subjected to 10 μs pulses of constant voltage from +225 kv to +400 kv once per second until a catastrophic breakdown occurred to a distant ground plane. The number of pulses withstood by a specimen prior to breakdown at some voltage is referred to here as its pulse life, a function of voltage as may be seen in Figure 2. This functional relationship has been examined for several mixtures of resin and filler and appears to be, in the range,

$$\text{Pulse Life} = \frac{Vo}{V}\, e^{a(V_o - V)} \quad \text{pulses}$$

where for these materials $275 \leq Vo \leq 325$, the extrapolated single-pulse intercept, is in kilovolts and $.10 \leq a \leq .33$ is a function of the filler, assuming its larger values when filler is added.

Figure 2 shows the effects of glass fillers for some mixtures with SRIR, the experimental curves favoring somewhat the data that represent the more resistant specimens. The general pattern of these curves indicates the increased influence of fillers for the longer pulse lives as compared with the one-pulse breakdown threshold where the effect is small. This behavior, then, is cumulative and can be attributed to the physical interruption of the treeing phenomenon by the filler particles and the delay involved as the tree detours around these obstructions. In some cases -- where the glass is smooth, the glass epoxy bond weak, and local packing dense enough to permit contact between filler particles -- the fillers hasten breakdown by presenting a more easily tracked surface along the glass-epoxy interface. Figure 3 shows such a track, which may be followed from the electrode -- pointing up in the center -- as it passes intimately around three .65-inch spheres and out of the solid at the upper left corner of the picture. At this location a rather unique tracking pattern may be seen, the discharge having confined itself to a ribbon-like path encompassing the primary tree until the interface could no longer contain it and it left the sphere from the ribbon's edges at about 25°. It is noteworthy that the tree seems to have wasted little

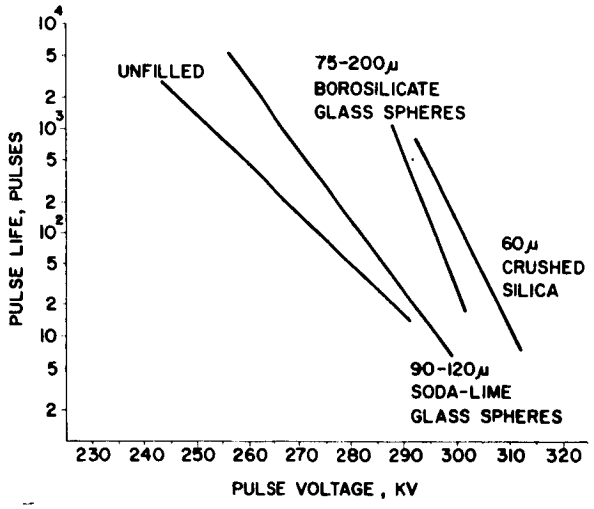

Fig. 2. Electrical Pulse Life, Versus Voltage, of the Four Dielectric Systems Under Study.

Fig. 3. Glass-epoxy Interface Breakdown Enhanced by High Incidence of Contact Between Filler Particles.

energy in seeking the locations of sphere contact through which it might continue to propagate, all the while within the interface. In fact, of the two other tree branches found in the material, the one in the center of the picture may be seen going directly to a point of filler contact. Such interface tracking is minimized by sand-blasting or otherwise spoiling the surface of the fillers. Reducing filler packing density also increases pulse life, apparently by reducing the incidence of contact between filler particles.

The introduction of fillers into the resin system appears to increase the dielectric strength also, and in like manner. AC short-time tests on 1/8-inch thicknesses of 1) SRIR, 2) SRIR and 20 μ glass spheres in a 1:1 ratio by weight, and 3) SRIR and the same spheres with twice the packing density. The results indicated that the more densely packed material was a better dielectric than the unfilled resin, and that the less densely packed material where filler contact was lower was the best of the three, exceeding the strength of the unfilled resin by 13.5 per cent on the average.

Reference

1. Carroll, B. and Smatana, J., "Transparent Cold-Shock-Resistant Epoxy Casting Resin," SCR-173, Sandia Corporation, Albuquerque, April 1960.

CORRELATION BETWEEN ELECTRICAL PULSE RESISTANCE AND MECHANICAL SHOCK RESISTANCE FOR FOUR CASTING RESINS

Jerome Allyn

Sandia Corporation
Albuquerque, New Mexico

Study of the electrical breakdown path obtained with pulsed, non-uniform fields, suggests that mechanical fracture may be important in the breakdown process. Therefore, the purpose of this study was to see if any correlation exists between electrical pulse and mechanical shock resistance. It was hypothesized that materials having poor mechanical shock resistance would have good high voltage pulse resistance.

I. Materials

The materials chosen for investigation were SRIR, TIR, Sylgard 182, and Adiprene-L 100-100, Moca 6.6. All these materials are semi-transparent casting resins, presently being evaluated for high voltage applications. SRIR and TIR are semi-rigid in their static behavior, whereas Adiprene-L and Sylgard 182 are more flexible.

II. Testing Method

The mechanical shock condition was obtained by means of exploding wires embedded in the four casting resins. This method was felt to be suitable because of the following reasons: (a) The energy delivered to different composition samples would be reasonably constant for a particular storage capacitor voltage. (b) The exploding wire process would rapidly strain the surrounding material. (c) The stress pattern would be similar to that thought to occur during dielectric breakdown. (d) The samples could be easily examined for damage after being tested.

The extent of fracture induced by the exploding wire was used as an indication of the shock-withstanding ability. Framing camera pictures were also taken to give an idea of fracture initiation time and fracture velocity. The shock-withstanding ability was then compared to electrical pulse life data, as described by Milton[1], and single pulse partial breakdown path length data as a test of the hypothesis stated earlier.

III. Sample Configuration

Cast cubical samples were used to facilitate viewing of the interior. Figure 1 shows a schematic of the configuration used. Gas checks were used in Sylgard 182 and Adiprene-L to prevent the gas from blowing out the ends. They were not needed in SRIR and TIR due to their more rigid behavior.

IV. Experimental Apparatus and Measurements

The basic circuit, used for the study, was proposed by Tucker[2]. The circuit as constructed was as small and robust as possible to keep resistance and induced voltage to a minimum. For diagnostic purposes, the current through the wire was

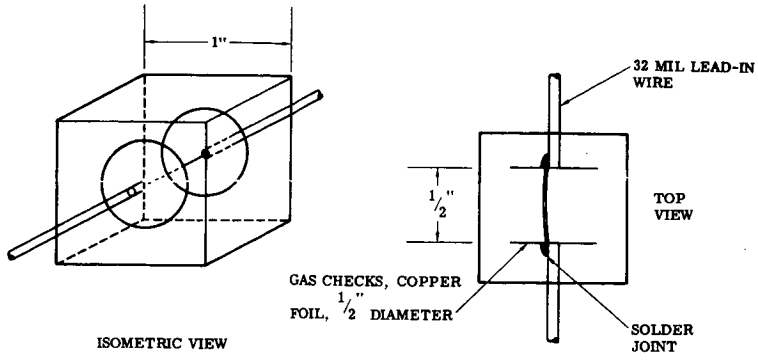

Fig. 1. Exploding Wire Sample Configuration, With Gas Checks.

monitored by means of a current viewing resistor. The voltage across the wire was monitored by means of a voltage divider. The amount of energy into the wire was found by recording, before and immediately after the event, the capacitor voltage. In this manner, the energy released in the wire could be found using the formula, $E = 1/2C(V_1^2 - V_2^2)$. By assuming that a certain fixed percentage of this energy, on the order of 50 per cent, was absorbed in the circuit, one could get a general feeling for how much energy was released in the sample. Although it has not been utilized by the investigators to date, a more exact method exists for determining the energy released in the wire[3].

V. Experimental Procedure

The testing procedure was simple and obvious. Basically, it consisted of exploding the wire at various energies, synchronizing the framing camera to properly record the event, and observing the results.

VI. Experimental Results

The results of the exploding wire test revealed the shock resistant properties of the four materials. SRIR and TIR, the two more rigid materials, were each blown completely apart for released capacitor energies of about seven joules. Few cracks formed in these two materials. Once a crack started, it tended to enlarge quickly at the expense of any others. The failure mode appeared to be a mixture of tension and shear.

Adiprene-L and Sylgard 182, on the other hand, were very resistant to shock. For released energies of about 13 joules, the Adiprene-L and Sylgard 182 samples had damage extending around the wire axis in about a 1/32 and 1/8 radius, respectively. The failure mode in both materials was definitely tension.

The test results have been summarized in the following table, along with the pertinent electrical data.

Table of Pulse Data

Material / Property	SRIR	TIR	Sylgard 182	Adiprene-L
Electrical Pulse Life at 200 kv	> 4300	> 2500	< 20	< 200
Partial Breakdown Path Length at 236 kv, Inches	1/4-3/8	1/4-3/8	1/2-3/4	Complete Breakdown
Exploding Wire Shock Resistance	Poor	Poor	Good	Excellent
Exploding Wire Fracture Radius, For 14 Joules/In., Inches	1/4-1/2	1/4-1/2	1/16	Negligible

VII. Discussion of Results

As can be seen from the table, SRIR has the longest pulse life and the shortest partial breakdown path length of any of the four materials tested, and yet it, along with TIR, has the poorest shock resistance. On the other hand, Adiprene-L, which suffered complete breakdown in the partial breakdown path length test, had the best resistance. The only obvious conclusion is that shock resistance is inversely correlated with pulse life and path length for these materials, a conclusion that is as expected. Since this is the case, then it would seem that poor shock resistance, or dynamic brittleness, is important in the make-up of a good high voltage insulator. Perhaps the rapid failure associated with this brittleness quickly absorbs the released energy from a partial breakdown. To use a more specific and physical interpretation, perhaps the rapid failure quickly relieves the high temperature and pressure in a suddenly formed partial breakdown filament. This rapid relief would reduce the charge density in the filament and thus would reduce the field at the filament tip. Naturally such a result would promote high voltage resistance.

References

1. Milton, O., "Application of the Pointed Electrode in Evaluating Pulse Life of Casting Resins," 33rd Annual Meeting, Conference on Electrical Insulation, NAS-NRC, Cleveland, Ohio, Oct. 11-14, 1964.

2. Personal Communication.

3. Anderson, G. W. and Neilson, F. W., Exploding Wires, Edited by W. G. Chace and H. K. More (Plenum Press, Inc., New York, 1959), p. 97.

THE MEASUREMENT AND ANALYSIS OF THE DIELECTRIC STRENGTH OF GLASSES

W. H. Barney

Corning Glass Works
Corning, New York

The work of this report is concerned with the analysis of the "critical" voltage. The meaning of the term "critical" implies that below this voltage the sample will not electrically fail.

Electrical contact was made to the sample through two solid hollowed electrodes, which made contact to the circumference of two gold circles, fired on to both sides of a 2 mm thick disc sample. Heat was conducted from the circumference of the gold circles to the solid electrodes. This allowed the center of the sample electrode configuration to heat faster and to break down electrically. Thus, accurate temperature measurements could be made at the predictable point of dielectric failure.

Neglecting the heat loss by radiation, the rate of heat introduced into the sample by the electrical energy is equal to the rate of sample heating plus the rate of heat loss by conduction. The relationship can be expressed by the following equation[1]:

$$V^2/\rho = k\frac{dT}{dt} + \beta T \qquad (1)$$

In this equation, ρ represents the resistivity, T is the sample temperature above furnace temperature, k is the specific heat times the amount of material being heated and the geometric factor of the electrical resistance, and β represents the thermal conductivity times the geometric factors of both heat loss and electrical resistance. Since the various geometries are difficult to determine, the values for k and β were measured as a function of temperature for the various glasses.

The various values of β can be determined by measuring the temperature of the sample as a function of time following "stabilized" voltage application. A "stabilized" voltage represents a value slightly below "critical." This means that the temperature of the sample will increase and then stabilize. It will not increase indefinitely to sample failure.

This means that $\frac{dT}{dt}$ in equation (1) is zero and β can be determined directly. After determining the various values of β, the slope at some arbitrary temperature is measured. Then the various values of slope, temperature, and β can be inserted into equation (1) and solved for k.

Thus, all the parameters of equation (1) are now known. However, the various parameters are a function of temperature and, as a result, the equation is a non-linear first order differential equation.

However, the equation can be solved using either non-linear analysis techniques, a computer, or iteration manipulations. The analysis and iteration techniques were used and found to be in excellent agreement.

The curves in Figure 1 indicate excellent agreement between the measured and the calculated dielectric strength of five different glasses. Data was taken using a sixty cycles per second power source over a temperature range of 700°C to room temperature.

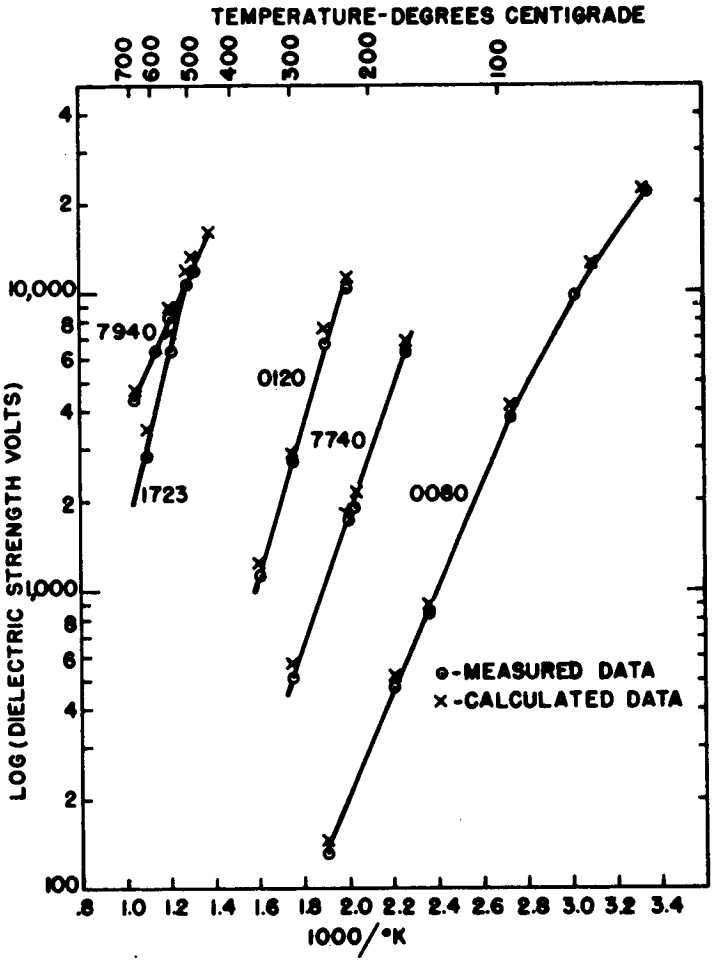

Fig. 1. The Calculated and Measured Critical Voltage as a Function of 1000/°K for Various Corning Code Glasses at Sixty Cycles Per Second Frequency.

This work is presently being expanded to include different source frequencies, sample thickness, and electrode sizes. Several organic materials have also been measured, and good agreement between measured and calculated data was achieved. However, it was found necessary that the material's electrical response be similar to glasses.

Reference

1. Wagner, K. W., "The Physical Nature of the Electrical Breakdown of Solid Dielectrics," A.I.E.E., Vol. XLI, 1922, p. 288.

MINIMUM DIELECTRIC STRENGTH AREAS IN KRAFT CAPACITOR TISSUE

E. P. Bullwinkel

Peter J. Schweitzer Division
Kimberly-Clark Corporation
Lee, Massachusetts

The present work stems from a desire to find out what factors characterize areas of minimum dielectric strength in kraft capacitor tissue (KCT), especially in the form of multiple sheets. While these microscopic areas are easily located by any suitable scanning electrode technique, their physical preservation proves to be more difficult. Thus, the dissipation of only a few microjoules in a 10 micron thick sheet of KCT during breakdown suffices to destroy the area of interest.

For a scanning device, a lathe is used which carries on centers an insulated brass cylinder (5" x 24") to which electrical connection is made by means of a slip ring. One or more sheets of KCT to be tested are affixed to this cylinder and then scanned in a helical fashion by means of a small electrode mounted on the lathe tool carriage. Also mounted on this carriage are two miniature spray guns which can be fired electrically to produce indexing marks for the location of the "failed" areas.

The circuitry (Figure 1A) used with the scanning device is simple and makes use of a thyratron diverter to quickly remove the test voltage following a breakdown. An over-all delay of ~ 0.1 μ second is achieved by using a high speed discriminator-trigger circuit based on a secondary emission pentode[1].

As seen in Figure 1B, the sample between the electrodes is actually two dielectrics in series, viz. paper and air. During the scanning, the air is continually being broken down which results in spurious pulses appearing across the phototube cathode resistor. The discriminator is employed to reject these pulses from the much larger ones which result when the paper itself breaks down. (While air breakdowns generate extremely corrosive ions, experiment shows that the paper substance can withstand quite a few such breakdowns without apparent harm).

The behavior of the paper on breakdown is of some interest. It appears that initially the paper switches rapidly ($< 10^{-8}$ sec.) to a conductive state from which it can be returned unharmed to its normal insulating state if care is taken to limit the time spent in the conductive state and the current density. The 917 phototube is used in the present circuit as a current limiting device where it functions as an almost perfect constant current generator (Cf. Region II of Figure 1C). We estimate that by use of this device (in conjunction with the rapid turn-off time) that the paper sample is only required to dissipate a few nanojoules during breakdown.

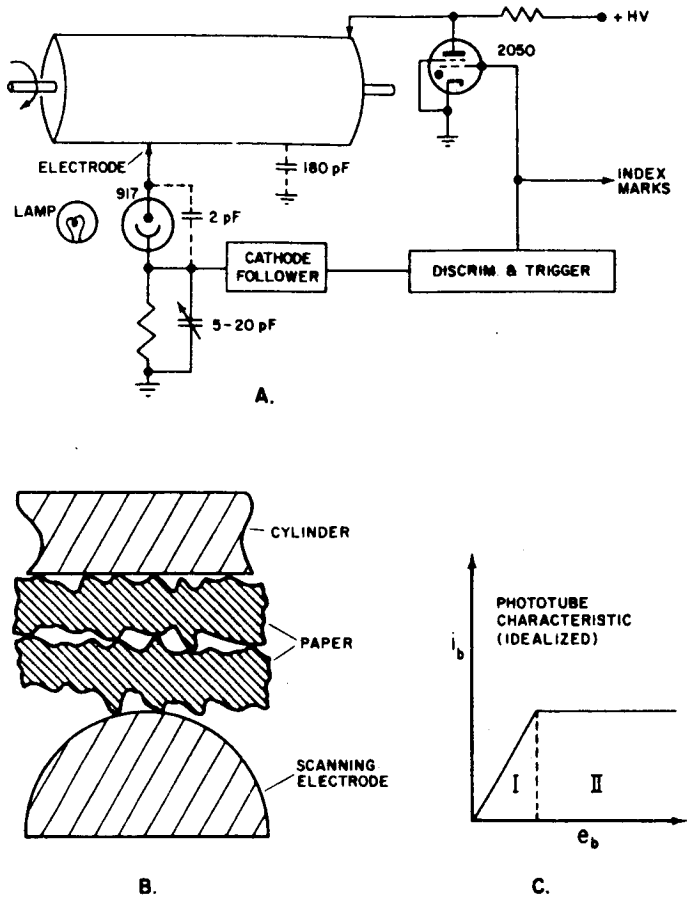

Fig. 1. Scanner (Schematic).

In scanning a sample, the test voltage is selected so that, on the average, one or two breakdowns per square foot are produced. Following this scanning, each indexed breakdown area of each sheet comprising the sample is examined as follows. First the area is subjected to the Stain Test[2] to reveal the presence of any microscopic hole or fissure. (This very sensitive test consists of applying alcohol to one side of the sheet while the other side is in contact with a sheet of spirit duplicating paper. If there is any opening or fissure present, the alcohol quickly wicks through it and solubilizes the dye on the duplicating paper sufficiently to cause a stain pattern to appear on the sheet being tested). Secondly, each breakdown area is examined microscopically by transmitted light to detect the presence of any opaque particles. (Such particles are usually found to be conductive). If no positive results are obtained with either of these two tests, the cause of failure is listed as "unassignable."

In using the above described equipment and tests on a single sheet of KCT we find, not unexpectedly, that the cause of failure is invariably assignable to either a hole or an opaque (conductive) inclusion. However, when two sheets of KCT are examined, we find, as shown in Tables 1 and 2, that the majority of failures fall into

the "unassignable" category. (The designation "hole" in these tables is not meant to imply anything as to size or shape, but merely indicates that the Stain Test result was positive). The nature of these "unassignable" causes is under active investigation.

Table 1

Sample: 2 sheets of 0.5 mil (12μ), 1.0 Density Paper

Test Voltage: 1.3 kv

Area Scanned: 13 ft.^{2}

"Causes" of Failure	No. of Failed Areas	% of Total
Unassignable	17	65
Opaque particle in one sheet	6	23
Opaque particle in both sheets	0	0
Hole in one sheet	3	12
Hole in both sheets	0	0
	26	100 Total

Table 2

Sample: 2 sheets of 0.66 mil (17 Micron), 0.75 Density Paper

Test Voltage: 1.4 kv

Area Scanned: 20 ft.^{2}

"Causes" of Failure	No. of Failed Areas	% of Total
Unassignable	7	54
Opaque particle in one sheet	0	0
Opaque particle in both sheets	0	0
Hole in one sheet	4	31
Hole in both sheets	2	15
	13	100 Total

References

1. Moody, N. F., Electronic Eng., 1952, 24, 214.

2. Developed by the late Dr. R. J. Hemphill, General Electric Company, Pittsfield, Massachusetts, ca. 1940.

PULSED VOLTAGE TESTS WHICH DETERMINE THE CRITERION FOR INSULATOR FLASHOVER IN DRY AIR

S. I. Reynolds

General Electric Research Laboratory
Schenectady, New York

I. Introduction

Uniform field flashover tests confirmed by photo-multiplier measurement of light pulses from discharges were reported at the 1963 Annual Meeting of the Conference on Electrical Insulation[1]. The system under study consisted of a dielectric rod (1"D.) and series air gap placed in the center of uniform field flat metal electrodes having a diameter larger than the dielectric rod (3"D.). The discharges occurring between the dielectric rod and metal electrodes were shown to be responsible for triggering the main gap (i.e., the region with no dielectric in place) flashover in dry air below the sparking potential of the main gap by supplying electrons and photons to the main gap.

This report concerns the measurement of the discharge magnitude in coulombs in discharges occurring in a series air gap between rods of #0080* Corning glass and the upper electrode. Non-destructive pulsed voltages of 20 millisecond duration are used. The discharge magnitude in coulombs obtained from current measurements was found to be proportional to the photon light output in arbitrary units using a properly controlled photo-multiplier.

Current measurements are determined by the voltage drop across a 160 ohm 1/2 watt carbon resistor. The discharge current flowing is equal to the measured voltage divided by 80 ohms, the value of the 160 ohm resistor shunted by the 160 ohm 517 scope.

II. Test Procedure

The voltage V_g across the series gap produced by different values of the applied voltage, V_o, (above the sparking potential V_s) were calculated as follows:

Eq. (1) $$V_g = \frac{V_o}{\frac{t_d}{t_a \epsilon} + 1}$$ where t_d is the dielectric thickness, t_a the air gap spacing in millimeters and ϵ the dielectric constant of the glass. In almost all cases tests were made at over voltages greater than 1 kv above the sparking potential of an equivalent metal to metal gap.

*Test samples furnished by W. H. Barney - Corning Glass Company.

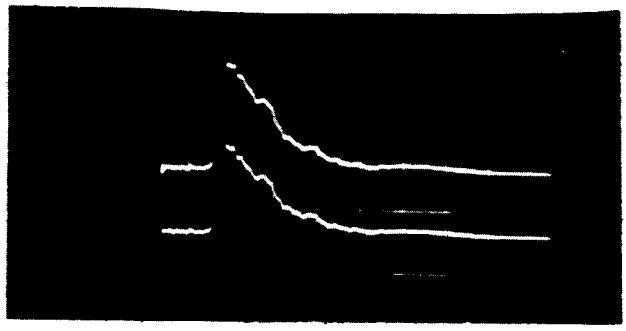

CURRENT PULSE
SWEEP 50n SEC/CM

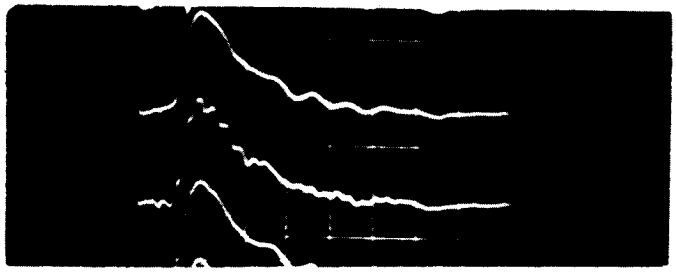

LIGHT PULSE
PHOTOMULTIPLIER
SWEEP 50n SEC/CM

Fig. 1. Streamer-like Discharges Between Insulator and Metal Electrode.

The discharge magnitude in coulombs is obtained by integration of the area underneath the voltage pulse as shown in Figure 1. This area Eq. (2) $\int_0^\infty I_e\,(t)\,dt$ where $I_e\,(t) = \frac{V(t)}{R}$ where $V\,(t)$ is the voltage pulse amplitude as observed on the scope. As can be seen, the current and photon pulse duration occurring at high over voltages is so rapid that only electron initiated streamer like discharges are involved.

For light photon measurement in arbitrary units the integrated area under the voltage time curve is Eq. (3) $\int_0^\infty V\,(t)\,dt$ where $V\,(t)$ is the voltage output from photo multiplier.

The coulomb discharge magnitude from discharge in the series air gap is equal to Q where $Q = c\,V_g$. V_g is obtained from equation (1).

Devins[2] has assumed a streamer extinction voltage of V_e to examine the expected dependence of discharge magnitude on the gap and thickness of the dielectric. This assumption predicates that a fraction of the dielectric surface t is discharged leaving V_e on that portion of the dielectric not discharged.

III. Test Results

Hundreds of discharge measurements were made on a 3 mm thick rod of #0080 glass in a uniform field gap at a number of over voltages, for a number of series air gap settings, to determine the discharge magnitude.

The results of these tests for five different gaps from 0.4 to 1.4 mm are shown in Figure 2 as photon light output as a function of over voltage up to flashover of the main gap. The light value at which flashover occurs within an order of magnitude is constant with flashover of the main gap at approximately the same voltage. Above 0.4 mm the ratio $\frac{V_d}{V_a}$ is almost constant where V_a is the sparking potential for the main metal to metal gap and V_d is the initiated flashover caused by discharges in the dielectric to metal gap due to the presence of the insulator.

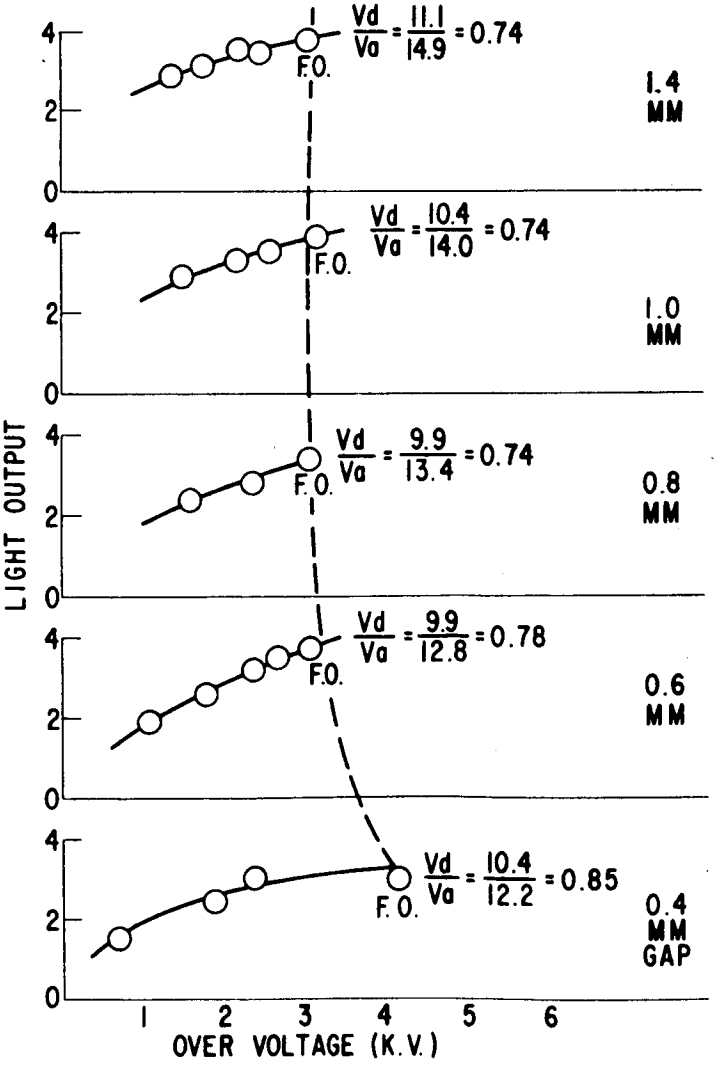

Fig. 2. Light Output Dependence on Over Voltage for Five Series Air Gaps.

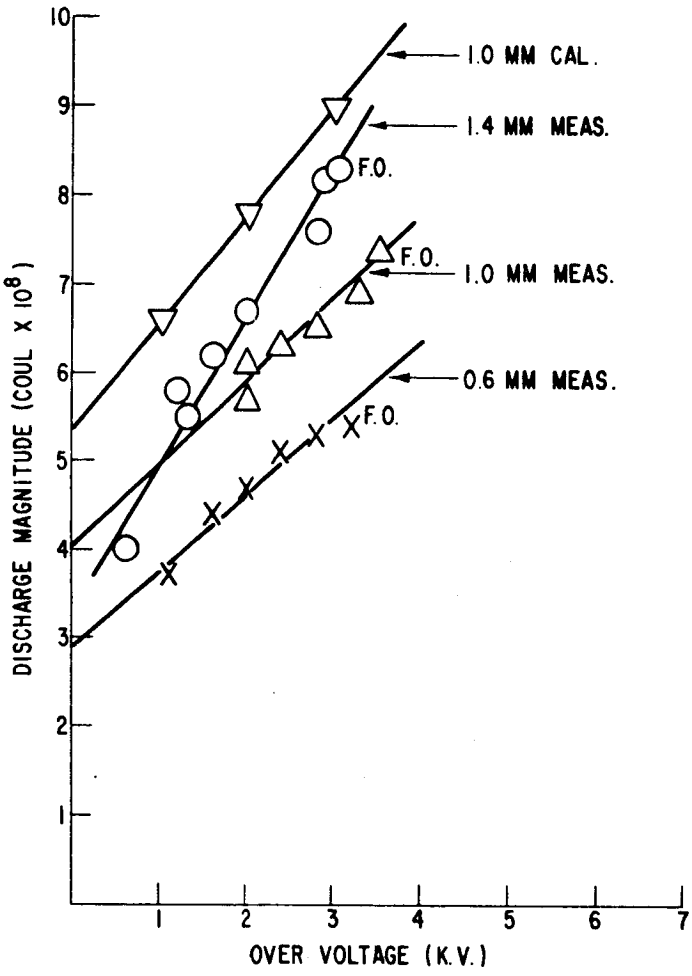

Fig. 3. Discharge Magnitude in Coulombs Versus Over Voltage for Three Series Air Gaps.

The discharge magnitude in coulombs in terms of lateral spread of charge over the dielectric surface at 0.6, 1.0, and 1.4 mm gaps to a glass rod 3 mm in length are shown in Figure 3. The measured coulombs for the three gaps just preceding flashover are as follows:

Series Gap MM	Main Gap MM	Over Voltage kv	Meas. Dis. Mag. Coulombs	$\frac{V_d}{V_a}$
0.6	3.6	3.2	5.4×10^{-8}	0.78
1.0	4.0	3.5	7.4×10^{-8}	0.77
1.4	5.0	3.0	8.3×10^{-8}	0.74

Assuming that the entire capacitance of the dielectric is completely discharged the calculated capacitance 12 pico farads of the glass was used to determine the discharge magnitude of 9×10^{-8} coulombs at 3 kv over voltage.

Calculation of capacitance at 1.0 mm gap from measured coulomb discharge gave a value of 9 pico farads independent of over voltage. This may indicate, as shown by

Devins, that a fraction of the dielectric surface still retains a charge. The calculated extinction voltage, V_e, is equal to $V_o - \frac{Q}{C}$, assuming the complete area of the sample to be involved in the discharge. The 1 mm gap V_o = 7.5 kv for O.V. of 3 kv and $V_e = 7.5 - \frac{6.8 \times 10^{-8}}{12 \times 10^{-12}}$ or 1800 volts extinction voltage. This is about three times higher than the 600 volt value obtained by Devins on similar tests working at small over voltages.

IV. Conclusion

The results of these tests indicate that one can possibly predict by calculation the discharge magnitude and lowering of main gap flashover if an insulator is placed in a uniform field gap in dry air with a series air gap existing between the insulator and electrode when subjected to dc or pulsed voltages.

With proper control of a photo-multiplier circuit the light output from a discharge is found to be proportional to the discharge magnitude so that confidence can be placed on the photo-multiplier method to study non-uniform field flashover phenomena.

A few preliminary tests indicate that variation in dielectric rod thickness and area do not change the effect of predicted initiation of discharge by a large factor.

V. Acknowledgement

The author wishes to express his appreciation for the many helpful suggestions and discussions with Dr. J. C. Devins during the progress of this work.

References

1. Reynolds, S. I., Annual Report, Conf. on Elec. Insul., NAS-NRC Publication 1141, 107 (1964).
2. ASD Technical Report 61-693 Aeronautical Systems Division, Air Force Systems Command, U. S. Air Force, Wright-Patterson Air Force Base, Ohio.

THE RELATION OF CORONA PULSE MEASUREMENT TO THE SIZE OF INTERNAL VOIDS OR OTHER ORIGIN

Thomas W. Dakin and Carroll N. Works

Westinghouse Research Laboratories
Pittsburgh, Pennsylvania

Corona pulse detection and measurement have become important and popular tools of insulation engineers. Yet there is still no very exact quantitative criterion of what a given corona pulse magnitude means in terms of the size of internal voids, or other location where it occurs. Also, there is no good quantitative correlation between measured corona pulse magnitude and the damaging effects to be expected from the corona. The latter, of course, depends on the energy of the discharges, and the type of insulation involved, as well as environmental conditions. This investigation has been directed particularly toward determining the relation of corona pulse size to the size of internal gas spaces within insulation, and to the nature of the insulation. The magnitude to be expected for observed corona pulses also has a critical bearing on the sensitivity to be required of corona detection equipment.

One would normally expect, for a given corona pulse charge transfer, at some "internal site," that the observed corona pulse at the electrodes or terminals would decrease with increasing series insulation, C_s, with thickness t_s, and voltage, V_s, and increase with gap capacitance, C_a, with thickness, t_a, and voltage V_a, which is discharged. This is expressed in the relation:

$$\Delta Q_{external} = \Delta Q_{internal} \frac{C_s}{C_a} = \Delta Q_{internal} \frac{t_a \epsilon_s'}{t_s} \qquad (1)$$

This relation is derived on the basis of a plane gap in series with a solid in a uniform field arrangement of dielectrics. It is assumed in this case that the added charge to the system, ΔQ_{ext}, really appears across C_s rather than the series combination of C_s and C_a, as has previously been assumed to be the case and which leads to a slightly different ratio of the charges. The relation may be generalized for other geometries. For example, in the case of a coaxial arrangement with an annular gas space with outer and inner radii of r_{a2} and r_{a1} in series with solid insulation, having outer and inner radii, r_{s2} and r_{s1} become:

$$Q_{ext} = \frac{Q_{internal} \epsilon_s' \log(r_{a2}/r_{a1})}{\log(r_{s2}/r_{s1})} \qquad (2)$$

It should be noted in this case that a particular sized discharge in a given thickness gap would produce a larger observed discharge if the gap were nearer the central conductor than the outer conductor.

The above-mentioned geometrical effects on the observed corona pulse size are superimposed on other effects which influence the size of individual discharges, such as the nature of the surface, and particularly the resistivity of the surface. To determine any systematic dependence of the coulomb pulse charge on the nature of the surface and the gap spacing, a careful study has been made of the corona pulse height with parallel plane uniform field gaps between two insulator surfaces and between metal and insulator, and with annular coaxial cylinder gaps between a plastic insulator surface and a central conductor (as in a bushing). A much less extensive preliminary study of some plane parallel gaps was reported in 1954 by one of the authors of this paper. The advance in the state of the corona measurement art since that time and the fact that there were a number of unanswered questions and little systematic data on expected corona pulse sizes in different situations prompted the present study.

It should be remembered that it is possible to calculate simply the corona pulse charge to be detected at the electrodes if one knows the effective voltage decrease produced by a single discharge across a gap of known area within an insulation system where a known thickness of insulation appears in series with the gas gap which is discharged. In the case of a parallel field with a flat series gas cavity, the internal charge is simply:

$$\Delta Q_{internal} = C_a(V_c - V) = \frac{\epsilon_o A}{t}(V_c - V) \qquad (3)$$

where V_c is the critical discharge voltage across the gap of thickness t and V is the residual voltage after the discharge occurs. Combining Eqs. (3) with (2) or (1) then gives the observed charge. Mason, Reynolds and others have shown, in detailed studies of the small areas, A, affected by individual discharges, that these areas are irregular and lacking in uniform surface charge. Thus V in Eq. (3) can only be an effective "average" value. It would seem that only idealized or limiting values of corona pulse charge can be calculated. An empirical study of observed pulses seems necessary to define their range of values.

It is well known that observed corona pulse charge values vary both during a single cycle and with time over a number of cycles. The distribution in pulse sizes for a uniform plane gap has been measured for quite a number of cases and is reported here (Figures 3 and 4), but it is reasoned that a critical quantity is the maximum pulse size, which occurs regularly almost every cycle.

Individual discharges affect only a limited area. Erosion leading to breakdown is seldom uniform over the affected area and the depth of erosion at a particular spot is influenced only by the individual discharges occurring repeatedly at that spot. Unfortunately in practical situations one (almost) never has an area affected by discharges, which is so small that discharges occur each cycle regularly and at only that spot.

In this paper and in the authors' testing practice it is custom to observe on the oscilloscope what is called the maximum corona pulse per cycle. While this is slightly subjective, it is generally repeatable within 20 per cent by different observers. The coulomb charge value is measured by comparison to a calibration pulse of known magnitude, using published procedures. The maximum pulse can be regarded as the pulse which occurs about every 6 cycles (at 60 cycles). Sometimes a peak reading voltmeter is used which responds accurately to pulses of that repetition frequency or greater. Meter readings and oscilloscope observations usually agree well.

Figure 1 shows a typical graph of pulse size versus gap spacing for a plane parallel gap not restricted in area edgewise, but with a 1" diameter electrode (in oil) above the upper solid dielectric layer. The lower electrode was 3.5 inches in diameter. The test arrangement permitted an easy change in insulator surface and quick continuous variation in gas gap spacing, while the series insulation thickness was held constant. Part of the variation with spacing noted in the size of the observed pulse is due to the geometric factor given in Eq. (1). Also in Figure 1 is graphed, for comparison, internal pulse magnitude calculated with Eq. (1). This quantity should be independent of the series insulation thickness, and this curve may be used to estimate the expected magnitude to be observed with the same gap in series with any given insulation thickness, through Eq. (1). It was hoped (somewhat vainly) that a master set of curves similar to Figure 1 for different insulation materials and conditions could be determined.

In Figure 1 is also graphed, for illustrative purposes, the energy of the maximum discharge. This is calculated from the well-known relation: $W = 1/2\Delta Q_e V_e$, where ΔQ_e is the observed pulse magnitude (at the terminals) and V_e is the voltage at the terminals when the discharge occurs. This voltage quantity is somewhat uncertain, since the phase is usually not recorded accurately, but it is reasoned that a proper value should be the corona threshold voltage, or in the case of an overvolted parallel gap, such as used in the experiments in this paper, the half width of the parallelogram seen on the oscilloscope with a capacitance bridge. In cases where the pulse size is increasing rapidly with overvoltage, it is suggested that the crest applied voltage be used in this energy calculation. This energy value is also equal to the internal discharge energy, and should be related to the corona damage.

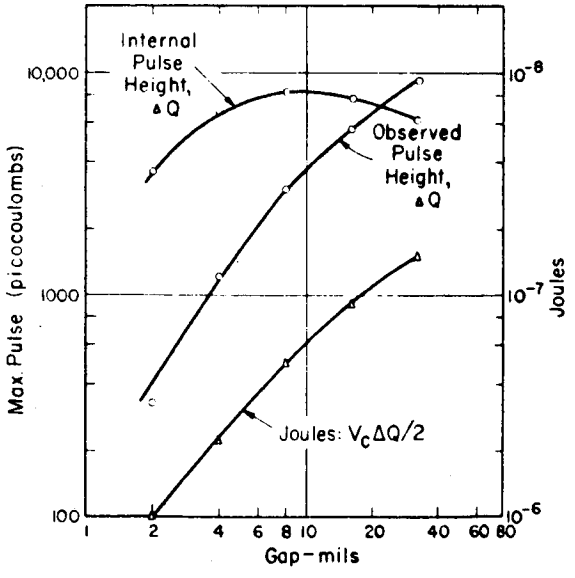

Fig. 1.

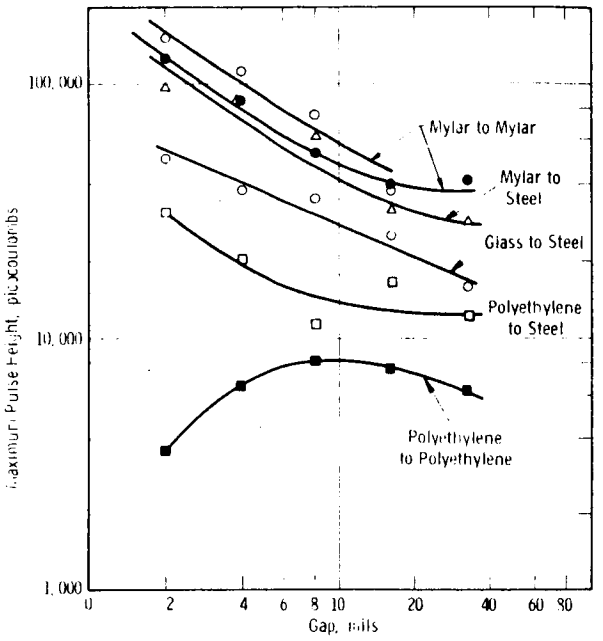

Fig. 2.

In careful studies of gaps with a variety of different surface conditions, curves as shown in Figure 2 were obtained. In this figure, only the internal charge, calculated from the observed charge is shown. These data were obtained under dry conditions with air, dehydrated with activated alumina, flowing very slowly through the system. The wide range of charge values and rather different trends of the charge-gap spacing curves obtained has frustrated analysis so far.

It is confirmed as previously reported that the pulse charge increases only moderately with overvoltage in the limited uniform planar gap. Increases of 2 or 3 fold were typical in going from the corona starting voltage to twice this voltage. This is contrasted with the conduction edge corona on the surface of insulation where the pulse size increases steadily with overvoltage through as much as several orders of magnitude.

The effect of humidity on the pulse size as noted qualitatively by Devins and others is very pronounced. With polyethylene surfaces and other materials, the pulse size decreases an order of magnitude or more with increased humidity. This does not seem to be associated with a change in observed corona starting voltage, which, for the planar gap, was nearly unchanged with humidity.

Measurements of the corona pulse size for a coaxial geometry ($\sim$0.25" diameter) with gaps from 2 to 32 mils between various insulating materials gave observed internal charge magnitudes of the order of 10,000 picocoulombs, generally overlapping the majority of the curves of Figure 2. This indicated that there was essentially no difference between flat and curved parallel surface gaps.

A considerable number of pulse size distribution curves have been measured such as illustrated by Figure 3. All of the distribution curves show an approximately exponential shape with a large number of small pulses. There is a regularly reproducible wave on the major exponential trend, indicating a somewhat large number of large pulses and very small ones, with a depression in the middle. Measurements were made on an area of about 1 inch diameter with a counter which counted all of the pulses above a preset threshold level, which could be set accurately down to 1 per cent of the largest pulse level. The data of Figure 4 indicated that the largest pulses covered areas of 0.1 to 0.3 square inches. Much smaller areas and smaller charges would be encountered with small area voids. As a check on the accuracy of this counting

technique, the integrated pulse charge per cycle was computed from curves such as Figures 3 and 4 and compared with the integrated pulse charge per cycle measured on a capacitance bridge. The agreement was within 15 per cent for the larger gaps where the measurements are more accurate and within 40 per cent for the 2 and 4 mil gaps.

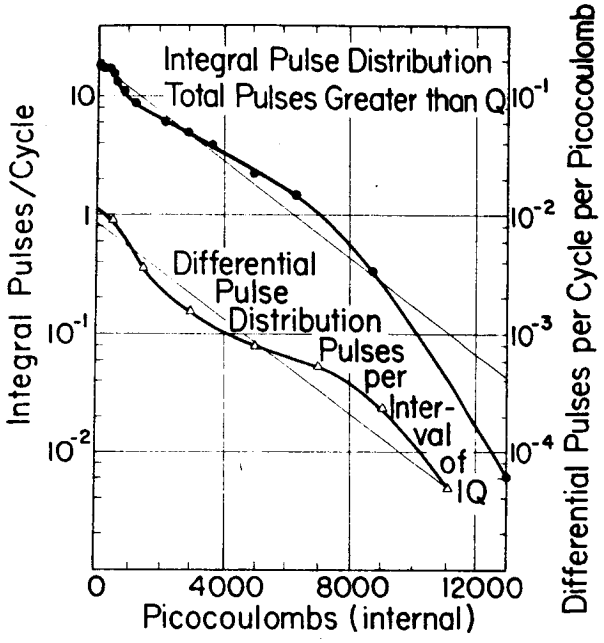

Fig. 3.

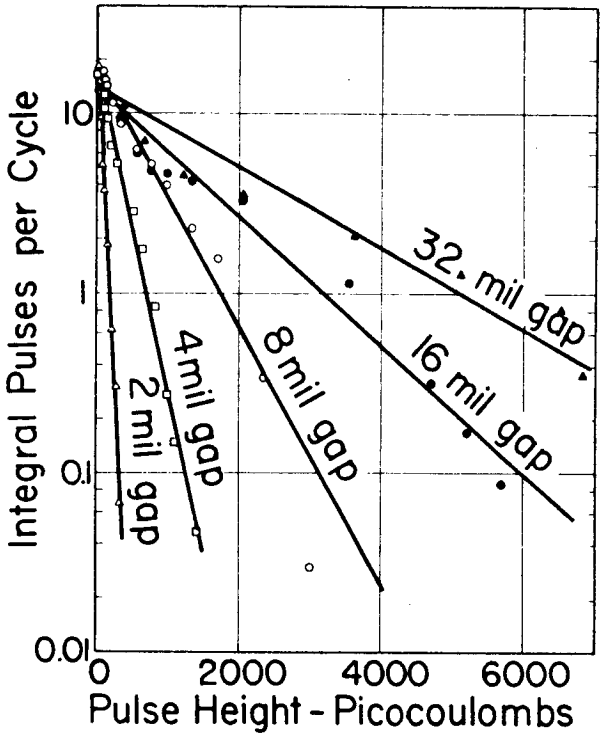

Fig. 4.

DESIGNING FOR MAXIMUM FLASHOVER VOLTAGE IN 10^{-7} VACUUM AND AT MODERATE GAUGE PRESSURES OF ELECTRONEGATIVE GASES WITH DIRECT VOLTAGE AT HIGH TEMPERATURES

W. T. Starr

General Electric Company
Schenectady, New York

In this paper we will examine some of the results obtained when insulators are placed into gaps between electrodes. The results are not claimed in any sense to represent the ultimate, but they do show that we have a long way to go to achieve the ultimate and do illustrate the effectiveness of certain designs in approaching the ultimate.

Vacuum Breakdown and Flashover

In really high vacuum fields as high as 800 kv per cm have been attained without breakdown when no insulator was in the gap[1,2,3]. When an insulator is placed in the gap and the vacuum is limited to 0.1 micron, rather large amounts of gas remain on surfaces and these residual gas films determine the behavior.

The observed results depend in a large degree on the apparatus used for testing. This is because gas is liberated during conditioning of the electrodes and the insulator. If the volume of the apparatus is large or the pumping speed is large the gas migrates quickly out of the gap leaving the residual pressure low and the strength of the gap is restored. All that is noted is a spit and a slight pressure increase. On the other hand, if the volume or the pumping speed is low, the liberated gas decreases the electric strength of the gap and the discharge spreads, releasing more gas until the current builds to large values. These intense discharges may vaporize electrode metal depositing it on the insulator in a way that reduces the electric strength of the insulator. Some of this can be compensated by conditioning with large resistors in series with the gap. In all our work reported here a 1.5 megohm resistor was in series. The volume of our apparatus was 9 liters and the apparatus was directly connected to a diffusion pump by a 2 inch diameter tubing two feet long.

The apparatus is shown in Figure 1. A 42 inch long 3-1/2 inch inside diameter alumina tube is mounted vertically with a Hoskins furnace at its center. The temperature of the outer surface of the alumina tube is measured with a thermocouple which is removed before voltage is applied to prevent, if possible, the breakdown of the wall.

At high temperatures the inner wall is an efficient radiator so that the electrode temperature is within 1 or 2°C of the inner wall temperature at 500°C. At 250°C the temperature difference would be about twice as big. The apparatus is shown in Figure 1. The detail of the electrode arrangement is shown in Figure 2.

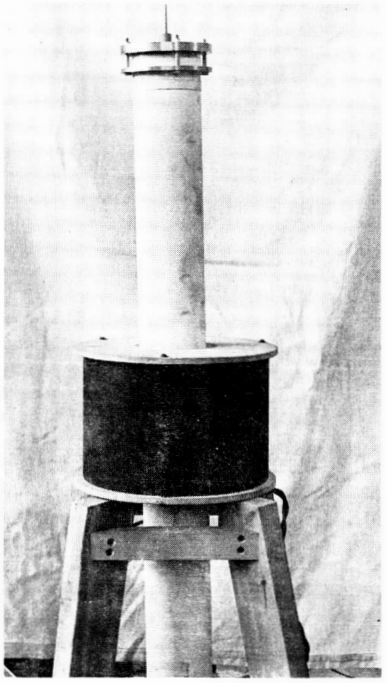

Fig. 1. Apparatus for High Temperature Insulator Tests in Vacuum.

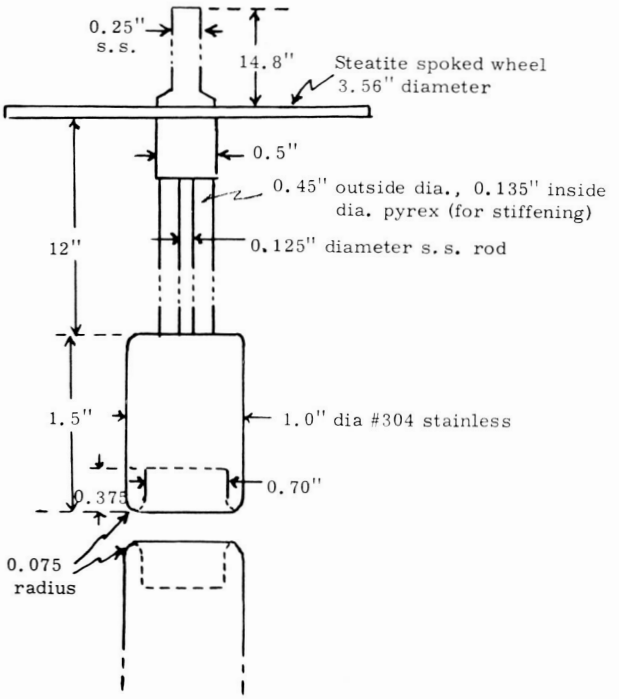

Fig. 2. Electrode System.

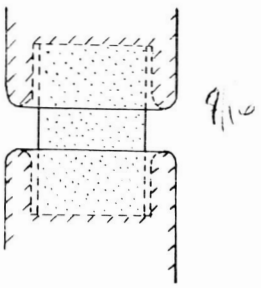

Fig. 3. 99.9% Alumina.

First an attempt to minimize the effect of the insulator on the breakdown strength was made by mounting the insulator in deep depressions in the electrodes. Kofoid had shown that this was effective[4]. Sample discs of insulating materials were placed in the depressions as shown in Figure 3 and the insulator was tested. With a 1 inch long 99.9 per cent alumina, so that the spacing between electrode edges was 0.25 inch, a first breakdown occurred at 68 kv, second at 90 kv, third at 107 kv, fourth at 110 kv, and it was possible to hold the voltage at 116 kv with considerable sparking.

With a 1.5 inch long 99.9 per cent alumina, conditioning occurred as follows at 300°C. First, 70 kv; 2nd 80 kv; 3rd, 116 kv; the insulator was then left at 300°C for 40 hours and the test repeated. Breakdowns occurred at 145 kv, 175 kv, and 165 kv, 150 kv and 142 kv. After 18 hours more conditioning, at 300°C without voltage, the insulator failed at 125 kv. Again after further conditioning failure occurred at 110 kv. When the insulator was inspected a band of dark material was found opposite the lower edge of the positive electrode.

These data indicate that it is possible to attain insulator strengths of 170 kv if the insulator is properly degassed before voltage is applied and if conditioning is done properly. This is over twice Kofoid's reported values.

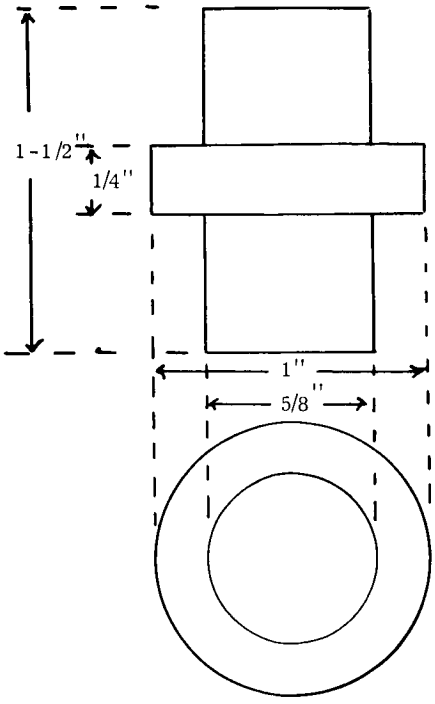

Fig. 4. 620 Mycalex Insulator.

It was reasoned that bursts of gas liberated at the positive electrode inside the well in the electrode would pass through the very intense field at the protruding edge of the positive electrode and result in discharges. If a skirt were applied to the insulator surface, it would shield the well from the bombarding ions and electrons originating at the negative electrode, reduce the gassing rate and make conditioning easier. Therefore, an insulator with the shape shown in Figure 4 was made from Supramica 620 and this was tried. The insulator in this case was conditioned for 20 hours at 225°C at 0.1 microns and cooled to room temperature before test. In this case, the voltage was increased to 190 kv before a failure punctured a hole in the wall of the test chamber. During this test the first conditioning sparks occurred at 105, 115, and 120 kv but the pressure increase due to these sparks was not even detectable at 0.01μ sensitivity. At 125 kv, one spark resulted in a 0.04μ pressure increase and at 140 kv, a 0.07μ increase, 0.03μ of which was permanent. The pressure increased monotonically with voltage from .08μ at 70 kv to 0.24μ at 190 kv. This is distinctly different from the behavior of the 1.5 inch long alumina insulator without a skirt in which case breakdowns were accompanied by pressure increases of .06μ and the pressure was much less stable at voltages as low as 80 kv.

Finally, the Mycalex insulator was tested at 220°C after 24 hours at this temperature. The insulator started gassing at 150 kv and visual postmortem indicated that the skirt had broken down. The gassing behavior was similar to that at room temperature at voltages below 150 kv. There was no band of discoloration as had appeared on the alumina.

Further experiments are planned in which the depression is on the negative electrode only. According to Kofoid this should be equal to the double depression system.

Since skirts are so effective, perhaps with skirts on the insulator, the depression can be eliminated. In order to test this hypothesis an insulator was made with attached studs as shown in Figure 5. This insulator was made with Forsterite ($2MgO \cdot SiO_2$) for we wished to maximize the thermal breakdown voltage. Gassing started at 85 kv at 330°C. About ten gassing events occurred in the eleven minutes between

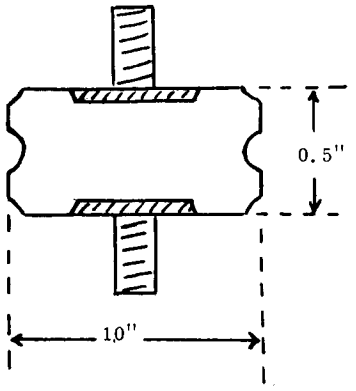

Fig. 5. Forsterite Insulator (Cross Section).

85 and 115 kv at which flashover occurred. On a second test at 350°C, 18 hours later about five bursts occurred between 110 kv and the 120 kv breakdown voltage. A third test with reversed polarity (negative) repeated the behavior of the first test with failure at 110 kv instead of 115 kv. A fourth test with positive polarity was made with no sparks below 105 kv and failure at 125 kv. A fifth test at 508°C produced some sparks at 85 kv and failure at 110 kv. A sixth test produced failure (considerable gassing) at 50 kv. The specimen had failed on the fifth test and it is believed that the failure was due to thermal runaway.

The thermal breakdown voltage for a uniform field with no lateral cooling is given by the following equation

$$V_2 = 8ke^b\, m \left[e^{\frac{m}{\theta_o}} - e^{\frac{m}{\theta_c}} \right] \left[\left(\frac{\theta_c}{m}\right)^2 + 2\left(\frac{\theta_c}{m}\right)^3 + 3\left(\frac{\theta_c}{m}\right)^4 \cdots - \left(\frac{\theta_o}{m}\right)^2 - 2\left(\frac{\theta_o}{m}\right)^3 - 3\left(\frac{\theta_o}{m}\right)^4 \cdots \right]$$

where k is the thermal conductivity (0.03 watts/cm^2 °C/cm for Forsterite)

e = 2.71828

θ_o is the surface temperature in °K, (i.e. electrode temperature)

θ_c is the critical central temperature above which the temperature increases at an increasing rate with time. It is determined from electrical conductivity (k_e) vs. temperature (θ) data.

$$\theta_c = \frac{m\theta_o}{m - 1.19\theta_o}$$

where m is the number which fits the measured variation

$$-\ln k_e = \frac{m}{\theta} + b$$

where b is a number taken from this variation.

For F-202 Forsterite "m" and "b" and 10,240 and 10.8 respectively. Thus at 508°C, V = 177 kv.

Now, this does not appear to be very good agreement with the experimental result of 110 kv. However, a small relatively conducting inclusion could easily result in the observed degree of lowering.

Incidentally, the bursts of gas released can transfer the high voltage to the walls of the test chamber and break it down resulting in a small leak. We have had excellent success in repairing such leaks with ML varnish.

Next, we would like to present some data on flashover problems of insulators in a gas ambient. Theoretically it should be possible to achieve the strength of the gas without the insulator in it and under certain conditions it is possible. If the insulator does not disturb the imposed field and, as a correlary, if there are only very small voids between the insulator and the electrode the electric strength measured is equal to that of the gap without the insulator. One-half inch and 1 inch diameter Teflon rod and 5/8 inch diameter alumina rod, all 1/2 inch long, have been tested in a 6 inch diameter Rogowski gap with results equal to the breakdown voltage of the gap without the insulator. Each rod specimen was ground so that its ends were really flat. All that is required to lower the flashover voltage to between 40 per cent and 60 per cent of theoretical is a very small void between the end and the electrode. This result has been achieved in air, SF_6 and FC-75 at pressures from atmospheric to 15 psig. In air a small singing corona starts at about 80 per cent of theoretical but it does not result in flashover. This result is not new except that to our knowledge it had not been achieved with a ceramic insulator.

The reduction of electric strength to about 40 per cent of theoretical is a serious limitation in design and of course, if some means can be devised to insure that voids are eliminated it would be a great boon. Also, when hardware is attached to an insulator, the field is disturbed and it is hard to know exactly how close to the theoretical maximum the measured result actually is. It is a safe bet that whenever conditioning is observed (the strength increases with repeated testing) the result is lower than it need be.

The results of several tests are given in the following table. The values in the per cent of theoretical column are interesting. Straight sided cylinders of Teflon gave the best results. The F-202 insulator of Figure 5 is fair. A straight sided cylinder of Alumina (Figure 7) is good. Skirts on the alumina did not help (Figure 6). End caps on the insulator produce particularly poor insulators.

The values in the per cent of theoretical column are derived by assuming that 150 kv is normal for a 3/8 inch gap at 14.3 psig of SF_6, that the gap strength increases linearly with gap length and with absolute pressure.

References

1. Maitland, A., J.A.P. 33, No. 8, 1962.
2. Brode, I., J.A.P. 35, 1964, p. 2324.
3. Bettler, P. C., AEC Report MDDC 1695, 2-17-47 Declassified 2-12-48.
4. Kofoid, M. J., Elec. Eng., March 1961, p. 182.

Insulator Design	Ambient Mat'l.	Ambient Press. psig	Min. Sparking Voltage kv	Max. Conditioned Voltage	Breakdown 1st	2nd	3rd	4th	5th	6th	Percent of Theoretical Breakdown Min.	Breakdown Max.	Sparking Min.	Sparking Max.
Figure 5	SF_6	6			96^+	96^+	100^+	94^-	95^-	100^-	66	70		
	SF_6	15.2			130^+	137^+	137^+	120^-	128^-	131^-	58	66		
Figure 6	SF_6	15	94	107	113^+	113^+		108^-	110^-	108^-	52	55	45	52
No Insulator	SF_6	14.3		(3/8" gap)	152^+	148^+	154^+	138^-	146^-	150^-	92	103		
Figure 7	SF_6	15	55	70	73^+	73^-					70	70	53	68
Figure 8	SF_6	6			130^+	155^+	140^+	138^+	140^+	110^+	69	96		
Figure 9	SF_6	6			150^+	140^+	151^+	140^+	140^+		87	94		
Figure 10	SF_6	8.7			127^+	127^+	127^+							
	FC_{15} 150C	18.3												
Figure 11	SF_6	15			90^+	96^+	100^+				49	55		
Figure 10	SF_6	15			177^+	183^+	155^+	190^-	168^+	190^+	38	46		

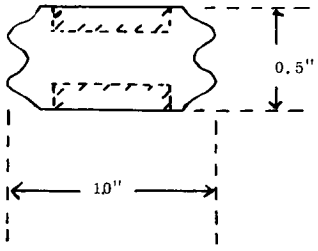

Fig. 6. 94% Alumina.

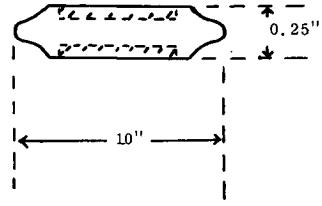

Fig. 7. 94% Alumina.

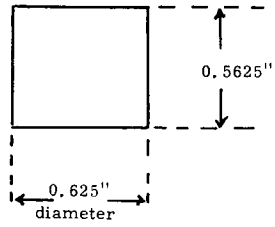

Fig. 8. Teflon Cylinder. (With Small Void at Edge.

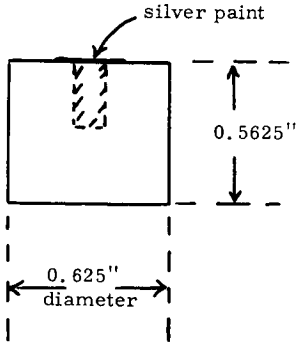

Fig. 9. Teflon With Drilled Hole.

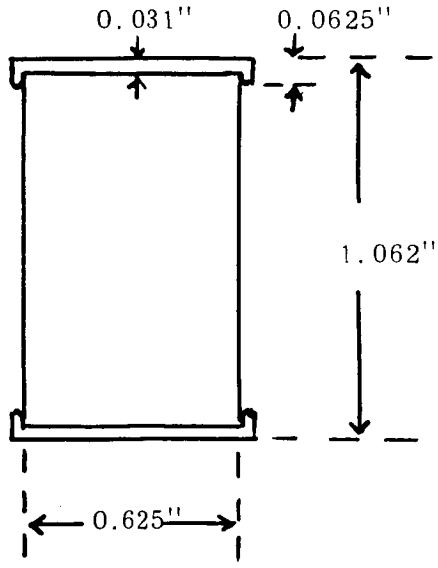

Fig. 10. Capped Alumina Insulator.

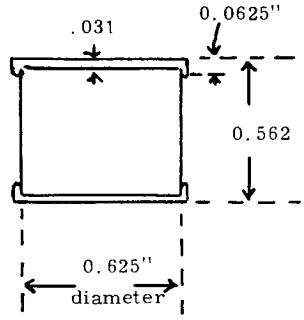

Fig. 11. Alumina Insulator With Metal Cap. (Cross Section).

EVALUATION OF ELECTRICAL INSULATION FOR RADIATION TOLERANT EQUIPMENT

C. L. Craig and J. Rogers

Sperry Gyroscope Company
Division of Sperry Rand Corporation
Great Neck, New York

I. Introduction

Review of the available literature on the effect of steady-state nuclear radiation on electrical insulation several years ago revealed that most of the data presented were of limited value for design purposes because of one or more of the following reasons:

a. Standard dosimetry techniques were lacking.

b. The radiation environment used was different from that encountered in many applications.

c. The degree of deterioration of the material was not adequately described.

d. The material tested was not adequately identified.

The radiation environments that materials must resist vary widely, depending on the application. Therefore, we felt it desirable to establish a gamma-neutron relationship that would, when the individual neutron flux and gamma dosage is known, allow an estimation of effects on a material from any radiation environment. Also, values for both threshold (initial) and significant damage to materials were required in order to estimate the probable effect of radiation from different environments in various applications.

II. Facilities and Specimens

Samples of commercially available insulating materials were exposed to mixed radiation in three different reactors. Cobalt-59, cadmium covered cobalt, and sulfur-32 monitors were used for neutron dosimetry. A specially designed carbon-wall CO_2 ionization chamber was used to determine gamma radiation levels.

As space for samples is at a premium within a reactor, reduced-size specimens were used for all mechanical property evaluations and some of the electrical tests. To validate the data obtained, a separate check of the results obtained with small specimens, as compared to standard size test specimens, was run. This comparison indicated that no significant difference in values was obtained when reduced-size specimens were used.

After exposure, the materials were evaluated for changes in critical properties, using standard hot laboratory procedures where applicable. Monitoring of transient property changes during irradiation was performed in a limited portion of the evaluations.

III. Radiation Dose Considerations

For reactor irradiation data to be of value in calculations, either the radiation energy absorbed by the test sample or the energy to which it is exposed must be determined. The energy absorbed by the sample frequently is used to define the dose, especially when working with pure chemicals. Knowledge of (1) the exposure environment, (2) the quantitative elemental structure of the sample, and (3) the absorption coefficients of each element present are all required to calculate absorbed dose. This makes calculations of the absorbed dose for heterogeneous insulating materials or components extremely difficult because of the complex and frequently unknown molecular structures usually present. Therefore, exposed dose usually is used in presenting results of reactor irradiation tests on engineering materials. However, the energy in the reactor environment is comprised of several different levels and types. Samples may see radiation flux within a reactor as follows:

thermal neutrons - 10^{8} to 10^{15} n/cm^2 - sec
epi-thermal neutrons - 10^{7} to 10^{14} n/cm^2 - sec
fast neutrons - 10^{6} to 10^{14} n/cm^2 - sec
gamma photon - 10^{6} to 10^{12} ergs/gC - hr

The ratio of the components of this energy spectra will vary from reactor to reactor or within a reactor depending on location, and within a location depending on the shielding effects of the capsule walls. This makes it difficult to compare results from one test program to another, or to use test results from one program to predict results in new applications based on identical exposure environments.

We attempted to solve this problem by calculating the single total radiation dose by summation of the component energies. A separate test program indicated that thermal neutrons usually are an insignificant factor in radiation damage of materials. For all practical purposes, it has been found that the dose obtained from epi-thermal neutron flux (nv_et) may be considered as the primary neutron component in damaging materials. Reactor radiation exposure dose then can be computed as a single value by summation of the epi-thermal neutron flux and the gamma level by use of the approximation: ergs/gm C = 3.04×10^{-7} nv_et[1]. Comparisons of results obtained in different reactors and locations in reactors then becomes practical.

IV. Tests Results

The effects of steady state reactor irradiation on the electrical insulating materials and forms tested are listed in Table 1. In all cases, the radiation exposure is given as a total dose in ergs per gram carbon and includes both gamma and neutron components.

---

(1) Format for Reporting Radiation Effects Data, REIC, Battelle Memorial Institute, Columbus, Ohio. REIC Memorandum No. 10, May 1959.

Table 1

TOTAL RADIATION DOSE, ERGS/GM C

MATERIAL	FORM*	THRESHOLD DETERIORATION	MAJOR DETERIORATION
Silicone Resin-glass	S, T, W	2×10^{11}	5×10^{11}
Silicone Resin-mica Paper	S	10^{11}	3×10^{11}
Epoxy Resin, Silica Filled	E	5×10^{10}	5×10^{11}
Cross Linked Polyester	W	5×10^{10}	2×10^{11}
Modified Terephthalate Polyester	W	2×10^{10}	5×10^{10}
Epoxy Resin-glass	S, C	2×10^{8}	5×10^{10}
Isocyanate Resin-glass	T	10^{10}	3×10^{10}
Polyester-alkyd	E	10^{10}	3×10^{10}
Polyurethane	W	10^{10}	3×10^{10}
Silicone Enamel	W	3×10^{9}	2×10^{10}
Polyethylene Terephthalate	S	5×10^{9}	8×10^{9}
Mineral Oil (Uninhibited)	E	10^{9}	10^{10}
Isocyanage Modified Polyester	W	10^{9}	8×10^{9}
Kraft Paper	S	5×10^{9}	8×10^{9}
Silicone Rubber	T	10^{9}	3×10^{9}
Polyvinyl Formal	W	3×10^{8}	3×10^{9}
Polyethylene	S	3×10^{8}	2×10^{9}
Polyvinyl Chloride, Compd.	T, W	3×10^{8}	10^{9}
PTFE-glass	S, C	8×10^{7}	10^{9}
FEP Fluorocarbon	S	5×10^{7}	10^{8}
TFE Fluorocarbon	S, T, W	3×10^{7}	6×10^{7}

*Forms: S = sheet; T = tubing; W = wire insulation; C = copper clad laminates; E = encapsulant or impregnant.

The sheet and tubing samples included in Table 1 were evaluated on the basis of tensile strength, ultimate elongation, dielectric strength, creased dielectric strength and fold brittleness after different level irradiations. Note that some materials, such as kraft paper, withstand the radiation with little apparent effect, then, as the level increases, they rapidly deteriorate. Others, such as epoxy-coated glass cloth, show some reduction of properties at relatively low radiation levels, but maintain usable properties until relatively high dosages are reached. This indicates that the threshold dose (initiation of property damage) is not necessarily the limiting factor in designing for radiation resistance.

The magnet and hook-up wire insulations were evaluated by changes in dielectric strength of irradiated twisted pair specimens, half of which were wrapped around a small mandrel before test.

Copper-clad laminates were tested as comb type patterns for both transient (in pile) and permanent (out of pile) effects on insulation resistance. Epoxy-glass cloth, used for printed wiring applications, and PTFE - Fluorocarbon glass cloth, used for microwave applications were tested. The results showed an appreciable increase in conductivity of a transient nature at relatively low radiation levels. Partial recovery was attained after removal from the radiation environment at lower dosages. As the dosage increased, the recovery became less until the out-of-pile values dropped to the transient values obtained. Insulation resistance readings during recovery were taken at times ranging from 3 to 48 hours after removal from the reactor, or when approximate equilibrium was reached. Approximately one week later, values of 2000 megohms on the TFE laminate and 15,000 megohms on the epoxy were obtained, indicating that further recovery can be expected as the materials lose their radioactivity.

A polyester-alkyd type impregnating varnish, a silica-filled anhydride-catalyzed epoxy encapsulant and non-inhibited mineral oil were tested. The cured varnish showed initial discoloration and hardening at about 10^{10} ergs/gm C and became brittle and black at about 10^{11} ergs/gm C. The filled epoxy resin showed initial hardening and slight darkening at about 5×10^{10} ergs/gm C, but was still in usable condition after 5×10^{11} ergs/gm C. The mineral oil was first affected by an increase in neutralization number at about 10^{9} ergs/gm C. Both neutralization number and high temperature viscosity increased substantially at about 10^{10} ergs/gm C. Oxygen absorption increased about 18 per cent after 6×10^{10} ergs/gm C, indicating marked degradation of oxidation resistance.

V. Evaluation of Results

The exact composition of many of the materials tested was unknown. All were commercial products, compounded and processed with some degree of proprietary formulation and technique. Even so, results on materials in different forms and somewhat different formulation, but of similar general composition, were very similar. Silicone-resin coated glass fibre consistently withstood over 10" ergs/gram C before damage was evident. At the other extreme, non-reinforced polytetrafluoroethylene in all forms failed between 10^{7} and 10^{8} ergs/gram C.

In the series of tests described, in-pile transient property changes were checked on only one class of material - copper clad glass reinforced laminates. As previously noted, conductivity of both laminates tested increased at relatively low radiation levels, while recovered out-of-pile values of conductivity remained low until at high radiation levels they gradually degraded to the transient values. Recovered values of conductivity were obtained on the other materials tested but have not been reported as they consistently remained low until major deterioration of the material was evident. However, assuming that the results obtained on the copper-clad laminates are typical, transient reductions in insulation resistance of several decades may be expected at low radiation levels with all the materials tested.

VI. Conclusions

The primary types of radiation causing damage to materials are epi-thermal neutrons and gamma photons. The most practical technique of monitoring and recording radiation levels with heterogeneous systems is by use of exposed dose, as the information required to determine absorbed dose usually is unavailable. The concept of total exposed dose, derived from postulated relationships between neutron and gamma radiation, is presented. This technique allows direct comparison of results from different test programs and has produced equivalent results from similar tests in different reactors and different locations within a reactor.

The radiation tolerance of electrical insulating materials varies widely; electrical properties are affected first with some materials, and mechanical properties with others. When no appreciable reduction in properties can be tolerated, selection of insulation suitable for total radiation dosage over 10^{10} ergs/gm C is limited. However, if significant reductions in mechanical or dielectric strength can be tolerated without damage to the system, a number of insulating materials can be utilized at relatively high radiation levels.

EFFECT OF HUMIDITY ON THE DIELECTRIC PROPERTIES OF SOME POLYMERS

D. L. Killam

The Hydro-electric Power Commission of Ontario
Toronto, Ontario, Canada

Measurements of surface resistivity, volume resistivity, permittivity and dissipation factor, as a function of relative humidity at room temperature, have been made on samples of a number of polymeric insulating materials (see Table 1). The work was undertaken to supplement knowledge and understanding of the behavior of insulating surfaces under voltage stress, particularly as related to the interpretation of periodic high direct voltage maintenance tests on the insulation of power apparatus.

Table 1

List of Polymers Tested

1. Polypropylene	10. Polyurethane - rigid
2. Polyethylene - natural	11. Chlorosulphonated polyethylene
3. Polyethylene - with carbon black	12. Polyamide - water resistant grade
4. Polystyrene	13. Polychloroprene
5. Polyethylene terephthalate	14. Ethylene-propylene-dicyclopentadiene
6. Polymethyl methacrylate	15. Polyurethane - flexible
7. Polyvinyl chloride - rigid	16. Polymethyl methacrylate
8. Polyvinyl chloride - plasticized	17. Polyamide
9. Polyoxymethylene	18. Cellulose acetate

As expected, exposure to an atmosphere at high relative humidity, leads to reduced resistivities and increased permittivities and dissipation factors. Some relationship between changes in dielectric properties and per cent water absorbed was indicated, but this was in general not pronounced (Figures 1 and 2 of the report).

A close relationship between measured surface resistivities and volume resistivities was noted, suggesting that measurements of surface conduction actually included appreciable components of the volume conduction adjacent to the surface under test, for most of the polymers tested (Figures 3 and 4 of the report).

Several hypotheses are offered as to the form in which the water sorbed (absorbed or adsorbed) by the polymers may exist or be bound within the material. In most cases the water molecules contributed to polarization, like free water. Generally, the findings may be summarized as follows:

1. Direct voltage resistivities (both surface and volume) of the various materials tested, in equilibrium with an atmosphere over the range of 50 to 90 per cent

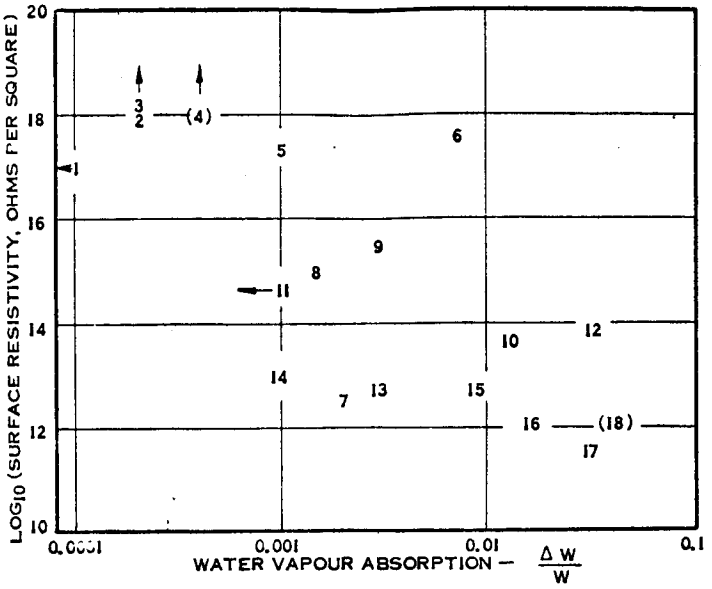

Fig. 1. Surface Resistivity at 90 Per Cent rh vs. Water Absorption.

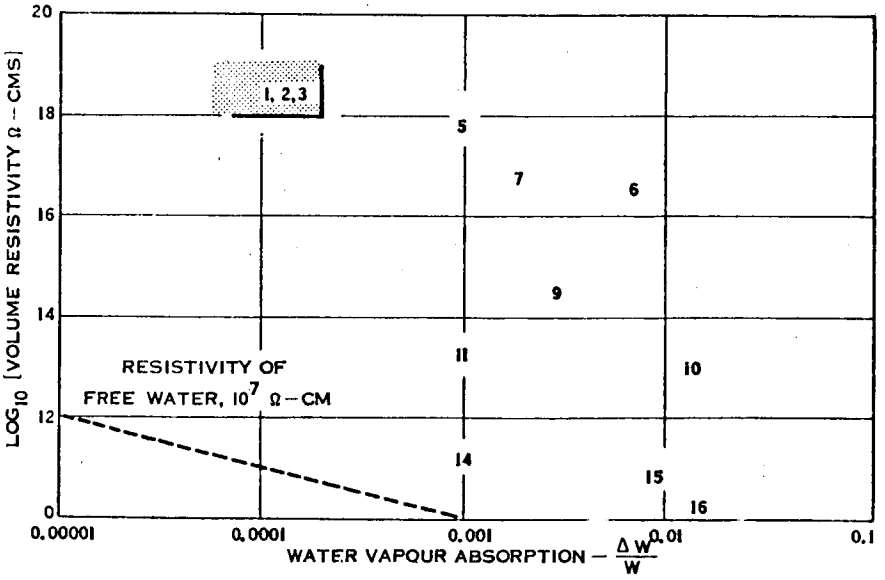

Fig. 2. Volume Resistivity at 90 Per Cent rh vs. Water Absorption.

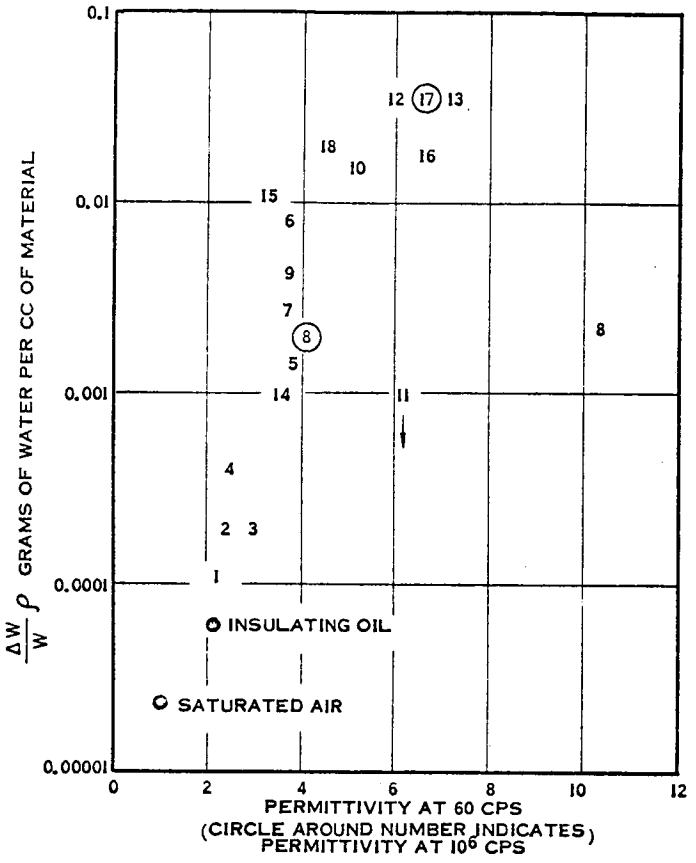

Fig. 5. Water Sorption vs. Permittivity.

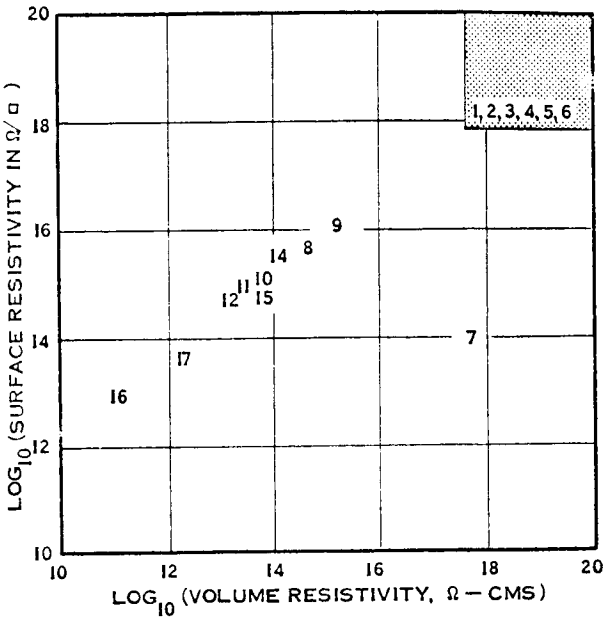

Fig. 3. Surface vs. Volume Resistivity - 50 per cent rh.

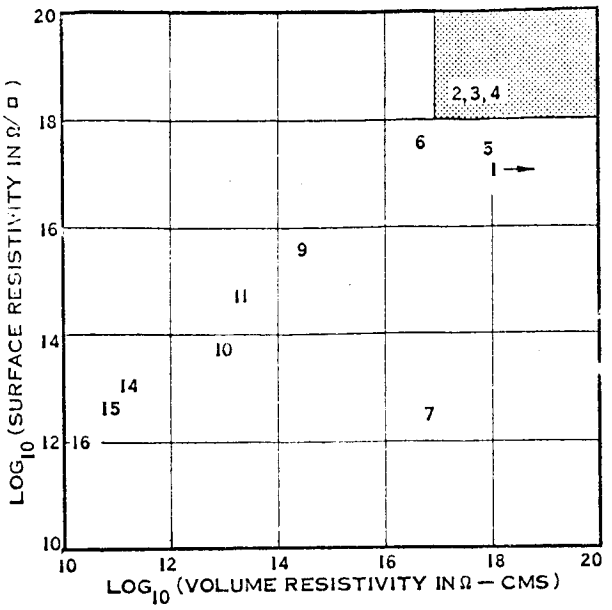

Fig. 4. Surface vs. Volume Resistivity - 90 per cent rh.

rh, at room temperature, varied over eight decades from 10^{10} to over 10^{18} ohms per square or ohm-centimeters.

2. Exposure to high humidity (90 per cent rh) reduced resistivities (at 50 per cent rh) by up to 2.5 decades.

3. Surface resistivity measurements of clean surfaces of many polymers are probably measurements of the resistivity of the volume adjacent to the surface.

4. The water repellent or non-wetting materials, like polyethylene, had the highest resistivities, the lower permittivities and the smallest water vapor sorptions. The similarity of capacitance change measurements along a surface and of a volume showed that water permeated the bulk of these materials. Generally, sorption was higher for the higher permittivity materials as polar materials exerted stronger binding forces on the water molecules (Figure 5).

5. Increased humidity resulted in increased capacitance roughly according to the polarization contributed by the sorbed water.

6. Dissipation factor increase was an insensitive general indication of water content at 100 cps.

Future work under consideration includes measurements of the effects of temperature variations in the zero to 100°C range.

A DUMBBELL MODEL FOR DIELECTRIC DISPERSION IN PARAFFIN-LIKE SOLIDS

Martin G. Broadhurst

National Bureau of Standards
Washington, D. C.

Dielectric dispersion in molecular crystals which results from orientational relaxation of permanent dipoles usually deviates from a simple Debye dispersion in such a way that the relaxation can be described by more than a single relaxation time. A simple model featuring two stable sites separated by a fixed potential barrier predicts a single relaxation time. Additional sites lead to additional relaxation times and a broadened dispersion. There has been no satisfactory theory which predicts that a broadened dispersion should result from a simple two site system.

The site structure of the n-paraffin chain in the usual orthorhombic paraffin crystal strongly suggests that the dipolar long paraffin chain compounds are simple two site systems in the low temperature crystal phase and yet the dielectric dispersions they exhibit are invariably broader than expected from a simple exponential decay. Hence, one wonders if dispersion broadening is to be expected even with a simple two site system.

To answer this question, it was decided to devise a model which would be as simple as possible and still include the essence of the following features of the n-paraffin lattice. The rotation of an n-paraffin molecule in its lattice is about a single axis along the chain axis under the influence of attractive van der Waals and repulsive overlap forces between its hydrogen atoms and those of adjacent molecules. These interactions are responsible for the shapes and positions of the orientational potential wells and barriers as well as for the transfer of the thermal energy necessary for the reorientation of a molecule.

Consider as a model (Figure 1) a row of vertical dumbbells, short compared to their separation, with their tops connected by springs at their equilibrium length and constrained to move with one degree of freedom about their fixed centers in the

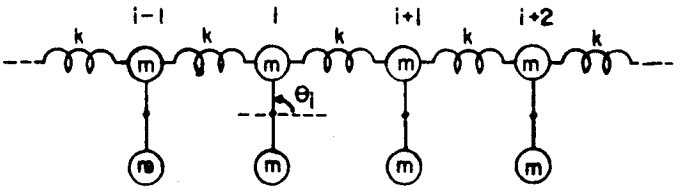

Fig. 1. A Schematic Diagram of a Segment of the Dumbbell Chain Model Showing Coupling Springs of Force Constant k and Rigidly Connected Masses. Calculation is Simplified by Assuming the Forces Between Dumbbells Act Only Horizontally.

plane of the figure. These dumbbells approximate the projection of the paraffin chain onto the plane of the crystal end layer where the masses represent the CH_2 units. The harmonic approximation to the interactions is adequate since normally interactions in an actual crystal occur at distances where the approximately correct 6-12 potential can be approximated by a quadratic. Also no generality can be gained by the use of more springs because of our approximation that the dipoles are short compared to their separation.

The acceleration of the i^{th} dumbbell in Figure 1 is given by

$$\ddot{\theta}_i = \frac{k}{2m} \sin \theta_i \, (4 \cos \theta_i - \cos \theta_{i+1} - \cos \theta_{i-1})$$

where m is the mass of each end of a dumbbell, θ_i is the angle that dumbbell i makes with the horizontal and the factor 4 accounts for 2 fixed springs in addition to the two coupling springs to approximate the effect of the second dimension in a two dimensional lattice and to fix the spatial orientation of our model. If the sin and cos are approximated by triangular functions, one obtains for the ratio of the potential energy to the moment of inertia for dumbbell i, with vertically fixed nearest neighbors,

$$V_i^o = 4A \, (\theta_i^2/\pi - 4\theta_i^3/3\pi^2), \; 0 \leq \theta_i \leq \pi/2, \; A = k/2m$$

with numerically equivalent expressions for the other three quadrants up to $\theta_i = 2\pi$. This potential energy V_i^o is shown in Figure 2. It exhibits two identically equivalent sites for $\theta = \pi/2$ and $3\pi/2$, separated by identical barriers centered about $\theta = 0$ and π. When either of the neighbors is out of its equilibrium position (as they generally will be when the system is set in motion), then V_i changes so that for any θ_i, V_i can be described by a probability distribution function, which can be obtained as a part of the solution to this problem.

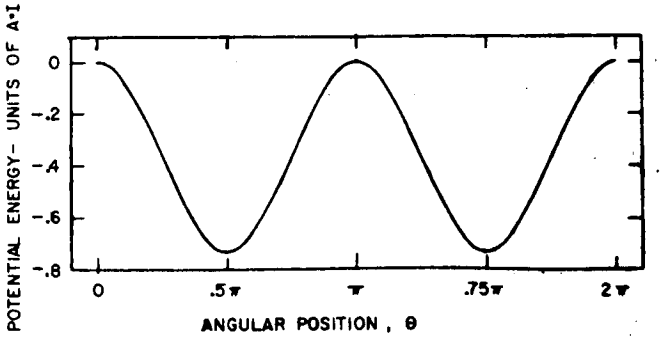

Fig. 2. Potential Energy Function for a Dumbbell With Vertical Neighbors, in Units of A · I Where A is the Ratio of the Spring Constant to Twice the Mass and I is the Moment of Inertia of a Dumbbell.

The numerical integration of this problem was programmed for the IBM 7094 for a one-thousand-dumbbell chain with the ends tied together. Numerical values of k and m were chosen to approximate the mass and vibrational frequency of an n-paraffin chain. Initial conditions involved assigning exponentially weighted random velocities to the dipoles, with the average energy being chosen to give an approximate decay time of 30 vibrational cycles (about 1/4 the average barrier height), and the program was run for 100 cycles. The correlation or decay function $(N_1 - N_2)/N$ was calculated as a function of time, where N_1 is the number of dumbbells which are in the same site they were in at t = o, and N_2 is the number that are in the site opposite the one they were in at t = o. (For a fixed barrier model, $(N_1 - N_2)/N = e^{-kt}$, where k is the probability of switching sites).

Figure 3 shows the positions of the dumbbells in a segment of the dumbbell chain at a series of closely spaced times. Examples of dumbbell flipping are evident. The decay function for our model is shown by the points in Figure 4, which are compared to a simple exponential function and a Cole-Cole circular arc function using $\alpha = 0.12$. It is seen that the circular arc function is a more accurate description of this model's orientational relaxation. The fluctuations in the curve are the result of having a statistically small number of dumbbells.

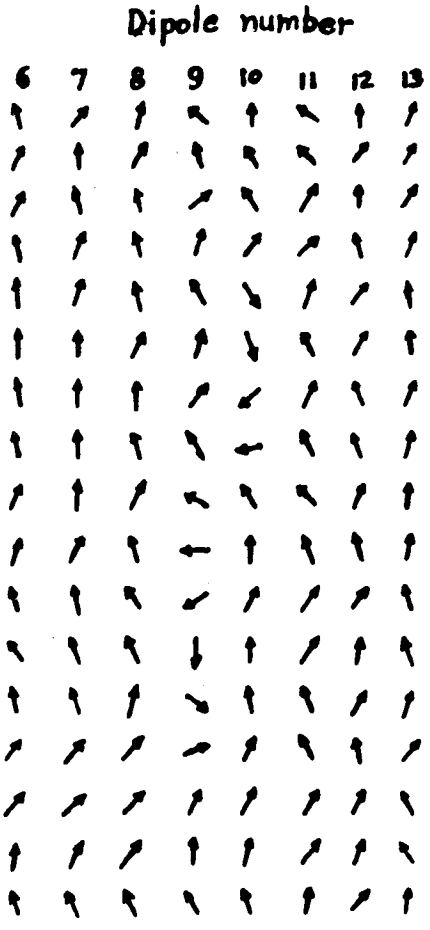

Fig. 3. The Angular Positions of the Dumbbells in a Segment of a Chain as a Function of Time. Each Row Gives the Positions a Small Time Increment (About 1/4 Cycle) Later Than Those Shown by the Preceding Row. Note That Part of the Chain Becomes Quiescent While Another Portion Flips. In This Example Two Dipoles Flip Completely Around and the Counting Scheme Registers no Change.

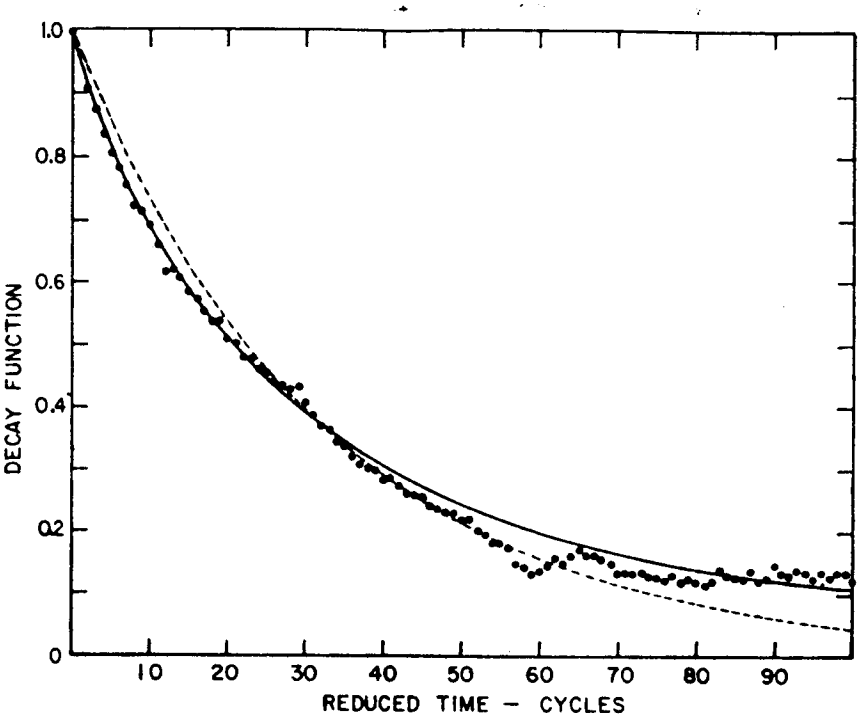

Fig. 4. Computer Calculations of the Quantity $(N_1 - N_2)/N$ as a Function of Reduced Time for a 1000 Dumbbell Chain. The Curves Represent the Cole Cole Decay Function

$$\sum_{n=o}^{\infty} \frac{(-1)^{n-1}}{R(1+\beta n)} (X)^{\beta n} ,$$

(Where X is Reduced Time) With the Solid Curve for $\beta = 0.88$ and the Dashed Curve for $\beta = 1$ (Simple Exponential).

Although these results are only preliminary and yet to be proven not dependent on artifacts in the calculations, it appears that the simple two position model used here does give a decay function which would lead to a broader-than-Debye dielectric dispersion (after assigning a small dipole moment to the dumbbells), and it is reasonable to suspect the barrier fluctuations to be responsible for this broadening. If this proves to be true, then the phenomena of dispersion broadening due to thermal fluctuations of the potential barriers to rotation could be expected in real crystals as well.

CRITERIA FOR THERMAL FAILURE OF INSULATING MATERIALS

W. T. Starr and E. J. McGowan

General Electric Company
Schenectady, New York

Corrections to the theory of thermal breakdown for the variability of electrical loss, for the presence of superimposed temperature gradients and for the presence of corona have been checked. If k_t is thermal conductivity, k_e is electrical conductivity, and β is a constant (0.22) when the electrodes are maintained at ambient temperature, θ_o, throughout the test, then thermal breakdown voltage of a slab is given by[1]

$$V = 4\sqrt{\frac{\beta k_t}{\gamma k_{e\theta_o}}}$$

$k_{e\theta_o}$ is k_e at θ_o (from measurements), and γ is obtained as follows.

1. Determine the variation of conductivity, k_e, with θ in the temperature and frequency region of interest. For alternating voltage, the real part of the conductivity is given by $k_e = fe' \tan \delta / 1.8 \times 10^{12}$.

2. Plot the data on semilog paper - i.e., log k_e vs. θ in °C.

3. Lay a ruler tangent to the curves at θ_o.

The value of γ is the ratio of 2.303 to the temperature range spanned by one decade of k_e as indicated by the ruler.

When k_e is taken as the maximum value expected for the test specimen, results agree with theory within 20 per cent.

For cable, the breakdown voltage is halved as is expected[2].

When one electrode is hotter than the other, and the hotter one is thermally insulated as in a cable with conductor losses, the value of β is given by

$$\beta = 0.22e^{-\gamma \Delta \theta_o}$$

where $\Delta\theta$ is the temperature difference. θ_o is the temperature of the cooler electrode.

When corona is present as in a test of a slab between a flat thermally insulated electrode and a 1/4 inch diameter rod (thermally insulated) electrode, the calculated failure voltage is about twice that found. The test setup is shown in Figure 3 and curves of k_e vs. θ for several materials are included.

References

1. Copple, Hartree, Porter, and Tyson, J.I.E.E. 85, 1939.

2. Whitehead, S., Dielectric Breakdown of Solids (Book), Oxford Press, 1951.

Table 1

Corona-Thermal Failure of Ceramics

Material	Thickness in.	Expected Thermal Failure kv/temp.	Firing or Softening Temps. °C (Approx.)	600°C kv	600°C secs	500°C kv	500°C secs	400°C kv	400°C secs	300°C kv	300°C secs	200°C kv	200°C secs
Steatite	0.10	4.0	1350			3.6**	25						
Grade L-5 (r.f.)	0.10	at				3.6*	2						
	0.10	400C				3.6	2	4.5	30	7.2	15	8.1	30
	0.055					5.3	2			7.2	55	9.0	45
Forsterite	0.125	18.7	1500	7.1	45								
		at		8.8	50	7.2	10	9.0	30	9.9	10	10.8	5
	0.062	500C		6.3	50	6.7	45	8.1	10				
Zircon Porcelain	0.125		1250			4.5	10	5.4	30	6.3	45	8.1	10
Supramica 500	0.0625	3.9 at 400C	900					2.7	10	5.4	20	7.2	30
Micamat (inorganic bonded)(General	0.063		1250-1400	6.3	20	5.4	30	6.3	30	8.1	30	9.0	30
	0.063					6.3	10						
	0.125					7.2	30					11.7	15
	0.125					7.2	30						
	0.125					6.3	60						
1732 Glass (Corning)	0.072		1600	7.2	20	9.0	5	9.0	10				
7940 Quartz (Corning)	0.074	21.6 at 500C	1600	10.8 } flash-		9.9	60						
				10.8 } over		11.0 } flash-							
						11.0 } over							
						9.0	50						
94% Alumina	0.128	16.9 at 500C	1600	8.1	55	9.0	50	9.9	30				
Phlogopite mica	0.010					3.6	15						

*Rod electrode 1/16" above surface: ** Rod electrode 1/8" above surface.

Table 2

Dissipation Factor

Material	150C 1 kc	150C 10 kc	250C 1 kc	250C 10 kc	350C 1 kc	350C 10 kc	500C 1 kc	500C 10 kc
Quartz #1	.00002	.00001	.0001	.00006	.002	.0003	.07	.01
Quartz #2	.00004	.00004	.0070	.0008	----	-----	3.8	.41
1723 Glass	.00074	.00068	.0017	.0012	.0050	.0028	.10	.025
7740 Pyrex	.19	.07	3.4	.67	----	-----	---	----
94% Alumina	.0019	.0009	.0080	.0040	.038	.014	.35	.10
Steatite	.011	.006	.14	.04	.66	.23	---	----
Zircon Porcelain	.07	.08	.08	.09	----	-----	.70	.20
Forsterite	*.00076	*.00048	.0038	.0031	.013	.005	.179	.051
Mica	*.00050	*.00025	.0060	.0014	.017	.007	.069	.024
Micamat S-1342	.0042	.0030	.0182	.0076	----	-----	.18	.070
Supramica 500	.0059	.0033	.054	.017	.067	.019	9.1	1.6

*100C

Table 3

Dielectric Constant

Material	150C		250C		350C		500C	
	1 kc	10 kc	1 kc	10 kc	1 kc	10 kc	1 kc	10 kc
Quartz #1	3.96	3.96	3.96	3.96	3.95	3.95	4.17	4.15
Quartz #2	3.92	3.92	3.93	3.92	----	----	4.12	3.94
1723 Glass	6.59	6.58	6.67	6.66	6.76	6.72	7.47	7.18
7740 Pyrex	6.3	5.6	11.4	8.2	----	----	----	----
94% Alumina	9.12	9.11	9.34	9.26	9.80	9.54	12.9	10.7
Steatite	6.38	6.31	7.14	6.62	11.1	7.65	----	----
Zircon Porcelain	13.4	12.0	16.9	15.0	----	----	28	20
Forsterite	*6.82	*6.81	7.03	7.00	7.18	7.12	8.77	7.60
Mica	*7.05	*7.05	7.09	7.07	7.20	7.10	7.57	7.21
Micamat S-1342	3.50	3.48	3.55	3.50	----	----	4.35	3.80
Supramica 500	7.13	7.09	7.49	7.23	7.53	7.22	29	19

*100C

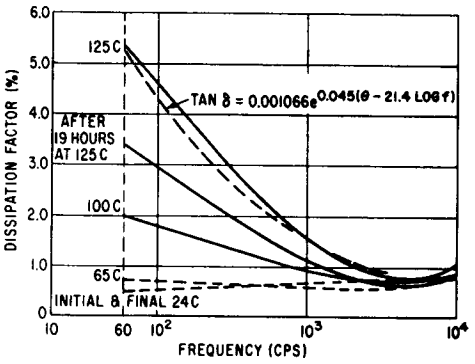

Fig. 1. Tan δ of Lot #2 Butyl Rubber.

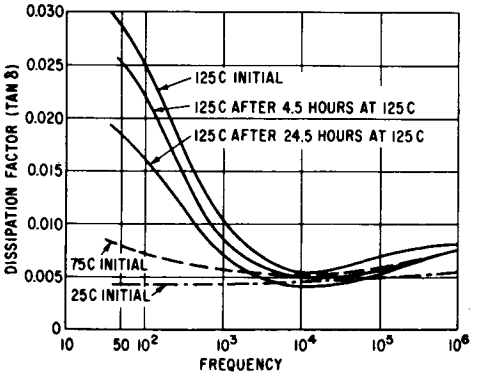

Fig. 2. Tan δ of Lot #5 Butyl Rubber.

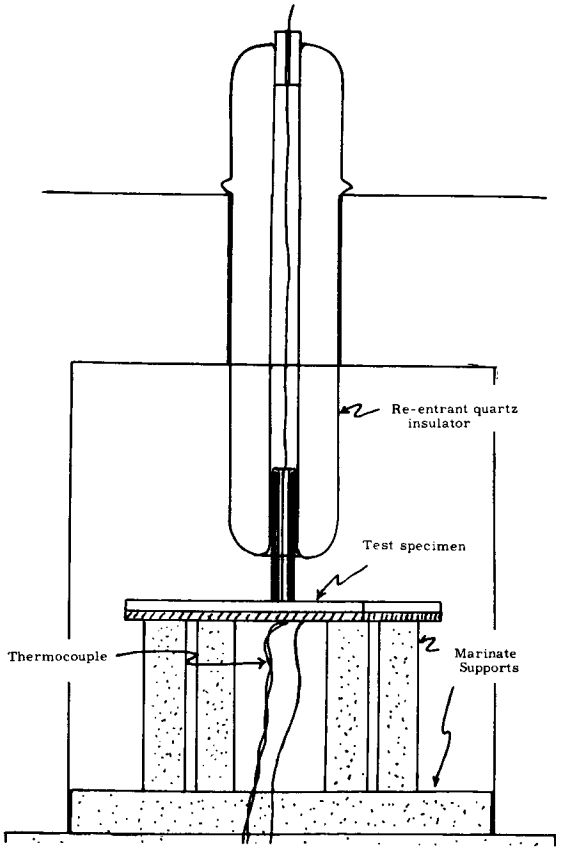

Fig. 3. Cross-sectional View of Furnace with Ceramic Test Specimen in Place.

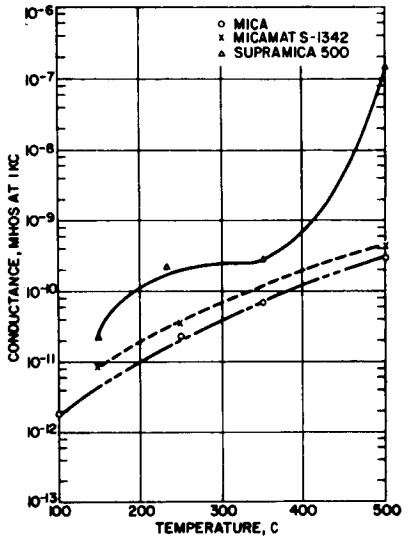

Fig. 4.

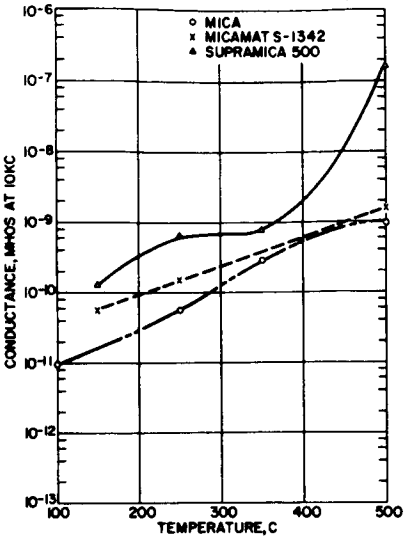

Fig. 5.

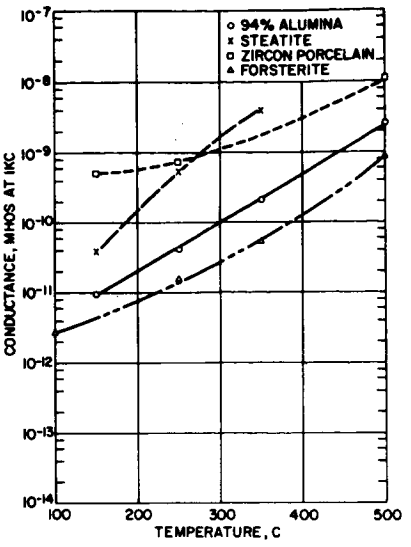

Fig. 6.

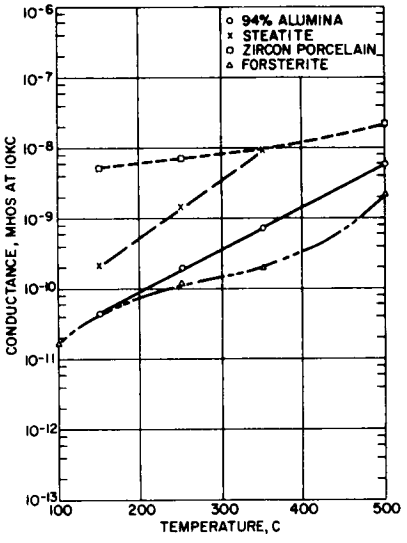

Fig. 7.

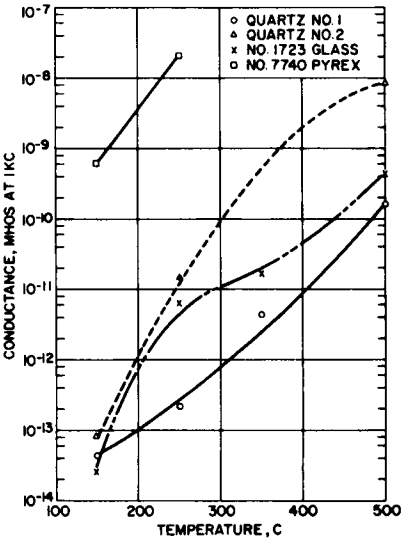

Fig. 8.

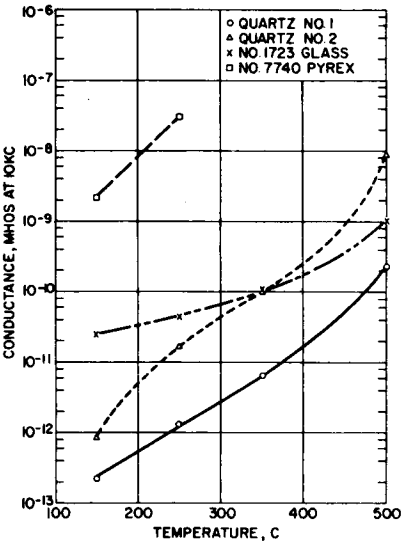

Fig. 9.

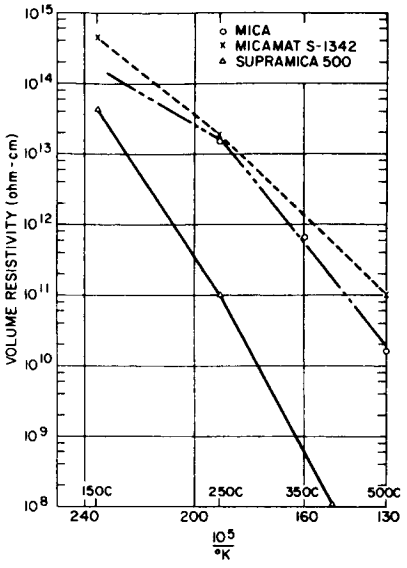

Fig. 10.

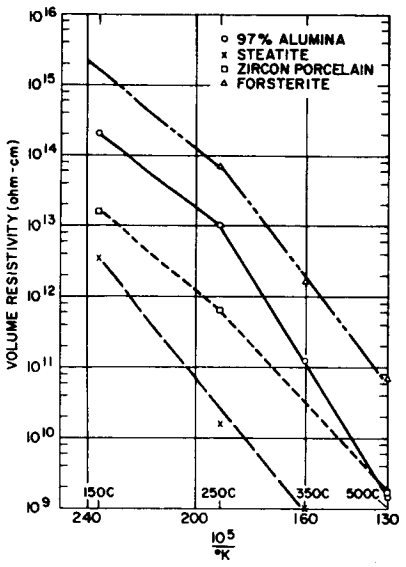

Fig. 11.

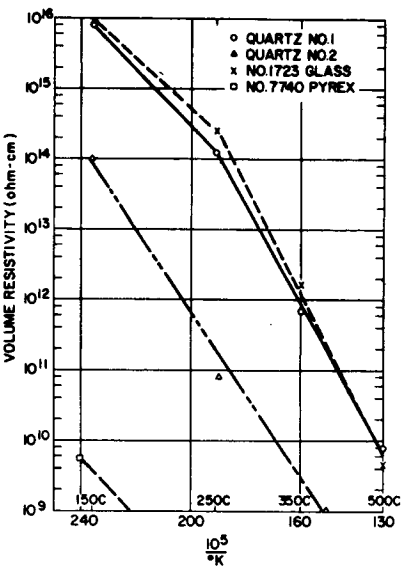

Fig. 12.

APPENDIX I

PAST CHAIRMEN

Conference on Electrical Insulation

1920 - 1921	Dr. Frank B. Jewett*
1922 - 1938	Dr. John B. Whitehead*
1927 and 1933	Mr. William A. Del Mar**
1939 - 1947	Dr. Ward F. Davidson*
1948	Dr. S. O. Morgan
1949	Dr. John D. Piper*
1950	Dr. Charles F. Hill
1951	Dr. Arnold H. Scott
1952	Dr. Arthur R. von Hippel
1953	Mr. Donald W. Kitchin
1954	Dr. David A. McLean
1955	Dr. Robert G. Breckenridge
1956	Dr. A. H. Sharbaugh
1957	Dr. Thomas W. Dakin
1958	Mr. Earl R. Thomas
1959	Dr. John D. Hoffman
1960	Mr. William McMahon
1961	Mr. S. I. Reynolds
1962	Mr. Philip J. Franklin
1963	Mr. Joseph Sticher

* Deceased
** Served as Chairman for 1927 and 1933

APPENDIX II

PROGRAM

Thirty-Third Annual Meeting

Conference on Electrical Insulation*

Union Carbide Corporation
Parma Research Center
Cleveland, Ohio

Monday through Wednesday, October 12 - 14, 1964

Monday Morning - October 12

Opening of the Conference . . . . . Louis J. Frisco
Chairman of the Conference

First Technical Paper Session - Louis J. Frisco, Presiding

Contributed Papers

Electrical Conductivity as a Function of Pressure in Five Conjugated Aromatic Monomers . . . . . R. G. Fitzgerald
Sandia Corporation

Cavitation in Transformer Oil Due to Electric Fields . . . . . .
N. Klein, Y. Amariglio, and E. Burstein
Israel Institute of Technology, Israel

The Effect of Hydrogen Acceptors on the Electrical Conductivity of Transformer Oil and Liquid Paraffin Under Very High Electrical Stress . . .
L. Angerer
Queen Mary College, England

The Effects of Radiation on Electric Conduction in Liquid Dielectrics. . . . . .
J. H. Calderwood and K. C. Kao
Royal College of Advanced Technology, England

Direct Current Conductivity of Polyethylene at High Field Strengths. . . . . .
G. Stetter
Technische Hochschule Munchen, Germany

Irradiation of Polyethylene and Electrical Conductivity. . . . . K. Yahagi
Waseda University
and
K. Shinohara
Institute of Physical and Chemical Research, Japan

Effect of High Energy Radiation on Electric Conduction of Polyethylene . . . . .
M. Ieda, M. Kosaki, Y. Yamada, and U. Shinohara
Nagoya University, Japan

Dielectric Properties of Some Poly(Fluoroalkyl Vinyl Ethers) . . . . . .
H. Sorkin, W. W. Graessley, J. A. Manson, and J. H. Zufall
Air Reduction Company

---

*Supported in part by the National Aeronautics and Space Administration Under Task Order Contract NSR-09-012-902

Monday Morning - October 12 (Cont'd.)

Invited Paper

J. B. Whitehead Memorial Lecture . . . . . Dr. Kenneth S. Cole
National Institutes of Health
"Dielectrics Alive"

Monday Afternoon - October 12

Second Technical Paper Session - A. H. Sharbaugh, Presiding

Contributed Papers

Simultaneous Dielectric Constant and Compressibility Measurements on Liquids at High Pressure. . . . . N. L. Brown
Bureau of Commercial Fisheries

Net Positive Charge Accumulation at Dielectric Surfaces Under 60 cps ac Corona. . . . . N. M. Bashara and F. M. Green
The University of Nebraska

Electron Ionization and Attachment Coefficients in Perfluorocarbon Gases . . . .
J. C. Devins and R. J. Wolff
General Electric Research Laboratory

Insulating Films of Boron-Nitride on Copper Substrates . . . . . .
R. R. Haberecht, R. J. Patterson, and R. D. Humphries
Texas Instruments, Incorporated

Thermoelectric Power of Sapphire Single Crystals . . . . . .
John Hart
Brock University
and
S. Dasgupta
Carleton University, Canada

Tuesday Morning - October 13

Third Technical Paper Session - N. M. Bashara, Presiding

Invited Papers

Fabrication of Thin Film Insulation. . . . . H. L. Caswell
IBM Watson Research Center

Thin Film Electronic Components. . . . . .D. A. McLean
Bell Telephone Laboratories, Inc.

Parameter Measurements in Thin Dielectric Films. . . . . J. V. Cathcart
Oak Ridge National Laboratory

Conduction in Thin Oxide Insulators. . . . . T. W. Hickmott
General Electric Research Laboratory

Conduction in Thin Organic Insulators. . . . . N. M. Bashara
The University of Nebraska

Tuesday Afternoon - October 13

Fourth Technical Paper Session - A. J. Warner, Presiding

Contributed Papers

Experimental Verification of the WLF Superposition Technique . . . . . A. J. Bur
National Bureau of Standards

Dielectric Specimen Holder for Electronic Materials. . . . . .
E. C. Bamberger and J. L. Dalke
National Bureau of Standards

Tuesday Afternoon - October 13 (Cont'd.)

Charge Behavior of an Absorptive Dielectric . . . . . M. M. Perlman
College Militaire Royal, Canada

Annual Business Meeting of the Conference

Tuesday Evening - October 13

Banquet - Dr. Augustus B. Kinzel, Speaker
Vice President of Research
Union Carbide Corporation

"Innovation"

Wednesday Morning - October 14

Fifth Technical Paper Session - O. Milton, Presiding

Contributed Papers

A Rogowski Surface for Dielectric Strength Tests . . . . . O. Milton
Sandia Corporation

A Controlled Thermal Environment for Dielectric Breakdown Strength Studies . . . . . L. J. Seligman
Sandia Corporation

Pulsed, Non-Uniform Field Electric Strength of a High Polymer. . . . J. L. Wentz
Sandia Corporation

Application of the Pointed Electrode in Evaluating the Pulse Life of Casting Resins . . . . . O. Milton
Sandia Corporation

Pulse Life and Dielectric Strength of a Glass-Filled Epoxy Resin System. . . . . L. J. Seligman
Sandia Corporation

Correlation Between Electrical Pulse Resistance and Mechanical Shock Resistance for Four Casting Resins. . . . . J. B. Allyn
Sandia Corporation

Disruptive Breakdown Measurements of Solid Materials in a Non-Uniform DC Field. . . . . R. R. Charpentier
High Voltage Engineering Corporation

The Measurement and Analysis of the Dielectric Strength of Glasses . . . . . .
W. H. Barney
Corning Glass Works

Minimum Dielectric Strength Areas in Draft Capacitor Tissue. . . . . .
E. P. Bullwinkel
P. J. Schweitzer Division

Pulsed Voltage Tests Which Determine the Criterion for Insulator Flashover in Dry Air. . . . . S. I. Reynolds
General Electric Research Laboratory

The Relation of Corona Pulse Charge Measurement to Size of Internal Voids or Other Origin . . . . . T. Dakin and C. N. Works
Westinghouse Electric Corporation

Wednesday Afternoon - October 14

Sixth Technical Paper Session - Joseph Sticher, Presiding

Contributed Papers

Designing for Maximum Flashover Voltage in 10^{-7} Vacuum and at Moderate Gauge Pressures of Electronegative Gases with Direct Voltage at High Temperatures . . . . . W. T. Starr
General Electric Research Laboratory

Evaluation of Electrical Insulation for Radiation Tolerant Equipment . . . . . C. L. Craig and J. Rogers
Sperry Gyroscope Company

Effect of Humidity on the Dielectric Properties of Some Polymers . . . . . D. L. Killam
The Hydro-Electric Power Commission of Ontario, Canada

Dumbbell Model for Dielectric Dispersion in Paraffin-like Solids . . . . . M. G. Broadhurst
National Bureau of Standards

Criteria for Thermal Failure of Insulating Materials . . . . . W. T. Starr and E. J. McGowan
General Electric Research Laboratory

Closing of the Conference . . . . . L. J. Frisco
Chairman of the Conference

APPENDIX III

ATTENDANCE LIST

Ackerman, Carl F.	Union Mills Paper Manufacturing Company	New Hope, Pa.
Allyn, Jerome B.	Sandia Corporation	Albuquerque, N.M.
Angerer, L.	Battersea College of Technology	London, England
Arnold, Robert M.	The Arnold Engineering Company	Marengo, Ill.
Avila, Frank C.	General Electric Company	Fort Wayne, Ind.
Bader, George	General Cable Company	Bayonne, N. J.
Bailey, C. A.	General Electric Company	Bridgeport, Conn.
Barney, Willis H.	Corning Glass Works	Corning, N. Y.
Bashara, N. M.	The University of Nebraska	Lincoln, Neb.
Berg, Daniel	Westinghouse Research Laboratories	Pittsburgh, Pa.
Blake, D. L.	Owens-Corning Fiberglas	Ashton, R. I.
Blodgett, R. B.	The Okonite Company	Passaic, N. J.
Bowers, G. H., III	E. I. du Pont de Nemours & Company	Wilmington, Dela.
Brancato, E. L.	Naval Research Laboratory	Washington, D. C.
Breckenridge, R. G.	Atomics International	Canoga Park, Calif.
Brockman, Irvin H.	AMP Inc.	Harrisburg, Pa.
Brown, Norman L.	Bureau of Commercial Fisheries	College Park, Md.
Bullwinkel, E. P.	Peter J. Schweitzer Division	Lee, Mass.
Bur, Anthony J.	National Bureau of Standards	Washington, D. C.
Burke, F. E.	Canadian General Electric Company	Toronto, Ont.,Can.
Burrell, R. W.	Consolidated Edison Company of N. Y.	New York, N. Y.
Calderwood, J. H.	Royal College of Advanced Technology	Lancashire, England
Cariou, F. E.	Union Carbide Corporation	Cleveland, Ohio
Carr, C. O.	Union Carbide Corporation	Cleveland, Ohio
Carter, C. E., Jr.	Westinghouse Research Laboratories	Baltimore, Md.
Cathcart, John V.	Oak Ridge National Laboratory	Oak Ridge, Tenn.
Caswell, H. L.	IBM Corporation	Yorktown Heights,N.Y.
Charpentier, Robert R.	High Voltage Engineering Corporation	Burlington, Mass.
Chipman, George P.	General Electric Company	Coshocton, Ohio
Cleveland, H. W.	Eastman Kodak Company	Rochester, N. Y.
Cole, Kenneth S.	National Institutes of Health	Bethesda, Md.
Cox, Duncan B.	Cox and Company, Inc.	New York, N. Y.
Craig, C. L.	Sperry Gyroscope Company	Great Neck, N.Y.
Curry, Robert C.	Formica Corporation	Cincinnati, Ohio
Dakin, T. W.	Westinghouse Research Laboratories	Pittsburgh, Pa.
Dalke, John L.	National Bureau of Standards	Boulder, Colo.
Dasgupta, S.	Carleton University	Ottawa, Ont.,Can.
Dazzo, Albert	Celanese Plastics Company	Clark, N. J.
Derber, Robert J.	Fairbanks, Morse & Company	Beloit, Wis.
Devaney, Richard G.	Tennessee Eastman Company	Kingsport, Tenn.
Devins, John C.	General Electric Company	Schenectady, N.Y.
Dingman, Edward G.	IBM Corporation	Endicott, N. Y.
Doak, Samuel	Weyerhaeuser Company	Fitchburg, Mass.
Doty, C. T.	Minnesota Mining & Manufacturing Company	St. Paul, Minn.
Duncan, G. I.	General Electric Company	Fort Wayne, Ind.
Eager, George S., Jr.	General Cable Corporation	Bayonne, N. J.
Eich, Edward D.	Anaconda Wire & Cable Company	Hastings-on-Hudson,N.Y.
Erven, C. C.	Ontario Hydro Research Division	Toronto, Ont.,Can.
Eustance, John W.	General Electric Company	Hudson Falls, N.Y.
Farber, Herman	77-40 250th Street	Bellerose, N. Y.
Fisher, John	Electronic News	Cleveland, Ohio
Fitzgerald, Roy G.	Sandia Corporation	Albuquerque, N.M.
Franklin, Philip J.	Advanced Research Projects Agency	Washington, D. C.

Frisco, Louis J.	General Electric Company	Schenectady, N. Y.
Goba, F. A.	Canadian Westinghouse Company, Ltd.	Hamilton, Ont.,Can.
Goreau, T. N.	Natvar Corporation	Woodbridge, N. J.
Gorski, D. A.	Union Carbide Corporation	Cleveland, Ohio
Graves, H. K.	New York Naval Shipyard	Brooklyn, N. Y.
Greenburg, William	Electronic News	New York, N. Y.
Greer, R. C.	Union Carbide Corporation	Cleveland, Ohio
Hart, John	Brock University	St.Catharines,Ont.,Can.
Hayworth, Bruce R.	General Dyn/Astronautics	San Diego, Calif.
Heidt, Lawrence	Simplex Wire and Cable Company	Arlington, Mass.
Heiss, J. H.	Bell Telephone Laboratories	Whippany, N. J.
Hickmott, T. W.	General Electric Company	Schenectady, N. Y.
Hoeckelman, R.	Union Carbide Corporation	Cleveland, Ohio
Hoehn, W. G.	General Electric Company	Cincinatti, Ohio
Hoffman, John D.	National Bureau of Standards	Washington, D. C.
Hogle, Donald H.	Minnesota Mining & Manufacturing Company	St. Paul, Minn.
Hueber, Bernard	AMP Inc.	Harrisburg, Pa.
Humphrey, L. E.	Union Carbide Corporation	New York, N. Y.
Hutzler, J.	Union Carbide Corporation	Cleveland, Ohio
Ieda, Masayuki	Nagoya University	Nagoya, Japan
Jaczek, S. M.	Canada Wire & Cable Company, Ltd.	Toronto,Ont.,Can.
Jensen, W. F., Jr.	E. I. du Pont de Nemours & Company	Wilmington, Dela.
Jones, P. W.	Rostone Corporation	Lafayette, Ind.
Kallweit, Juerg-Heinrich	University of Alabama	Huntsville, Ala.
Kinard, Joseph R., Jr.	National Bureau of Standards	Washington, D. C.
Kinzel, Augustus B.	Union Carbide Corporation	New York, N. Y.
Kitchman, Lester Allan	Harry Diamond Laboratories	Washington, D. C.
Klein, Nicholas	Faculty of Electrical Engineering	Haifa, Israel
Krause, A. R.	TRW Capacitor Division	Ogallala, Neb.
Kuritza, O. M.	IIT Research Institute	Chicago, Ill.
Kurtz, M.	Ontario Hydro Research Division	Toronto, Ont.,Can.
Liao, T. W.	General Electric Company	Philadelphia, Pa.
Lusk, G. E.	G & W Electric Specialty Company	Blue Island, Ill.
McCarthy, James L.	Lake Publishing Corporation	Libertyville, Ill.
McCarty, Lewis V.	General Electric Company	Cleveland, Ohio
McDevitt, J. T.	Union Carbide Corporation	Cleveland, Ohio
McGowan, Edward J.	General Electric Company	Schenectady, N. Y.
McLean, D. A.	Bell Telephone Laboratories	Murray Hill, N. J.
McMahon, Eugene J.	E. I. du Pont de Nemours & Company	Wilmington, Dela.
McMahon, W.	Bell Telephone Laboratories	Whippany, N. J.
Mankoff, Lawrence L.	General Electric Company	Philadelphia, Pa.
Manley, Thomas C.	The Welsbach Corporation	Philadelphia, Pa.
Manning, M. L.	South Dakota State University	Brookings, S. Dak.
Manuel, James C.	Tektronix	Beaverton, Ore.
Meyer, Owen L.	Harry Diamond Laboratories	Washington, D. C.
Mildner, Raymond C.	Dow Chemical Company	Midland, Mich.
Miller, Marian F.	National Academy of Sciences	Washington, D. C.
Millington, James E.	Allis-Chalmers Manufacturing Company	Milwaukee, Wis.
Milton, Osborne	Sandia Corporation	Albuquerque, N. M.
Mitchell, George R.	Glastic Corporation	Cleveland, Ohio
Molzon, Arnold E.	Picatinny Arsenal	Dover, N. J.
Mopsik, Frederick I.	National Bureau of Standards	Washington, D. C.
Moses, Graham Lee	Westinghouse Research Laboratories	Pittsburgh, Pa.
Nielson, Erik R.	IIT Research Institute	Chicago, Ill.
Nothelfer, John J.	Nothelfer Winding Laboratories, Inc.	Trenton, N. J.
Olyphant, Murray, Jr.	Minnesota Mining & Manufacturing Company	St. Paul, Minn.
Orr, Robert W.	General Radio Company	West Concord, Mass.
Pappaioanou, George J.	Union Carbide Corporation	Indianapolis, Ind.
Pappas, Peter	General Electric Company	Scotia, N. Y.
Parker, S. B.	Delco-Remy Division of GMC	Anderson, Ind.

Patterson, R. J.	Texas Instruments, Inc.	Dallas, Tex.
Perkins, J. R.	E. I. du Pont de Nemours & Company	Wilmington, Dela.
Perlman, M. M.	College Militaire Royal	St.Jean, Que.,Can.
Peterson, G. R.	Allen Bradley Company	Milwaukee, Wis.
Petricola, A. J.	International Cellulose Research	Hawkesbury,Ont.,Can.
Philofsky, H. M.	Westinghouse Research Laboratories	Pittsburgh, Pa.
Pleitt, Richard J.	Charles Bruning Company	Mount Prospect, Ill.
Reed, Clive W.	General Electric Company	Schenectady, N. Y.
Reynolds, Robert E.	Detroit Edison Company	Detroit, Mich.
Reynolds, S. I.	General Electric Company	Schenectady, N. Y.
Ried, Kenneth A.	E. I. du Pont de Nemours & Company	Wilmington, Dela.
Riegelmann, Kermit W.	Field Emission Corporation	McMinnville, Ore.
Robinson, Preston	Sprague Electric Company	North Adams, Mass.
Rosch, S. J.	324 Woodworth Avenue	Yonkers, N. Y.
Sacher, E.	E. I. du Pont de Nemours & Company	Wilmington, Dela.
Saile, Charles J.	James G. Biddle Company	Plymouth Meeting, Pa.
Samoden, Robert A.	E. I. du Pont de Nemours & Company	Wilmington, Dela.
Scheid, Carl	General Electric Company	Milwaukee, Wis.
Shepard, R. L.	Union Carbide Corporation	Cleveland, Ohio
Schifreen, C. S.	Philadelphia Electric Company	Philadelphia, Pa.
Schmunk, E. W., Jr.	S. & C. Electric Company	Chicago, Ill.
Scott, Arnold H.	National Bureau of Standards	Washington, D. C.
Seligman, Lee J.	Sandia Corporation	Albuquerque, N. M.
Sharbaugh, A. H.	General Electric Company	Schenectady, N. Y.
Sletten, A. M.	Westinghouse Research Laboratories	Pittsburgh, Pa.
Sommerman, G. M. L.	Westinghouse Research Laboratories	Pittsburgh, Pa.
Sorkin, H.	Air Reduction Company	Murray Hill, N. J.
Spauschus, Hans O.	General Electric Company	Louisville, Ky.
Sparks, Norman D.	Union Carbide Corporation	Cleveland, Ohio
Starr, Wendell T.	General Electric Company	Schenectady, N. Y.
Stetter, Gunter	Technical University of Munchen	Munchen, Germany
Sticher, Joseph	The Detroit Edison Company	Detroit, Mich.
Swan, David W.	Minnesota Mining & Manufacturing Company	St. Paul, Minn.
Swiss, Jack	Westinghouse Research Laboratories	Pittsburgh, Pa.
Taimuty, S. I.	Stanford Research Institute	Menlo Park, Calif.
Taylor, J.	Monsanto Chemical Company	Springfield, Mass.
Thornhill, D. W.	National Academy of Sciences	Washington, D. C.
Timm, L. J.	U. S. Applied Science Laboratory	Little Falls, N. J.
Touchette, Alphe F.	General Electric Company	Somersworth, N. H.
Tucker, Robert W.	Harry Diamond Laboratories	Washington, D. C.
Umbaugh, C. W.	Union Carbide Corporation	Cleveland, Ohio
Valley, David J.	Union Carbide Corporation	Cleveland, Ohio
Wagener, Siegfried	Union Carbide Corporation	Cleveland, Ohio
Ward, R. A.	General Electric Company	Schenectady, N. Y.
Ware, P. H.	Simplex Wire and Cable Company	Cambridge, Mass.
Warner, A. J.	DeBell and Richardson, Inc.	Hazardville, Conn.
Waters, Paul F.	W. R. Grace and Company	Clarksville, Md.
Wentz, J. L.	Sandia Corporation	Albuquerque, N. M.
Wheeler, E. S.	General Electric Company	Schenectady, N. Y.
Wiitala, J. R.	Union Carbide Corporation	Cleveland, Ohio
Wikstrand, W. Carl	American Cyanamid Company	Stamford, Conn.
Wilson, Jerry D.	General Electric Company	Hudson Falls, N. Y.
Woodland, Paul C.	Dow Chemical Company	Midland, Mich.
Work, R. N.	Pennsylvania State University	University Park, Pa.
Works, Carroll N.	Westinghouse Research Laboratories	Pittsburgh, Pa.
Yahagi, Kichinosuke	Waseda University	Tokyo, Japan
Zimmerman, S. W.	102 Valley Road	Ithaca, N. Y.

APPENDIX IV

PUBLICATIONS OF THE CONFERENCE ON ELECTRICAL INSULATION

Single volumes in the series of Annual Reports of the Conference on Electrical Insulation are:

Year	NAS-NRC Publication Number	
1949	No Number (Order by Year)	$3.00
1950	Out of Print	
1951	No Number (Order by Year)	3.00
1952	" "	3.00
1953	NAS-NRC Publication 304	3.00
1954	" " 368	3.00
1955	Out of Print	
1956	NAS-NRC Publication 512	3.00
1957	" " 570	3.00
1958	" " 650	3.00
1959	Out of Print	
1960	Out of Print	
1961	NAS-NRC Publication 973	5.00
1962	" " 1080	5.00
1963	" " 1141	5.00

Single volumes in the series of annual Digest of the Literature on Dielectrics are:

Vol. XI	(1947)	Reprint	$5.00
Vol. XII	(1948)	Reprint	5.00
Vol. XIII	(1949)	Reprint	5.00
Vol. XIV	(1950)	NAS-NRC Publication 202	5.00
Vol. XV	(1951)	" " 231	5.00
Vol. XVI	(1952)	Out of Print	
Vol. XVII	(1953)	Out of Print	
Vol. XVIII	(1954)	NAS-NRC Publication 383	5.00
Vol. XIX	(1955)	" " 503	5.00
Vol. XX	(1956)	" " 562	5.00
Vol. XXI	(1957)	" " 599	5.00
Vol. XXII	(1958)	" " 713	5.00
Vol. XXIII	(1959)	" " 799	8.00
Vol. XXIV	(1960)	" " 917	10.00
Vol. XXV	(1961)	" " 1034	15.00
Vol. XXVI	(1962)	" " 1139	15.00
Vol. XXVII	(1963)	" " 1230	15.00

ORDER FROM: Printing and Publishing Office
National Academy of Sciences
National Research Council
2101 Constitution Avenue, N. W.
Washington, D. C. - 20418